Computational Studies on Small Molecule Activation via Cooperative Lewis Pairs

PhD dissertation

Tibor András Rokob

Supervisor:
Imre Pápai, D.Sc.
Head of Department

Chemical Research Center of the
Hungarian Academy of Sciences

Eötvös Loránd University
Doctoral School of Chemistry
Head of School: György Inzelt

Theoretical and Physical Chemistry,
Structural Chemistry PhD program
Head of Program: Péter Surján

2009

Contents

Foreword

The elucidation of reaction mechanisms has long been of particular importance in chemistry. Deep understanding of experimental results and systematization of seemingly independent information may pave the way for the development of new approaches; allowing more complex products to be synthesized, or faster, simpler, more efficient reactions to be invented. By now, computational chemistry has become a valuable tool that can complement experimental mechanistic studies, rationalize trends and provide new insight at the molecular level.

During my PhD work, I have been involved in studying the reactions of sterically crowded Lewis acid–base pairs. These pairs have recently been found experimentally to provide coexistent, reactive Lewis centers, and to undergo or induce chemical transformations unprecedented for main group compounds. Beginning in 2006 with the seminal experiments of Douglas W. Stephan and coworkers, the ability of certain pairs to cleave dihydrogen and to act as hydrogenation catalysts was demonstrated. These results attracted immediate attention of the scientific community, as such processes required so far either transition metal systems, or extreme conditions. The experimental results underline that Lewis acid–base cooperation can be a viable design principle for systems devoted to activating small molecules.

Our computational results made possible to formulate plausible mechanisms for the activation of hydrogen and ethylene. Studies of the related catalytic hydrogenation processes and calculations on the thermodynamics of the hydrogen splitting reaction helped to interpret a large body of experimental data, and to derive principles that may prove useful in designing new systems. Our work, published in five research papers [1–5], is now summarized in this dissertation, with the hope of providing a useful reference for anyone interested in this promising area of chemistry.

Acknowledgements

I would like to express my grateful thanks to all the people who have shared my efforts or helped me in any way during my work. Without them, this dissertation could have never been written.

First, I am deeply indebted to my supervisor, Imre Pápai. It has been delightful for me to work together with him, and it would be hard to enumerate all things that I have learned from Imre in these three years. I am also grateful for the continuous support I have got, both in the academic career as well as in personal life.

I was really lucky that I could work together with Andrea Hamza, Tibor Soós and András Stirling on the topics discussed in the dissertation. I thank for the inspirating environment and for the long talks in which the final versions of the concepts and papers were matured. Special thanks to Tibor for calling our attention to this topic.

The extraordinary support from György Hajós, Director of the Institute of Biomolecular Chemistry, and from Gábor Pálinkás, General Director of the Chemical Research Center for me as well as for the Department of Theoretical Chemistry is highly appreciated.

I am obliged to Szilárd Varga, my ex-roommate at the Bolyai College, who has always been ready for help or discussion, on scientific topics just as on anything else. I am particularly grateful for his suggestion, made almost four years ago, that I should contact Imre concerning a PhD work.

I thank all Colleagues from the Department of Theoretical Chemistry and the Department of Synthetic Organic Chemistry for providing lots of help and a very enjoyable atmosphere at work.

My scientific work could not have been successful without a solid background I have always been able to count on. It would be hard to suitably thank the continuous love, support and patience I received from my parents and my fiancée. I wish to also express my gratitude to all my friends for sharing good and bad moments with me.

Notations and Abbreviations

A	Lewis acceptor
B	$B(C_6F_5)_3$ [tris(pentafluorophenyl)borane]
B′	$-B(C_6F_5)_2$ [bis(pentafluorophenyl)boryl group]
cat.	catalyst
Cy	cyclohexyl [group]
D	Lewis donor
DFT	density functional theory
E	zero-point uncorrected gas-phase electronic energy
ee	enantiomeric excess
FLP	frustrated Lewis pair
G	solvent-phase Gibbs free energy
*i*Pr	isopropyl [group]
IRC	intrinsic reaction coordinate
Me	methyl [group]
Mes	mesityl (2,4,6-trimethylphenyl) [group]
MO	molecular orbital
NPA	natural population analysis
NMR	nuclear magnetic resonance [spectroscopy]
*o*Tol	*ortho*-tolyl [group]
PES	potential energy surface
Ph	phenyl [group]
SCS-MP2	spin-component-scaled MP2
*t*Bu	*tert*-butyl [group]
THF	tetrahydrofuran
TS	transition state

Notations of compounds are collected in Figures 1.13–1.15 on page 10.

In figures showing molecular geometries, the following atom coloring is used: carbon, hydrogen, fluorine, phosphorous, boron, nitrogen, oxygen. Selected bond lengths and other distances are given in ångströms.

Chapter 1

Introduction

1.1 The Lewis Concept and the Strength of the Dative Bond

Gilbert N. Lewis formulated his theory of acids and bases in 1923 [6,7]. By defining an "acid" as an electron pair acceptor and a "base" as an electron pair donor, this approach covers all reactions in which bonds are formed with both electrons coming from one fragment. The applicability of this concept is not limited to compounds with dative bonds: all reactions that are mainly governed by the interaction between a single doubly occupied and a single empty orbital to produce a favorable overlap can be classified as Lewis acid–base reactions. Such processes have fundamental significance in most areas of chemistry; for example, a broad range of organic chemical reactions between nonradical intermediates (electrophiles and nucleophiles) can be interpreted in this way [8,9].

In the Lewis acid–base concept, reference is made neither to the rate of the reaction, nor to the strength of the bond formed. Moreover, unlike the Brønsted acids and bases, a single, unified strength scale of Lewis acids or bases is insufficient to make general predictions, as acidity order often depends on the reference base chosen, and vice versa. Although a series of such scales have been developed [10], their usability is limited by the wide structural variety of Lewis acids and bases, which also made the formulation of an appropriate theory, qualitative or quantitative, challenging. A deep understanding of the nature of the chemical bond was necessary to determine the main factors affecting its strength.

The hard–soft classification, introduced by Pearson in 1963, "permits a useful systematization of a large amount of chemical information" [13]. Hard bases prefer hard acids, and form bonds with a stronger ionic character; whereas soft bases react better with soft acids, forming bonds with more covalent character. Quantum mechanics provides a simple explanation for this principle, which is broadly applicable to understand qualitative trends in bond strengths as well as relative rates or selectivities of chemical reactions [8].

Inspired by Mulliken's quantum mechanical description of the covalent bond [14], a quantitative model has been developed by Drago and Wayland that can predict bond formation enthalpies for a remarkably wide range of acid–base pairs [15,16]. This model assigns two numbers to each acid and base: their affinity for covalent (C) and ionic, electrostatic bonding (E). By using E and C parameters fitted to some experimental data, binding enthalpies can be calculated from their values for the acid (A) and base (B):

$$-\Delta H = E_\mathrm{A}E_\mathrm{B} + C_\mathrm{A}C_\mathrm{B}.$$

This simple approach provides not only very accurate predictions, but also a quantification of the hardness of the acids and bases via the E/C ratio. The obtained values usually agree with Pearson's qualitative classification.

Considering the success of the Drago–Wayland model to describe the electronic interaction between acids and bases, the cases in which it *fails* highlights other factors that influence bond strength. Among these, the most important is the *steric effect* [16].

Steric hindrance of the dative bond formation, as well as steric effects on a range of other processes, were extensively studied by Herbert C. Brown and coworkers from the 1940's [17, 18]. Their experiments with bulky acids and bases pointed out that dative bonds can be weakened, or their formation completely blocked by steric strain (see Figure 1.1). However, larger substituents do not exclusively mean larger repulsion. Recent theoretical studies highlighted that attractive secondary forces acting between the bulky groups may contribute significantly to the strength of the dative bond (an example is shown in Figure 1.2) [19].

In summary, the electronic properties, including the hard–soft nature of the Lewis centers, and the repulsive or attractive forces between the substituents all have importance in determining the bond strength, which can range from strong, irreversible interaction to no bond at all.

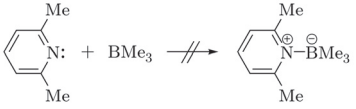

Figure 1.1: Example of sterically blocked dative adduct formation [17]

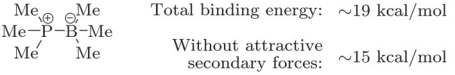

Figure 1.2: Significant contribution of secondary forces to dative bond strength [19]

1.2 Non-Classical Lewis Acid–Base Reactions

Steric congestion around the most reactive site of a molecule can often shed light on other possible places where reaction can occur. Under normal circumstances, such alternative pathways are usually kinetically or thermodynamically disfavored over the main reaction channel, but they may become predominant if the latter is unavailable due to steric reasons.

For Lewis acid–base pairs, this kind of reactivity was observed as early as in the 1960's. The research group of Wittig described the reaction of Ph_3C^- with the tetrahydrofuran (THF) adduct of BPh_3 [20]. Instead of the expected displacement of THF (i.e., a substitution on the boron), a ring opening reaction was observed (a substitution on the sterically more available carbon, see Figure 1.3). Reaction of bulky tertiary amines with the trityl cation afforded triphenylmethane and an iminium

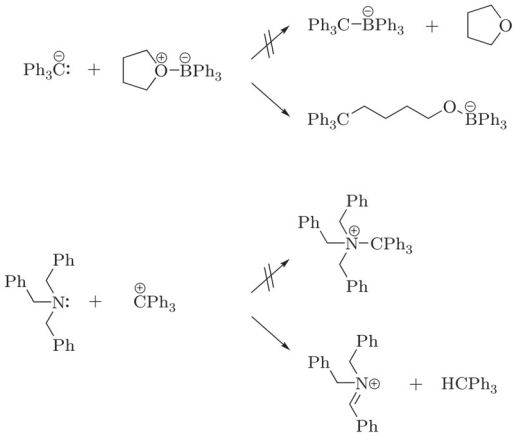

Figure 1.3: Early examples of non-classical Lewis acid–base reactivity [20–22]

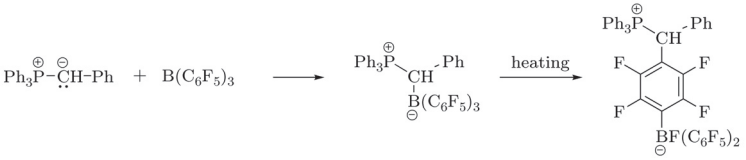

Figure 1.4: Reaction of a bulky ylide with $B(C_6F_5)_3$ [23]

cation via hydride abstraction [21,22]; the anticipated quaternary ammonium salt was not formed.

More recently, Erker and coworkers found that the reaction of triphenylphosphonium ylide $Ph_3P{-}CHPh$ with tris(pentafluorophenyl)borane $B(C_6F_5)_3$ yields a thermally unstable conventional acid–base adduct, which readily undergoes rearrangement (see Figure 1.4) [23]. Formation of the resulting compound can be interpreted as a Lewis acid–base reaction of the ylide with the *para*-carbon of the pentafluorophenyl ring, followed by fluoride migration.

Originating from their interest in Lewis acid activators for olefin polymerization [24,25,77], significant efforts have lately been made by the research group of Douglas W. Stephan to systematically explore the chemistry of sterically encumbered Lewis acid–base pairs. Stephan et al. showed that THF ring opening reactions can also be carried out with phosphines and $THF{-}B(C_6F_5)_3$ (Figure 1.5) [78]. Analogously to the ylide–borane system, phosphine attack on the aromatic rings of $B(C_6F_5)_3$ [76], as well as of Ph_3C^+ [79], was also observed. These reactions provided a new methodology

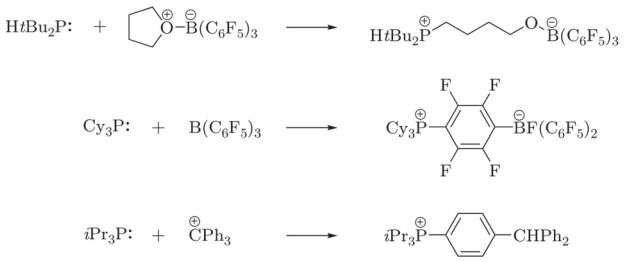

Figure 1.5: Reactions of bulky phosphines and Lewis acids [76, 78, 79]

for the synthesis of a series of phosphine–borane compounds and to tune the Lewis acidity of the borane center [76].

1.3 Ambiphilic Systems

Lewis pairs that show neither classical dative bond formation, nor any alternative reactivity, possess chemically interesting and often useful properties, owing to the simultaneous presence of free acidic and basic centers. Linking the donor and acceptor moieties into one molecule may create an organized ambiphilic environment, which is often more successful than its components alone. In all cases, careful design of the steric [26, 54–56] and electronic, e.g., hard–soft [57, 58] properties is necessary to avoid the unwanted self-quenching of the ambiphilic pair.

Important applications of such pairs include versatile ligands for transition metals, allowing the synthesis of complexes containing metal → Lewis acid dative bond [59, 60]; some selected examples are shown in Figure 1.6. The use of ambiphilic systems allowed the trapping of reactive intermediates, such as the Huisgen zwitterions of the Mitsunobu reaction (see Figure 1.7) [61, 62], and the phosphazide intermediate of the Staudinger reaction [63, 64]. Boronic acid derivatives containing a Lewis basic site were successfully used for chemosensing; fluorescent saccharide detection has a wide literature [65] but other methods such as electrochemical detection of hydrogen fluoride have also been reported [66].

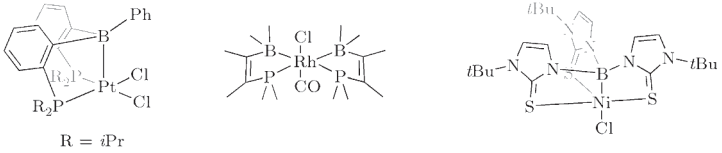

Figure 1.6: Examples of ambiphilic molecules as transition metal ligands [59, 60]

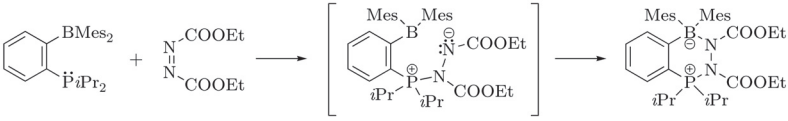

Figure 1.7: Trapping of the P−N bonded Huisgen zwitterion intermediate [62]

An increasing number of organic chemical transformations have been described using acid–base cooperative catalysis: the simultaneous binding or activation of nucleophilic and electrophilic fragments is reminiscient to enzyme mechanisms, and often yields excellent reactivities and selectivities [67–75]. A few examples, such as a [2+2] cycloaddition reaction of imino esters and ketenes (Figure 1.8) [67], and an asymmetric Strecker reaction (Figure 1.9) [68], indicate the broad applicability of this concept.

1.4 Hydrogen Activation

As part of their systematic exploration of phosphine–borane compounds, Stephan and his coworkers achieved the synthesis of the zwitterion [$^{+}$HMes$_2$P−C$_6$F$_4$−B(C$_6$F$_5$)$_2$H^{-}] via the treatment of the nonconventional adduct of HMes$_2$P and B(C$_6$F$_5$)$_3$ with chlorodimethylsilane (Figure 1.10) [80]. This species seemed of interest because it contains both a protonic and a hydridic hydrogen, attached to the phosphorus and boron atoms, respectively. The resulting colorless compound is stable on air, but it was found to release molecular H$_2$ in a clean reaction upon heating to 150 °C [80]. This finding was not completely unexpected: structurally somewhat related compounds, such as various hydride salts and aminoboranes, may similarly lose H$_2$, and they are nowadays intensively investigated as promising candidates for hydrogen storage materials [221, 222].

However, a rather surprising observation was made when the resulting phosphinoborane Mes$_2$P−C$_6$F$_4$−B(C$_6$F$_5$)$_2$ was reacted with H$_2$. In a rapid reaction, occuring at room temperature and atmospheric pressure, the starting zwitterion [$^{+}$HMes$_2$P−C$_6$F$_4$−B(C$_6$F$_5$)$_2$H^{-}] was re-formed [80].

Hydrogen activation on transition metals has long been known and well studied, but direct reactions of H$_2$ with stable main group compounds are quite rare. Known examples include alkali metal alkyl or aryl compounds [125], carbocations in a superacidic environment [126], the ArGeGeAr "digermyne" species [127], singlet (alkyl)(amino)carbenes [128], and the heavier group 14 element carbene analogue SnAr$_2$ [129] (see Figure 1.11).

Transition-metal-free H$_2$ activation in biological systems was also considered feasible [153–156]. However, the unique hydrogenase found in methanogenic archaea, which was assumed to act as a purely organic hydrogenation catalyst, was later shown to comprise an active iron-containing cofactor [157, 158].

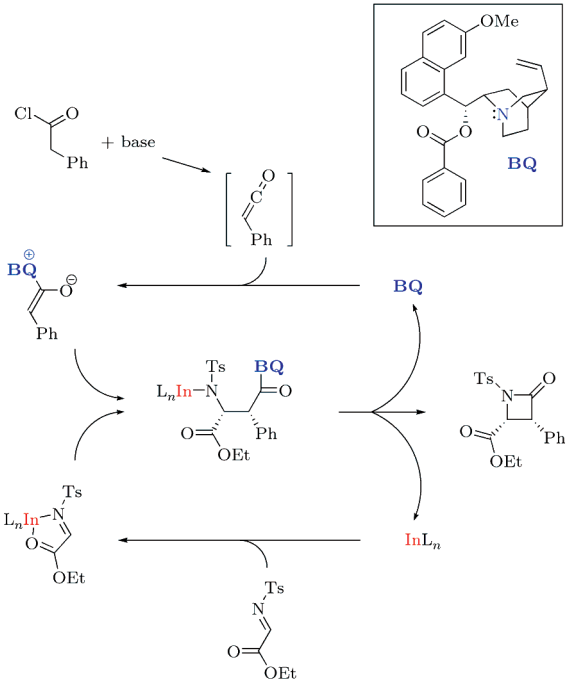

Figure 1.8: Cycloaddition reaction of an imino ester and a ketene, catalyzed by a Lewis acid (indium salt) and a Lewis base (benzoylquinine, **BQ**) [67]

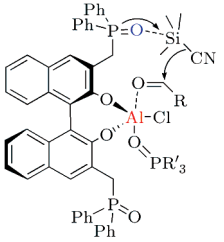

Figure 1.9: Catalytic asymmetric Strecker reaction between an aldehyde and trimethylsilyl cyanide [68]

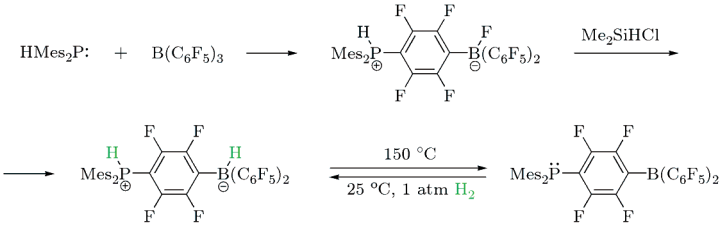

Figure 1.10: Synthesis and reactivity of a phosphonium hydridoborate zwitterion [80]

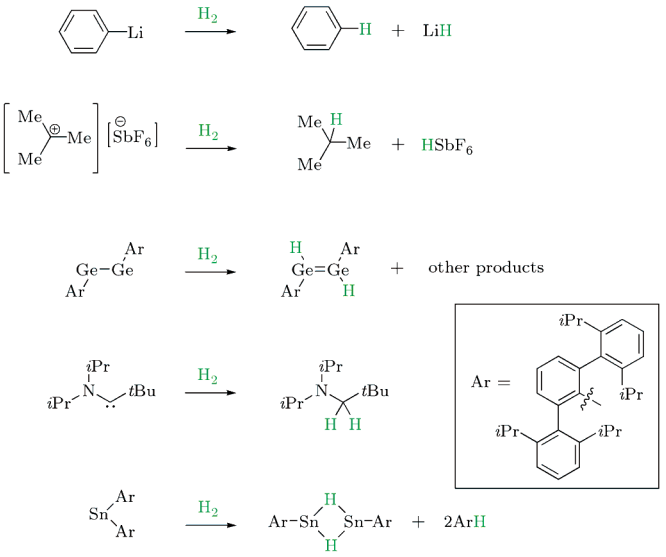

Figure 1.11: Activation of H_2 by main group compounds [125–129]

Although mechanistic details of the novel hydrogen activation process by phosphinoboranes were not extensively studied, Stephan et al. attributed this unique reactivity towards H_2 to the presence of unquenched Lewis donor and acceptor centers. The absence of any aggregation of this intramolecularly linked Lewis pair, as observed by NMR spectroscopy, turns this compound into an efficient ambiphilic system, with its Lewis centers available for an interaction with molecular hydrogen [80]. Stephan et al. coined the term "frustrated Lewis pair" (FLP) to this and similar compounds [76], which present extraordinary reactivity due to steric reasons [81, 82].

In a subsequent study, the Stephan group demonstrated that the phosphine and borane fragments need not be connected in order to effect hydrogen cleavage [83]. In these experiments, the simple phosphines $t\mathrm{Bu_3P}$ and $\mathrm{Mes_3P}$ were found to be unreactive towards $\mathrm{B(C_6F_5)_3}$, thus forming frustrated Lewis pairs. These systems are also able to heterolytically split hydrogen under mild conditions, yielding the appropriate phosphonium hydridoborate salts, albeit in a nonreversible manner (see Figure 1.12).

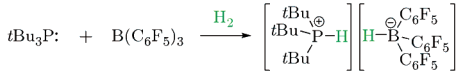

Figure 1.12: Activation of H_2 by a nonlinked phosphine–borane pair [83]

These landmark discoveries shed light on the potential of frustrated Lewis pairs to broaden the scope of metal-free bond activation, which has long been of interest due to the environmental and product toxicity concerns connected with transition metals [84, 85]. The results brought into focus the application of ambiphilic compounds for small molecule activation, which may lead to novel strategies in various branches of synthetic chemistry, and also to developments relevant to hydrogen economy.

Since the description of the above systems, a series of different donors (D) and acceptors (A) have been investigated, both as nonlinked combinations (D + A) and as part of linked systems (D∼A). On the donor side, application of various phosphine derivatives [86, 87] (including ferrocenyl phosphines [88, 89]), imine [90–92], amine [90, 93, 94], pyridine [95], and carbene [96–99] compounds has been described (Figure 1.13), albeit on the acceptor side, only borane derivatives [87, 91, 100, 101] have been reported (Figure 1.14). The applied linkers include *p*-$\mathrm{C_6F_4}$, methylphenyl [102], ethylene [103, 104] and ethenylene [105] moieties, but a directly linked phosphanylborane system [106] has also been described (Figure 1.15).

The most frequently used Lewis acidic molecule is the tris(pentafluorophenyl)borane $\mathrm{B(C_6F_5)_3}$, which has numerous applications in synthetic chemistry, for instance, as Lewis acid activator in olefin polymerization [12, 27–29]. From now on, we shall denote this compound by **B**. As part of linked systems, the bis(pentafluorophenyl)boryl fragment ($-\mathrm{B(C_6F_5)_2}$, referred to as **B′**) is exclusively utilized.

Most H_2 cleavage reactions readily proceed under mild conditions and produce high yields of the corresponding salts ($[\mathrm{DH}]^+[\mathrm{HA}]^-$) or zwitterions ($[^+\mathrm{HD}{\sim}\mathrm{AH}^-]$).

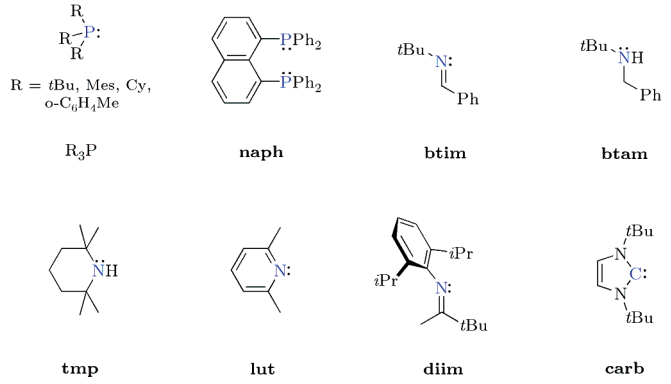

Figure 1.13: Some FLP donors described in the literature

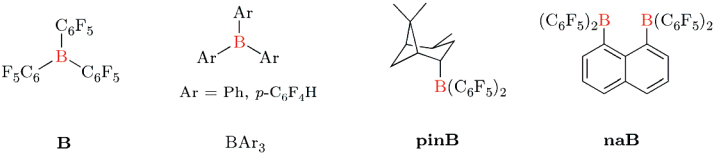

Figure 1.14: Some FLP acceptors described in the literature

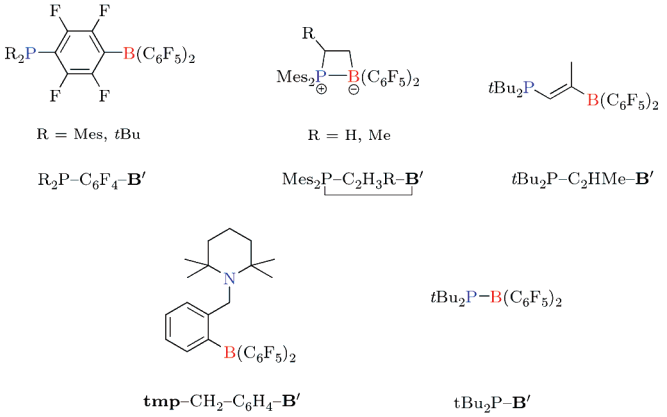

Figure 1.15: Examples of linked D∼A systems described in the literature

Some of these processes were even found to be reversible upon heating and/or reducing pressure [80, 86, 87, 94, 102]. Notably, several pairs form dative bonds, producing D−A adducts or rings (D≃A), and are yet reactive despite the presence of a dative bond [90, 93, 95, 103, 104, 106] (see Figure 1.16). The reactivity is thought to arise from the unbound forms, present at least in small concentration in equilibrium [103]. Existence of such equilibria has been known in the literature [30, 65] and it was indeed demonstrated by NMR measurements for some of these pairs, e.g., **lut**−**B** [95] and $Mes_2P{-}C_2H_3Me{-}\mathbf{B'}$ [104].

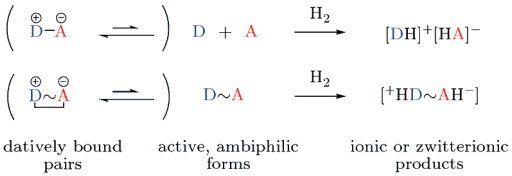

Figure 1.16: General equations of hydrogen splitting by FLPs

Early hypotheses about the reaction mechanism were formulated by the Stephan group [80]. These authors carried out a preliminary kinetic investigation of the hydrogen loss from the linked phosphonium borate $[^{+}HMes_2P{-}C_6F_4{-}\mathbf{B'}H^{-}]$, and found it to follow first-order kinetics. This observation, together with the calculated activation parameters, suggested an intramolecular H_2 elimination process. Stephan et al. proposed the reaction to occur via proton or hydride migration along the linker aromatic ring, followed by 1,2-elimination (see Figure 1.17). Activation of H_2 could then take place via the reverse pathway. On the other hand, these authors also carried out experiments with deuterated compounds, and observed scrambling of the deuterium labels, e.g., between $[^{+}HMes_2P{-}C_6F_4{-}\mathbf{B'}H^{-}]$ and $[^{+}DMes_2P{-}C_6F_4{-}\mathbf{B'}D^{-}]$ at elevated temperature, "which suggests a bimolecular high-temperature exchange process involving the intermolecular approach of BH and PH fragments in a transition state" [80]. The possible role of such transition states in the hydrogen activation process has not been mentioned.

In the case of the nonlinked phosphine–borane D + A pairs, a side-on coordination of H_2 to the borane, or an end-on coordination to the phosphine was suggested to initiate the reaction, followed by the attack of the other Lewis component (Figure 1.18) [83]. Both hypotheses seemed reasonable, as literature evidence confirmed the possibility of weak adduct formation between H_2 and phosphines [31] or boranes [32–35], albeit only in a low temperature noble gas matrix. However, experimental detection of such adducts with the active FLP components in solution at temperatures as low as 190 K was unsuccessful [83].

Facile, and in many cases, reversible activation of hydrogen by these systems immediately raises the question of practical applications. While it may be expected that new strategies for chemical hydrogen storage involve the concept of cooperative

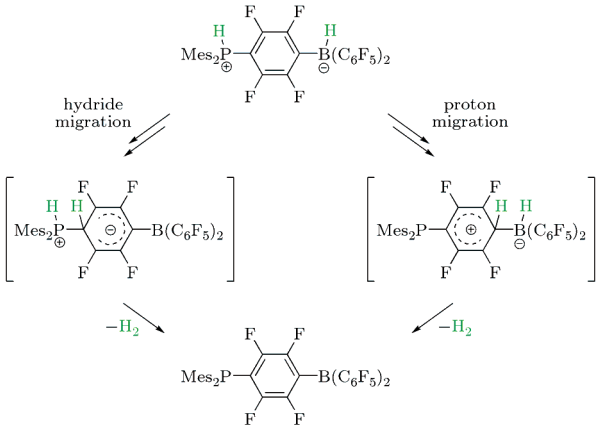

Figure 1.17: Proposed mechanisms for the hydrogen loss from $[^{+}\mathrm{HMes_2P{-}C_6F_4{-}}\mathbf{B'}\mathrm{H}^{-}]$. Hydrogen splitting was suggested to proceed via the reverse pathway [80].

Figure 1.18: Proposed pathways for the hydrogen activation by nonlinked pairs [83]

Lewis acid–base pairs, the present systems bind a very small amount of H_2 as compared to the mass of the FLP, so they are still quite inefficient for such use. On the other hand, they may be readily applicable as transition-metal-free hydrogenation catalysts, which possibility has indeed been demonstrated.

1.5 Catalytic Hydrogenation

Catalytic hydrogenations of unsaturated organic compounds constitute an important class of chemical transformations and find broad applications both in chemical industry and laboratory organic synthesis [223, 224]. The majority of hydrogenation reactions involve the direct use of H_2 as hydrogen source and they are catalyzed by transition metals. The role of metal centers and surrounding ligands in H_2 activation processes has been extensively studied for several decades and the details of homolytic and heterolytic H_2 splitting pathways are now well understood [225–233].

In the literature, several examples of transition-metal-free homogeneous catalytic hydrogenation involving H_2 have been reported, but these reactions usually require

rather drastic conditions [130–139]. A rare exception is a very recently discovered class of calcium-based catalysts, which operate at room temperature and moderate pressure (Figure 1.19) [140].

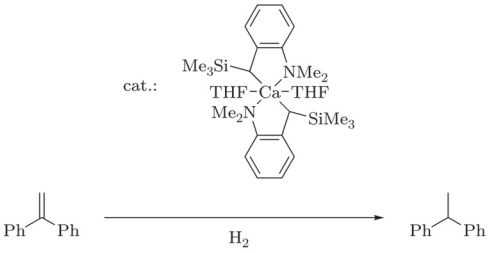

Figure 1.19: Example of a hydrogenation reaction catalyzed by a calcium complex [140]

Metal-free hydrogenation processes employing surrogates instead of H_2 have also been of interest. Main group hydrides are widely used reagents for reduction [9], and several procedures have also been described with the Hantzsch ester (Figure 1.20) [141–145], boron derivatives [146] or silicon compounds (Figure 1.21) [147–152] as hydride source.

A major breakthrough toward direct catalytic hydrogenation by non-transition-metals was achieved very recently by Stephan and coworkers by discovering that their phosphonium borate compound [$^+$HMes$_2$P–C$_6$F$_4$–**B**′H$^-$], which reversibly releases and binds H_2, also acts as a hydrogenation catalyst for imines, nitriles, and aziridines, and serves as a hydride source for the stoichiometric reduction of aldehydes [107]. Subsequently, numerous other frustrated Lewis pairs were also shown to exhibit similar reactivity, and the scope of substrates was extended to enamines and silyl enol ethers (see Figure 1.22) [86, 92–94, 102, 103, 105]. The catalytic reactions proceed at moderate conditions and catalyst loadings, but the substrates must be either bulky enough or protected by adduct formation in advance to avoid quenching of the catalytically active Lewis centers.

The experimental results also allow some conclusions about the mechanism to be drawn. The much higher rates of the reduction of electron-rich imines compared to electron-poor, e.g., sulfonated, ones by [$^+$HMes$_2$P–C$_6$F$_4$–**B**′H$^-$] indicate that this imine reduction is probably initiated by proton transfer from the phosphorus to the nitrogen atom [107]. This finding is also corroborated by the fact that [$^+$Cy$_3$P–C$_6$F$_4$–**B**′H$^-$] does not react with imines even on prolonged heating [107], and further supported by literature examples [145, 232]. The reduction is then supposed to be completed by a hydride transfer step.

In contrast, reduction of imines or nitriles protected as their **B** adducts necessarily begins with hydride transfer, as no basic site is present in the substrate [107]. As

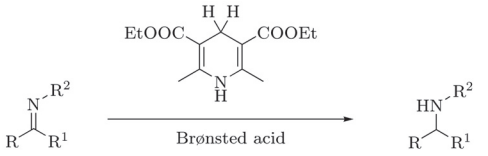

Figure 1.20: Hydrogenation via Hantzsch ester [141–145]

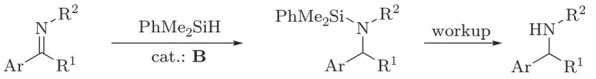

Figure 1.21: Imine hydrogenation using silanes [148]

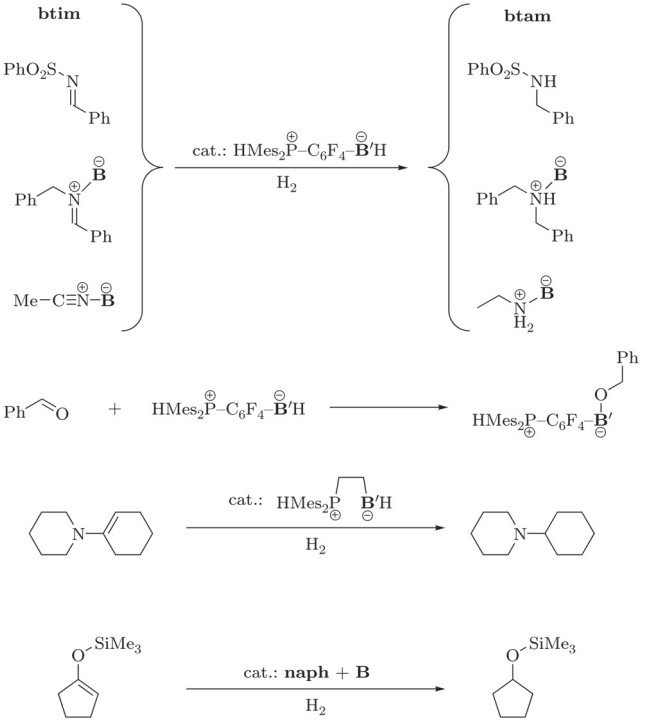

Figure 1.22: Examples of hydrogenation processes using FLPs [86, 105, 107]

mentioned, stoichiometric reduction of aldehydes only comprises a hydride transfer step, with the proton remaining on the phosphonium center.

As a further application of the FLP concept, Stephan's [90] and Klankermayer's [91] groups have independently showed that imines and aziridines can themselves act as the basic component of an FLP, and can therefore be hydrogenated using solely the Lewis acid **B** as catalyst (see Figure 1.23). Notably, Klankermayer et al. demonstrated the possibility of enantioselective hydrogenation in this context, using the chiral borane **pinB**, although only very modest enantioselectivity (13% *ee*) was achieved [91]. Catalytic imine hydrogenation was later also described with the bis-borane **naB** [100].

Experimental mechanistic studies by Stephan et al. on this reaction [90] allowed the formulation of a catalytic cycle (Figure 1.24a), which shares a number of features with the mechanism of the related **B**-catalyzed hydrosilylation reactions (Figure 1.24b, see also Figure 1.21) [148–150]. The reaction is thought to be initiated by the formation of an iminium borate ion pair as the result of hydrogen splitting, followed by hydride transfer yielding an amine–borane adduct. Thermal dissociation of this adduct delivers the amine and regenerates the free borane that can enter the cycle again.

1.6 Activation of Other Molecules

If one considers the number of research papers published by now, it is clearly the hydrogen activation reactivity that had the largest impact in FLP chemistry. However, FLPs also participate in a number of other uncommon reactions; in particular, they can react with a series of small molecules that are sometimes unreactive towards either component of the pair.

The ring opening of THF−borane adducts by the trityl anion was discovered rather early, and it has already been mentioned in Section 1.2, along with the recently observed analogous reactivity of phosphines. This reaction was later also described for other Lewis pairs (Figure 1.25) [95, 97–99, 108].

Addition of bulky Lewis pairs to olefins has long been known as well. In his 1966 review [26], Tochtermann cites that butadiene derivatives, which readily polimerize upon addition of Ph_3C^-, undergo a 1,2 or 1,4-addition reaction if BPh_3 (or its Al, Be, Mg analogues) is simultaneously present (Figure 1.26). Notably, 2,3-dimethylbutadiene also exhibits the addition reactivity, but it is inert towards Ph_3C^- alone.

Shortly after the discovery of hydrogen activation by phosphine–borane pairs, their addition to olefines was also reported [109, 110]. Intramolecular or intermolecular cleavage of the π-bond yields alkanediyl-linked phosphonium borates (Figure 1.26). Quite intriguing is the three-component reaction of the nonlinked phosphine–borane pair with ethylene or propylene, as these olefins do not react with either Lewis component [109]. The authors suggested that the reaction may be initiated by activation of the olefin by the borane, but no evidence for an interaction between them was observed, in disagreement with earlier low-temperature experiments with BF_3 [36] and related calculations for aluminum compounds [37]. As shown later,

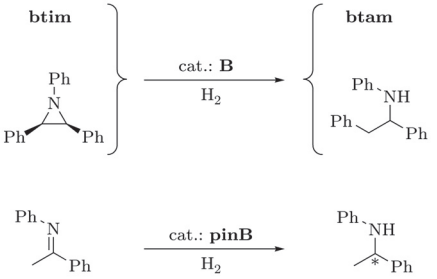

Figure 1.23: Lewis-acid-catalyzed hydrogenation [90, 91]

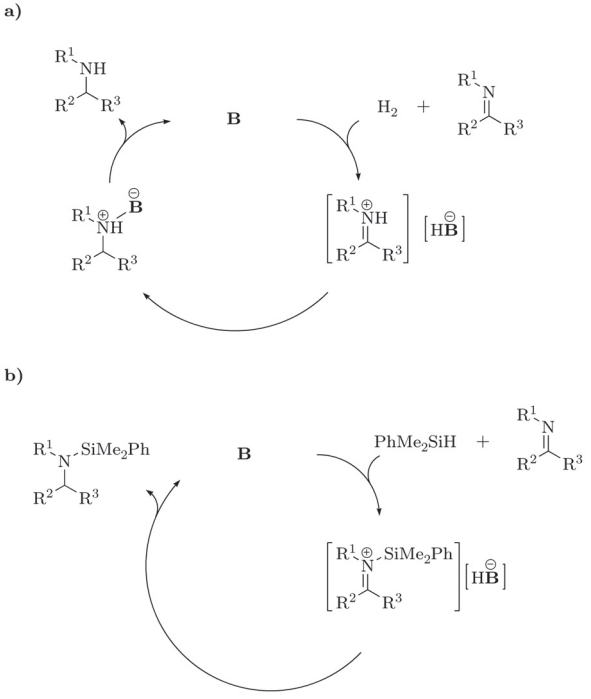

Figure 1.24: Mechanism of **B**-catalyzed reactions: imine hydrogenation (a) [90] and hydrosilylation (b) [148–150]

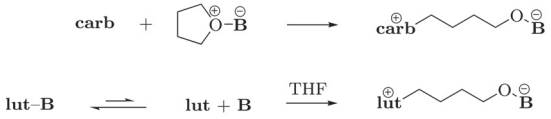

Figure 1.25: Examples of THF ring opening reactions [95, 97, 98]

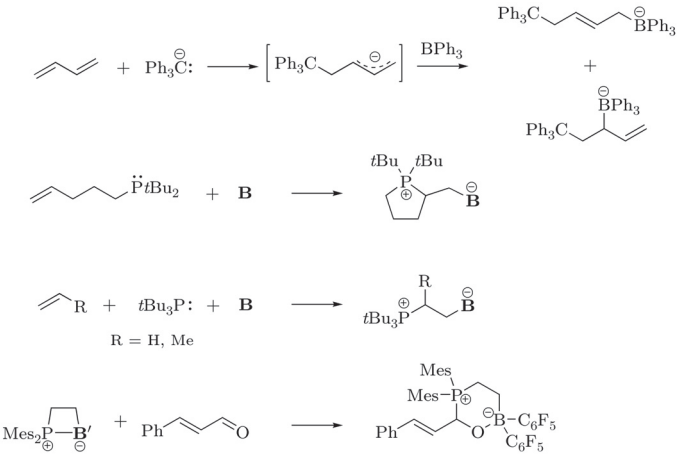

Figure 1.26: Addition of FLPs to double bonds [26, 109, 110]

phosphine–borane pairs react in analogous reactions with 1,3-dienes to give 1,4-addition products [111]. In contrast, α,β-unsaturated aldehydes exhibit 1,2-addition to the C=O group (Figure 1.26) [110].

Lewis pairs may show similar reactivity towards the π-bond of alkyne derivatives. Small yields of the corresponding addition product could be isolated when the highly unstable 1,2-didehydrobenzene was prepared in the presence of Ph_3P and BPh_3 (Figure 1.27) [38]. More recently, reactions of phosphine–borane and phosphine–alane D + A pairs with the stable phenylacetylene were reported [112]. The addition reaction was also shown to occur intramolecularly in triple-bond-containing D∼A systems, allowing simple preparation of π-conjugated molecules with unique electronic and photophysical properties [39]. As an alternative reaction pathway, phosphines may effect the deprotonation of terminal alkynes, leading to phosphonium alkynylborate or alkynylaluminate compounds (Figure 1.27) [110, 112].

An example of B−H bond activation using FLPs has been reported as well, leading to the isolation of a compound that can be formally characterized as the first oxygene-ligated borenium cation (Figure 1.28) [113]. Nevertheless, the cation is stabilized by electron donation from the phosphine, and its electron distribution is better described as a boryl phosphonium cation.

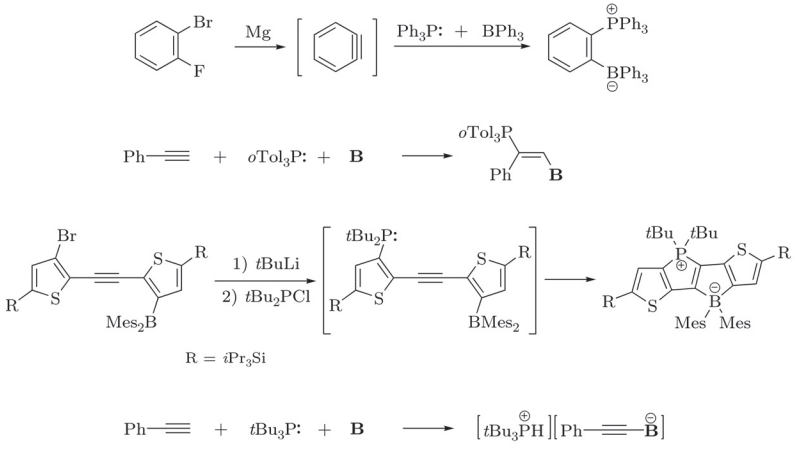

Figure 1.27: Reaction of FLPs with triple bonds [38, 39, 112]

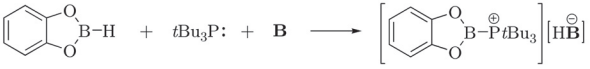

Figure 1.28: Synthesis of a stabilized borenium cation [113]

Sterically demanding carbene Lewis bases effect the deprotonation of various amine–$B(C_6F_5)_3$ adducts, which is in fact a heterolytic N−H bond activation [96]. For certain amines, this reaction yields neutral aminoboranes via pentafluorobenzene elimination; as expected, this pathway only requires catalytic amounts of the carbene (Figure 1.29). Under certain circumstances, carbene–borane pairs can also effect dehydrogenation of saturated C−C bonds (Figure 1.30) [99].

Despite its remarkable thermodynamic stability and limited reactivity, carbon dioxide readily reacts with FLPs in reversible reactions to form a novel type of carbonic acid derivative [114]. Last but not least, nitrous oxide forms addition compounds with phosphine–borane pairs featuring a P−N=N−O−B moiety (Figure 1.31) [115].

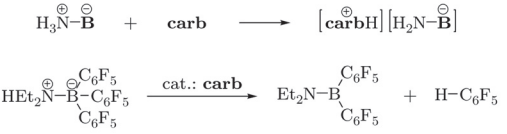

Figure 1.29: N−H activation by FLPs [96]

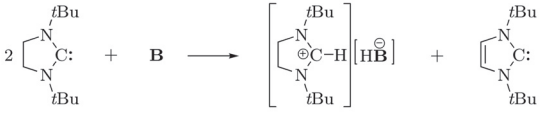

Figure 1.30: Self-dehydrogenation of a carbene–borane pair [99]

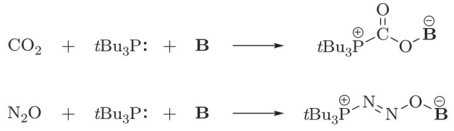

Figure 1.31: Reactions with carbon dioxide and nitrous oxide [114, 115]

1.7 Aims of the Present Work

Although developments in catalysis often proceed by trial and error, systematic approaches often lead more rapidly to success. For this purpose, however, detailed knowledge of the mechanism of these reactions is required. We thus initiated theoretical studies, which was at a time when only the first hydrogen/ethylene activation and catalytic hydrogenation studies were published. As more and more experimental works appeared in the literature, the number of questions theory could also raised. Our aims included:

- interpretation of the bond splitting reactivity, with particular emphasis on understanding why the seemingly termolecular reactions of nonlinked D + A pairs are as fast as observed;
- elucidation of the role and chemical significance of frustration;
- comparison of the hydrogen activation mode with other systems, including transition metals;
- analysis of the factors that render certain systems to be reactive towards hydrogen, and preclude others;
- identification of key intermediates and reaction pathways that form the basis of the catalytic hydrogenation processes.

In the subsequent chapter, the applied computational methodology is described. The detailed mechanism of bond activation of H_2 by the tBu$_3$P + **B** pair, and the role of frustration is discussed in Chapter 3. Applications of the model to other frustrated pairs as well as to ethylene activation are demonstrated in Chapter 4. Chapter 5 is devoted to the thermodynamics of the hydrogen activation, along with an assessment of the role of acid–base strength. Finally, mechanistic studies on catalytic hydrogenation are presented in Chapter 6. The dissertation ends with a short summary of the results, and an outlook towards possible future research and development.

The chemistry of frustrated pairs has been undergoing an active development during the time of my PhD work. In this period, several concurrent theoretical works or papers containing computational parts appeared, written by various research groups. These literature results are also briefly presented, mainly in Chapters 4 and 6, in order to provide the reader with a broader overview of the current theoretical understanding of FLP-type reactivity.

Chapter 2

Computational Methodology

2.1 General Considerations on Energetics

In spite of the enormous development of computational methods and computing capacity, realistic modelling of condensed phase reactions is still a demanding task. However, with an appropriate choice of methods and careful analysis of the results, meaningful interpretation of chemical phenomena is feasible for a wide range of systems.

Considering the characteristics of the reactions discussed here, and the available computational resources, we chose the approach of identifying stationary points (minima and transition states) on the zero kelvin gas phase Born–Oppenheimer potential energy surface (PES). After preliminary investigations on the first triplet excited states, we decided to investigate only the ground state PES.

Electronic structure methods that were used to locate the stationary points and to calculate energy differences on the PES include both density functional methods in the framework of the Kohn–Sham theory and wavefunction-based approaches. These methods are discussed in detail in the following sections.

For all intermediates and transition states (TSs), we carried out full geometry optimizations. The nature of the identified stationary points was confirmed by calculating the analytical second derivatives with respect to the nuclear coordinates. These results were also employed in determining zero-point energies and thermodynamic corrections in the ideal gas – rigid rotor – harmonic oscillator approximation [161]. The calculations were usually done for the standard temperature of $T = 298.15\,\mathrm{K}$, and a gas-phase concentration of $c = 1\,\mathrm{mol\,dm^{-3}}$, which corresponds to a pressure of $p = 24.46\,\mathrm{atm}$.

From the transition states, we initiated intrinsic reaction coordinate (IRC) calculations to identify the intermediates they connect. In the IRC approach, the minimum energy pathway from the TS to the related minima is followed in mass-weighted Cartesian coordinates [162]. These calculations usually failed to reach the appropriate minima, probably due to the exceptionally flat PES and the inaccuracies in the estimation of second derivatives. To locate the minima and to obtain a "pseudo-IRC" path for the reaction, we simply started geometry optimizations from the endpoints of the IRC calculations.

It is worth noting here that the size of the investigated molecules and the dominance of weak, nondirectional forces such as dispersion make the PES of most reactions not only flat, but also rather rugged, i.e., a series of close-lying stationary points can usually be identified. As these are not expected in our case to influence the chemical interpretation, exhaustive conformational searches have usually not been done.

In certain cases, the PES was mapped by carrying out relaxed scans. These were done by fixing a single geometrical variable at the desired values and allowing the remaining degrees of freedom to relax.

Experimentally, only apolar or moderately polar, aprotic solvents were used, which means that the participation of the solvent molecules in the reactions or specific solvation effects are not expected. We therefore decided to use continuum solvation methods for the determination of the solvent effect on the reactions. In the chosen

IEF-PCM method [163], the investigated species is put into a molecular-shaped cavity inside a homogeneous medium with a given permittivity, and the electrostatic energy associated with this process is calculated self-consistently. In addition, empirical terms for cavity formation, Pauli repulsion and dispersion between the solute and the solvent are also evaluated. The model provides solvation free energies in the Ben-Naim sense [164], and summing with the gas-phase free energies calculated for $c = 1\,\mathrm{mol\,dm^{-3}}$ allows solvent-phase free energies referring to this standard concentration to be determined.

In order to separate the various factors influencing the reaction mechanisms and thermodynamics, some of our calculations contain references to single ions solvated in apolar solvents, which are unlikely to be present under ordinary circumstances, but are easily accessible for calculations. Reference is made in particular to H^+, whose treatment requires the knowledge of its solvation free energy. Albeit none of our conclusions would be affected by an arbitrary choice of $\Delta G_{\mathrm{solv}}(H^+)$, we still attempted to obtain a meaningful value for it.

Due to its enormous polarizing power, the proton never remains "free" in the condensed phase, but attaches to other molecules [165]. Therefore, the solvation free energy of H^+ cannot be determined directly from continuum models; we employed the cluster-continuum approach instead, which treats some solvent molecules explicitly to grasp specific solvation effects, while the bulk solvent is described by a continuum approach [166, 167]. Details of the applied procedure are described in the Supporting Information of the respective publication [5].

Our computational approaches are certainly not expected to provide very accurate free energy data mostly due to the relatively large errors of the IEF-PCM solvent model [168] and the approximations employed in the calculation of gas-phase entropic contributions [169, 170]. However, in the present work, we wish to focus on the main characteristics of the mechanism, various trends in energetics and on the identification of the most important influencing factors. For these purposes we think the present approach is fairly adequate.

Throughout this dissertation, E denotes zero-point exclusive, gas-phase electronic energies, whereas G refers to solvent-phase Gibbs free energies.

2.2 Density Functional Methods

In this work, we carried out all geometry optimizations and frequency calculations, and also some of the single-point energy determinations, using Kohn–Sham density functional theory (DFT). Central element of this approach is a hypothetical system of noninteracting particles having the same electron density as the real molecule. This leads to a single-determinant description, with effective one-electron equations and orbitals. While this feature resembles Hartree–Fock theory, in principle, Kohn–Sham DFT can provide exact results, including electron correlation effects. However, the

exactness of Kohn–Sham theory hinges on the exchange–correlation (XC) functional, the exact form of which is not known.

A huge variety of approximate exchange–correlation functionals (or simply "functionals") have been developed, based on theoretical considerations on the functional form, and often also on parameter fitting to experimental data. The remarkable success of DFT is due to the suprisingly good accuracy provided by certain functionals with a computational cost comparable to Hartree–Fock theory or even smaller. Its major drawback, the impossibility of a systematic improvement towards the exact results, has not precluded it from becoming a valuable tool in the interpretation of chemical phenomena in relatively large systems.

One of the XC functionals employed in the present study is the widely used B3LYP, which was invented in 1994 [171–174]. Its remarkably good performance for various, structurally unrelated systems quickly led to its acceptance as a "black-box" method. However, B3LYP (and many other DFT methods in general) possess known weaknesses such as the absence of dispersion interactions as well as a tendency to underestimate the stability of larger molecules due to inappropriate treatment of medium-range correlation [175].

In spite of its disadvantages, we chose this functional for geometry optimizations at the beginning of our studies, as it yields reliable geometries for non-dispersion-dominated cases [176], and geometry optimization with significantly better performing functionals was not available in common software packages at that time. It is also noteworthy that together with double-ζ basis sets, partial error compensation might also be expected due to basis set superposition error [177, 178]. In order to obtain reliable energetics, we employed a more accurate ab initio method (SCS-MP2, see later) to calculate single-point energies on the B3LYP geometries, which is a common practice, e.g., in the Gaussian family of composite methods [179].

In the last few years, significant progress has been made in developing functionals for general usage by a wider community. The group of Donald G. Truhlar published the M05, M06 and M08 families of functionals, which are based on expressions fulfilling numerous exact constraints, with a large number (more than 20) of parameters fitted to experimental data [180–182]. These functionals provide not only excellent accuracy in general, but also reasonable energetics for dispersion interactions, at least around the equilibrium geometry of weakly bound complexes. Stefan Grimme and coworkers combined common functionals with an MP2-type perturbation expression of the Kohn–Sham orbitals and an empirical dispersion term, arriving at the B2PLYP-D and related functionals [183]. This approach again provides remarkable results, and even reproduces the correct asymptotic behavior of van der Waals forces, which is impossible solely with semilocal DFT functionals [184]. Several tests done by these authors confirm the superiority of the new functionals, and their applicability to problems that were not amenable to DFT treatment earlier. We also contributed to this area with a paper devoted to the assessment of functionals for the energetics and mechanism of conjugate addition reactions [185].

In the major part of our present work, we employed Truhlar's M05-2X functional [182], parametrized specifically for main-group compounds, in conjunction with a double-ζ basis set (6-31G* [186–190]) to optimize geometries. Relative electronic energies were either calculated with the same functional and a triple-ζ basis (6-311++G** [191–193]) or using the SCS-MP2 method.

An important question in practical DFT calculations is the choice of the appropriate integration grid for the computation of the XC contribution. Although efforts were made [182] to make the M05-2X functional free from a known singularity problem [194] shared by a series of related functionals, numerical errors of the integration can still cause convergency problems [195] or destroy the smoothness of the PES and make the calculation of derivatives, especially in flat regions, problematic [196]. We therefore used a relatively large ("ultrafine") grid consisting of 99 radial shells and 590 angular points per shell. However, similarly to Scuseria et al., we still identified problems in the calculation of the frequencies for the normal modes associated with the rotation of methyl substituents on aromatic rings [197]. Model calculations on a toluene molecule yielded imaginary frequency for the methyl rotation both in the minimum and the transition state of this motion. Significantly more demanding calculations on a larger grid (180 radial shells, 974 angular points) were found to adequately characterize the stationary points of toluene as minimum or first-order saddle point, which confirms that accurate determination of the curvature is hampered by the errors in numerical integration. However, considering that such calculations have enormous computational costs, and the effect on the calculated free energies is estimated to be only around $1\,\mathrm{kcal\,mol^{-1}}$, no further steps were taken to eliminate this error.

2.3 Ab Initio Methods

Conventional ab initio electron correlation methods provide a high and systematically improvable accuracy, but due to the unfavorable scaling property of their computational cost (usually at least with the fifth power of molecular size) and the need of large basis sets, they are hardly applicable for larger systems. However, various techniques, such as the local correlation methods [198] or the resolution-of-identity (RI) integral approximation [199–201] can significantly speed up such computations, without much compromise in accuracy. These algorithms are now implemented in various codes, allowing MP2 or sometimes even higher level calculations to be done routinely on systems with hundreds of atoms.

Considering that MP2 scales only with the fifth power with system size, it often provides an affordable, yet reasonably accurate solution. In 2003, Grimme proposed a method that significantly improves the performance of MP2 at practically zero additional computational cost [202]. The procedure is based on an empirical scaling of the parallel-spin and opposite-spin contributions of the MP2 correlation energy. The resulting method, called spin-component-scaled MP2 (SCS-MP2) is certainly not a pure ab initio method, as it contains two parameters determined in an empirical

way (nevertheless the method, and the values of the parameters do have theoretical motivation [202,203]). Later, a series of related methods were also published [204–206].

From a practical point of view, SCS-MP2 usually significantly outperforms MP2 (and earlier DFT methods like B3LYP as well), and often provides CCSD(T)-quality results without increasing computational costs with respect to MP2 [183]. We employed this method in the RI approximation with the cc-pVTZ basis set [207] to obtain reliable single-point electronic energies for the investigated species. Such calculations also served as a benchmark for energies calculated by DFT methods: we were pleased to find that the trends (and usually even the numerical values) obtained by M05-2X and SCS-MP2 agreed very well.

The SCS-MP2 calculations were done without any correction for the basis set superposition error (BSSE). The applicability of the usual correction schemes is limited to nonreactive systems [208], and for weak complexes, evidence was presented in the literature that the BSSE is well compensated by the one-electron basis set deficiencies in the SCS-MP2/cc-pVTZ combination [209]. The counterpoise-uncorrected values from this method were found to fall closer to the reference values than the corrected ones, and therefore, these are used throughout this dissertation.

2.4 Wave Function Analysis

Although the calculated energetics is of immense importance in determining which reaction pathways are feasible or preferred, it is as well important to provide a description of the mechanism and an explanation for the obtained numbers in terms of chemical concepts. The analysis of the wave function can reveal various interesting features of the electronic structure, which are essential for a complete mechanistic understanding [161].

A Hartree–Fock or Kohn–Sham calculation at convergence yields a single determinant wavefunction composed of the canonical molecular orbitals. Simple perturbation theory arguments indicate that in absence of strongly charged fragments and radicals, chemical reactivity is mainly determined by the interaction of the highest (doubly) occupied and lowest unoccupied molecular orbitals (HOMOs and LUMOs) of the reactants [8]. Inspecting the HOMO and the LUMO of a molecule can thus reveal affinity and sites for electron pair donation and acceptance, i.e., for Lewis basicity and acidity.

On the other hand, canonical molecular orbitals are delocalized over the entire molecule, and the electron density at a certain point usually stems from many MOs. This picture thus does not reflect our view of the electrons forming bonds and lone pairs. Furthermore, chemically analogous molecules such as homologous series of organic compounds have quite different canonical MOs, which means that functional groups and bonding properties are not readily identified. Appropriate methods that allow the bonding structure from the wavefunction to be determined are therefore necessary.

2.4.1 Bond Order Calculations

The concept of valence and bond order has long been of importance in chemistry [210]. Considering a simple MO picture of homonuclear diatomics, bond order can be identified with the half of the difference between the numbers of bonding and antibonding electrons, i.e., electrons on MOs constructed from bonding or antibonding overlaps of the atomic orbitals. However, the interpretation of this definition in polyatomic molecules is neither straightforward nor unambigous.

The first quantity which can be directly related to the classical bond order yet computable from the wavefunction was proposed by Wiberg [211]. Writing the first-order density matrix in an orthogonal atomic orbital (AO) basis, the Wiberg bond index between atoms A and B is determined as the sum of the squared absolute values of the off-diagonal density matrix elements corresponding to overlaps between orbitals on A and B. The generalization of this scheme to the commonly encountered case of nonorthogonal AOs was done by Mayer [212].

Mayer bond orders were applied in the present work to analyze bond formation and bond breaking along reaction pathways, and to determine whether these occur synchronously.

2.4.2 Natural Orbital Methods for the Description of Electronic Structure

Natural orbitals (NOs) for any wave function are the orbitals that diagonalize the first-order density matrix. The NOs with large occupancies (eigenvalues) provide a compact representation of the electron density associated with the wavefunction.* Weinhold and coworkers developed a methodology to apply this concept for the distribution of electrons into atomic and bonding contributions [213].

In the natural atomic orbital (NAO) analysis, eigenvectors of the diagonal *blocks* of the density matrix belonging to the individual atomic centers are first determined. These orbitals are then orthogonalized in a manner that preserves the form of the strongly occupied orbitals as much as possible (via an occupancy-weighted symmetric orthogonalization). The resulting orthogonal orbitals are called NAOs. The highly occupied NAOs provide a compact description of the wave function in terms of *atomic* orbitals.

In order to determine atomic charges, a population analysis using NAOs (natural population analysis, NPA) can be done. This procedure has many advantages, e.g., over the Mulliken scheme. In particular, natural charges converge to well-defined values as the basis set is improved, and agree well with other experimental or theoretical measures of charge distribution.

*The natural orbitals of single determinant wavefunctions are not uniquely defined. The density matrix is diagonal when represented in any set of orbitals obtainable from the canonical MOs with separate unitary transformations of the occupied and virtual subsets.

As the following step of the method, natural bond orbitals (NBOs) are determined. NAOs with large occupancies (say > 1.9) are identified as core and lone pair orbitals, and their contributions are removed from the density matrix. Each pair of atoms is then considered, and the corresponding two-by-two blocks of the density matrix are diagonalized. Bonding NBOs are identified as eigenvectors with large occupancies (say > 1.9). The remaining low-occupancy orbitals are the antibonding or Rydberg orbitals. The strongly occupied (core, lone pair, and bonding) NBOs constitute a "natural Lewis structure" of the molecule, while the occupancy of the antibonding and Rydberg orbitals is the sign for the deviations from this idealized Lewis picture.

In the NBO basis, the density matrix is partitioned into a block associated with the strongly occupied NBOs of the natural Lewis structure, and a block corresponding to the weakly occupied NBOs. The off-diagonal elements between these blocks represent the mixing of the filled and unfilled orbitals, carrying information about the chemically important delocalization effects, i.e., the partial breakdown of the Lewis picture.

2.4.3 Localized Orbitals

The single-determinant wavefunction is invariant to any unitary transformation among the occupied orbitals it is composed of. We can thus freely choose an appropriately transformed set of the canonical occupied MOs, which better suits our purposes. Localization is a procedure which provides MOs that are confined to a relatively small volume, with the goal of displaying the bonding structure and identifying transferable structural units of the molecule [161].

As no single criteria of "locality" exist, an arbitrary number of localization schemes can be defined. These procedures often start from the canonical MOs, and apply some iterative optimization method to find the extremum of an appropriately chosen quantity describing the compactness of the orbitals.

In contrast, the above discussed NBO analysis provides a very efficient and advantageous way of defining localized orbitals. Instead of localizing canonical MOs, this procedure is based on adding "delocalization tails" to the occupied NBOs. Namely, appropriate unitary transformations on the NBO orbitals are applied that sequentially zero all off-diagonal elements between the strongly and weakly occupied blocks of the density matrix. In case of a single-determinant wavefunction, this procedure yields a completely diagonalized density matrix, with orbital occupations of 0 or 2. The resulting orbitals are called the natural localized molecular orbitals (NLMOs) [214].

Due to their roots in NBO analysis, the occupied NLMOs reflect the Lewis structure of the molecule, and the appearing delocalization tails can be directly related to the resonance effects, representing departures from the strictly localized Lewis picture. Such effects can even be assessed quantitatively by inspecting the NBO contributions to each NLMO [214]. In the present work, we applied NLMO analysis to visualize weak electron donation effects as well as bond formation and breaking processes.

2.5 Applied Software Packages

Various softwares were employed to obtain the results discussed in this dissertation. The Gaussian 03 package (releases B.05 and E.01) [216] was used for electronic structure calculations with DFT methods, geometry optimizations, as well as for computation of frequencies, thermodynamic corrections, and solvation free energies. Single point SCS-MP2 calculations were carried out with the Turbomole program (versions 5.9.1 and 5.10) [217]. Version 3.1 of the NBO package, bundled as part of Gaussian, was utilized for NPA and NLMO analyses. Mayer bond orders were determined using the BORDER 1.0 program [218].

Initial geometries for the computations were created, the resulting structures were inspected and further edited with Molden 4.6 [219]. Visualization of molecules, electron densities and orbitals was carried out using Molekel 4.3 [220].

Chapter 3

Turning Frustration into Bond Activation: Basic Concepts

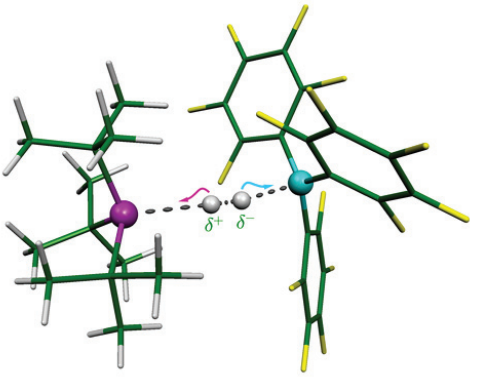

3.1 Introduction

We initiated our theoretical studies with the aim of gaining mechanistic insight into the intriguing bond activation reaction by FLPs. At that time, no computational results were available in the literature, and the reported experimental findings only referred to linked and nonlinked phosphine–borane pairs. We therefore began our investigations with the prototypical $t\mathrm{Bu_3P}$ + $\mathrm{B(C_6F_5)_3}$ + $\mathrm{H_2}$ system.

The model that emerged from our calculations was able to interpret the observed reactivity, and also highlighted important properties of frustrated pairs that render it feasible. The present chapter is devoted to the introduction of this model, and to the formulation of the key concepts that expand and clarify the meaning of "frustration".

3.2 Experimental Results on the $t\mathrm{Bu_3P}$ + B Pair

As noted in the introduction, Welch and Stephan carried out several experiments to explore the reactivity of nonlinked phosphine–borane pairs [83]. The reported NMR measurements at 25 °C and at −50 °C on the toluene solution of a stoichiometric mixture of the $t\mathrm{Bu_3P}$ + **B** pair showed no evidence of the formation of dative bonds. However, the exposure of the solution to $\mathrm{H_2}$ at 1 atm pressure and 25 °C temperature resulted in the formation of a white precipitate, which was isolated and identified to be a salt with the formula $[(t\mathrm{Bu})_3\mathrm{PH}]^+[\mathbf{HB}]^-$ (see Figure 3.1).

To interpret these results, the authors outlined two possible stepwise reaction mechanisms [83]. One pathway was assumed to begin with the side-on interaction of $\mathrm{H_2}$ with **B**, which bears some analogy to transition metal chemistry. The fact that weak $(\eta^2\text{-}\mathrm{H_2})\mathrm{BH_3}$ complexes were characterized theoretically [32–34] and in matrix isolation studies [35] clearly supports this hypothesis. Interaction with **B** is thought to induce polarization of the $\mathrm{H_2}$ molecule [83], the positive end of which is then attacked by the phosphine (Figure 3.1). Nevertheless, Stephan et al. did not observe any interaction between $\mathrm{H_2}$ and **B** by NMR spectroscopy at temperatures as low as 190 K.

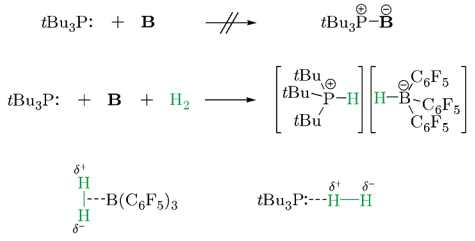

Figure 3.1: Experimental results on the reactivity of the $t\mathrm{Bu_3P}$ + **B** pair and the proposed intermediates [83]

As another possibility, the end-on interaction of H_2 with tBu$_3$P was outlined. Assuming lone-pair donation to the σ^* orbital of H_2, this reacion route could also produce a polarized hydrogen molecule, whose more negative atom can then be attacked by the borane (Figure 3.1). Interactions of Lewis bases and H_2 were indeed observed experimentally in argon or neon matrices, as well as analyzed theoretically, but they were only found to be of very weak, van der Waals nature [31, 40].

3.3 Possible Reaction Pathways*

3.3.1 Binary Interactions

In order to unravel the mechanism, we first explored the proposed $H_2\cdots$**B** and (tBu)$_3$P$\cdots H_2$ interactions by deriving potential energy curves with respect to X$\cdots$H distances (d_{XH}, X = B and P). Relaxed PES scans at the B3LYP/6-31G* level, followed by single-point energy calculations with the SCS-MP2/cc-pVTZ method yielded the results shown in Figure 3.2. It is apparent from the figure that both side-on and end-on approaches of H_2 to **B** are unfavorable due to Pauli repulsion. This is somewhat in contrast to previous studies that pointed toward the existence of a weakly bound $H_2\cdots BH_3$ complex, and prompted a closer investigation.

In line with the previous results, we were also able to identify the (η^2-H_2)BH_3 complex on the B3LYP/6-31G* PES. The calculated SCS-MP2/cc-pVTZ binding energy is $-2.5\,\mathrm{kcal\,mol^{-1}}$. However, our analysis revealed that the π system of the aromatic substituents in **B** exhibits an appreciable electron delocalization to the originally empty boron p orbital (see Figure 3.3), which limits the stabilizing donation of σ electrons of H_2. The repulsive potential energy curves obtained in our calculations are in agreement with experimental observations of Stephan et al. that $H_2\cdots$**B** adducts are unstable even at low temperatures.

As seen from Figure 3.2, the interaction between H_2 and tBu$_3$P is also found to be repulsive for the chemically relevant d_{PH} range. These results firmly suggest that other reaction channels should be considered to provide a rationale for the reactivity of the tBu$_3$P + **B** pair with hydrogen.

3.3.2 Weak Association of the Frustrated Pair

The reported hydrogen splitting reaction proved to be rather facile, which can hardly be explained in terms of a termolecular collision between the reactants. Although not observed by NMR experiments, we envisioned that secondary interactions may lead to weak association between the molecules of a nonlinked frustrated D + A pair. This idea is supported by recent quantum chemical calculations carried out for a series of classical phosphine–borane Lewis adducts [19], which revealed considerable contribution of dispersion interactions to the overall binding energy (see Figure 1.2 on page 3).

*This section is based on our results published in paper [1].

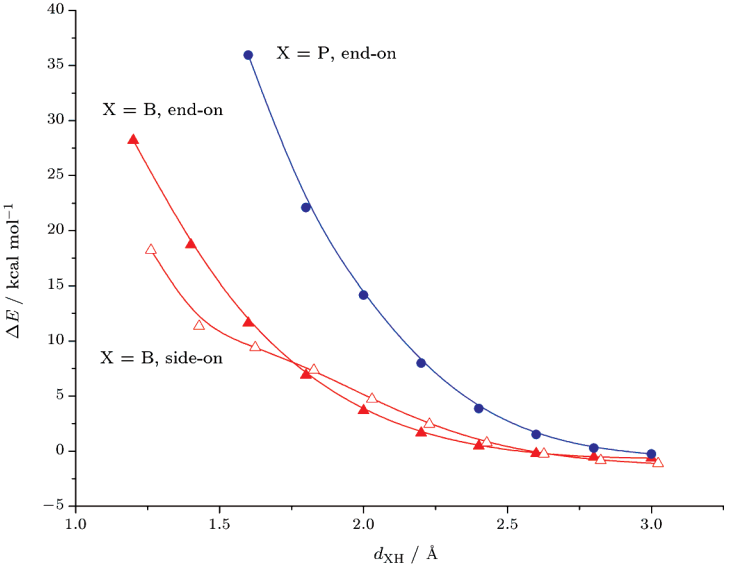

Figure 3.2: Interaction energy of H_2 with tBu$_3$P (blue dots) and **B** (red triangles) as a function of X···H distance

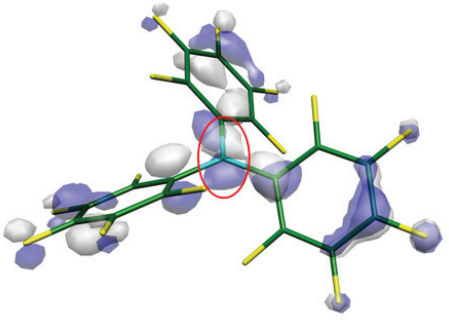

Figure 3.3: An occupied canonical MO of **B**, showing delocalization of electrons onto the boron p orbital (marked in red)

Keeping in mind that B3LYP performs poorly for the description of weak interactions, we explored the PES of this binary intearction by carrying out constrained B3LYP/6-31G* geometry optimizations at various fixed P···B distances, followed by single-point SCS-MP2/cc-pVTZ calculations. On the resulting potential energy curve (shown in Figure 3.4), a weakly bound tBu$_3$P···**B** complex (referred to as a "frustrated complex") can be clearly identified around $d_{PB} = 4.2$ Å (Figure 3.5). Noteworthily, a bound minimum also exists on the B3LYP/6-31G* PES at a slightly larger d_{PB} of 4.46 Å.

The bonding in this D···A adduct can be characterized as a combination of multiple C−H···F hydrogen bonds and dispersion interactions. The central BC_3 unit in **B** remains planar, indicating the absence of electron transfer. The association energy is predicted to be $\Delta E = -11.5\,\text{kcal mol}^{-1}$, which is about the half of the interaction energy found for strained classical Lewis adducts [19]. In order to assess the role of C−H···F interactions, similar calculations were also carried out for the tBu$_3$P···BPh$_3$ complex, which yielded a binding energy of $-8.5\,\text{kcal mol}^{-1}$. This underlines the importance of such interactions, but also indicates that their presence is not a prerequisite in the formation of frustrated complexes.

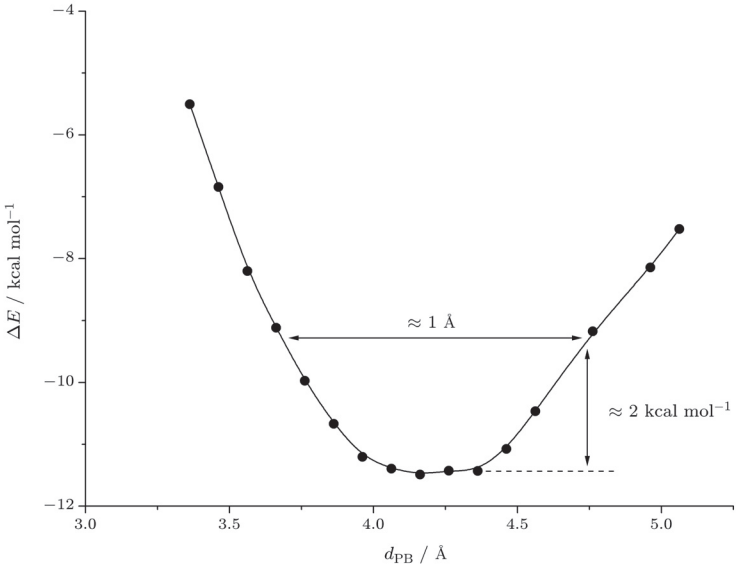

Figure 3.4: Interaction energy of tBu$_3$P and **B** as a function of the P···B distance

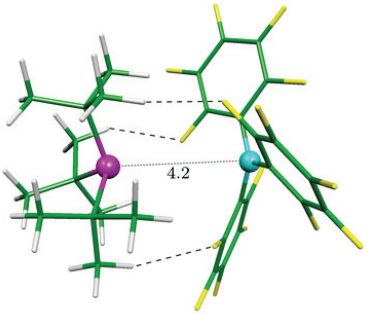

Figure 3.5: Structure of the frustrated $t\mathrm{Bu_3P}\cdots\mathbf{B}$ complex. C−H···F-type hydrogen bonds (with $d_{\mathrm{HF}} < 2.4\,\text{Å}$) are indicated with dashed lines. Distance is given in ångströms.

Although the exothermicity of binding is likely overcompensated by entropy loss, the surprisingly large stabilization energies suggest a certain degree of association even at room temperature. The absence of spectroscopic evidence for such association can presumably be attributed to the noncovalent nature of the bonding and to the low concentration of the adduct. Interestingly, the solution of a related pair, the $\mathrm{Mes_3P}$ + **B** mixture was observed to have a violet color [83], which was attributed by the authors to π-stacking of the electron-rich and electron-poor arene rings, pointing to some degree of intermolecular interaction.*

An important characteristic feature of the $t\mathrm{Bu_3P}\cdots\mathbf{B}$ complex is its structural flexibility, which stems from the dominance of weak non-directional long-range forces. As demonstrated in Figure 3.4, the P−B distance can be varied in a quite broad range at only a small energetic cost.

3.3.3 Stationary Points of the Reaction

Considering the flexible nature of the frustrated complex and the small size of the H_2 molecule, one expects that H_2 can easily reach the vicinity of the P···B axis of the adduct. In this way, a simultaneous interaction with both active centers of the phosphine–borane pair may be feasible, which is likely to be more favorable than the interactions with the separated centers step-by-step.

The potential energy surface of $t\mathrm{Bu_3P}$ + **B** + H_2 has been explored in this region, and we have indeed located a low-lying transition state ($\mathbf{TS}_{\mathrm{PB}}$) associated with the H−H bond cleavage (see the structure and the corresponding SCS-MP2/cc-pVTZ//B3LYP/6-31G* energy diagram in Figures 3.6 and 3.7, respectively). In the

*The research group of Repo and Rieger later presented NMR evidence of intermolecular N−H···F hydrogen bonding in the **tmp** + **B** FLP [93].

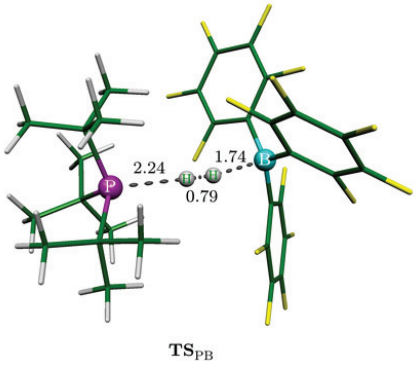

Figure 3.6: Transition state of hydrogen splitting by the tBu$_3$P + **B** pair

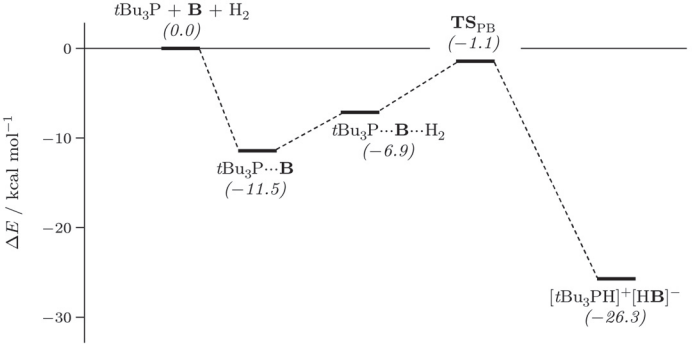

Figure 3.7: Electronic energy profile of the hydrogen splitting process by the tBu$_3$P + **B** pair, calculated at the SCS-MP2/cc-pVTZ//B3LYP/6-31G* level of theory

transition structure, the H_2 molecule is nearly aligned with the P···B axis, interacts with both active centers, and it is only slightly elongated suggesting an early TS for H−H bond cleavage. It is also worth noting that most C−H···F and van der Waals contacts between the phosphine and borane molecules are maintained in the TS.

On the reactant side of this TS, a weak ternary complex tBu$_3$P···**B**···H$_2$ can be identified, in which the hydrogen is bound by secondary forces to an open form of the tBu$_3$P···**B** frustrated complex (Figure 3.8a). Although this ternary complex lies somewhat above tBu$_3$P···**B** + H_2 in energy (Figure 3.7), PES scans indicate that no significant further barrier hinders its formation.

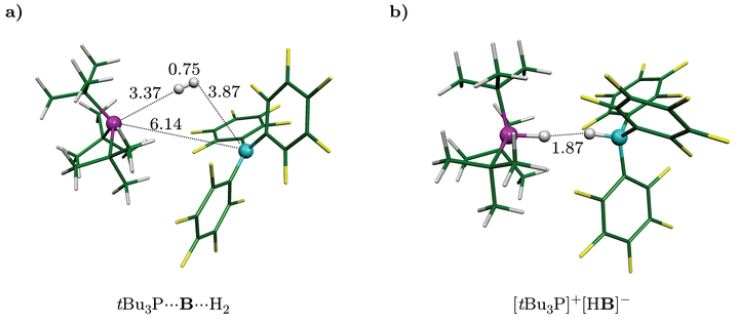

Figure 3.8: Energy minima associated with the TS of the hydrogen splitting process: weak ternary complex on the reactant side (a), phosphonium hydridoborate ion pair on the product side (b)

Following the reaction coordinate in the other direction, one obtains the $[t\text{Bu}_3\text{PH}]^+[\text{HB}]^-$ product with a notable gain in energy. The optimized structure of the product (Figure 3.8b) is consistent with experimental X-ray data [83], and indicates that mainly Coulombic attraction and a dihydrogen bond hold the ion pair together, but van der Waals forces also contribute to the binding.

3.4 Electronic Structure Analysis*

Not only do quantum chemical methods allow energetics and PESs to be calculated, but they also provide a manner to understand the electronic reorganizations that drive the reactions. In this section, we present an analysis of the hydrogen splitting process by FLPs from an electronic structure viewpoint. The $t\text{Bu}_3\text{P}$ + **B** pair, discussed above, is examined based on the M05-2X/6-31G* wavefunction.

3.4.1 Reactants

To understand the reorganization of electrons in the TS, it might be useful to start with the characterization of the reacting partners. The basic nature of the trigonal pyramidal phosphorus atom in $t\text{Bu}_3\text{P}$ is clearly borne out by the properties of the highest occupied molecular orbital (HOMO), which lies relatively high in energy, and can be described as an sp^3-type lone pair on the P atom (see Figure 3.9a).

Similarly, the lowest unoccupied molecular orbital (LUMO) of the borane molecule, having low energy and composed mainly of the empty boron p orbital, clearly indicates the affinity for electron pair acceptance on the trigonal planar boron atom (Figure 3.9b).

*The analysis presented here is based on our results published in paper [2].

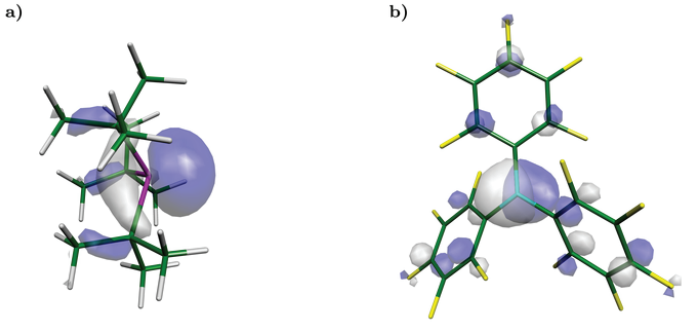

Figure 3.9: Frontier orbitals of the reactants: HOMO of tBu$_3$P (a) and LUMO of **B** (b)

In contrast, the hydrogen molecule has low-lying, compact occupied σ(H−H) and high-energy unoccupied σ^*(H−H) orbitals, and it is apolar. These properties make it a poor Lewis acid or base, and provide the rationale for its known low reactivity.

3.4.2 Binary Interactions with Hydrogen

Although the end-on interactions of H_2 with either component of the Lewis pair were found to be repulsive, their examination can yield useful insight into the ternary reaction, so first we shall start with the analysis of tBu$_3$P···H$_2$ and H$_2$···**B** interactions.

Figure 3.10 shows how a tBu$_3$P or a **B** molecule alone deforms the electron density of H_2 at the TS geometry. Notably, both binary interactions lead to the polarization

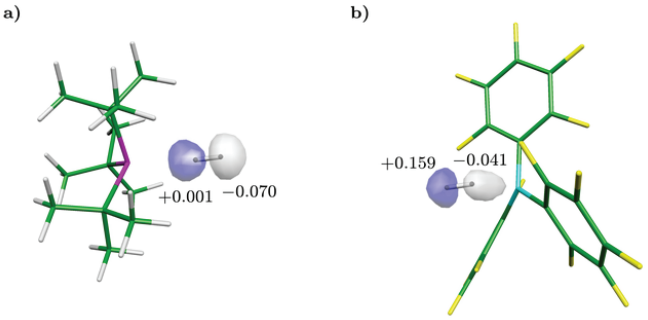

Figure 3.10: Calculated electron density differences of the tBu$_3$P + H$_2$ (a) and H$_2$ + **B** (b) systems at the TS geometry. Gray and blue surfaces (obtained with a cutoff of ±0.0025 au) indicate the electron density gain and loss as compared to the isolated components in the TS geometry. Numbers indicate NPA charges on the corresponding hydrogen atoms.

of H_2, and their most striking feature is the same polarization pattern (with respect to the P···H−H···B direction). The magnitude of the effect is also comparable in the two cases.

The polarization can be interpreted as a mixing of the original HOMO (σ) and LUMO (σ^*) orbitals of the H_2 molecule resulting in an asymmetric charge distribution along the molecular axis as indicated in Figure 3.11. This implies a certain degree of destabilization for the occupied orbital and stabilization for the unoccupied level of the molecule. As a consequence, an asymmetric, amphoteric H_2 species develops, which has spatially separated, enhanced Lewis acidic and basic characters as compared to the free H_2. In both cases, the interacting Lewis site induces the opposite Lewis property at the closer end of the H_2 molecule, in order to reduce the repulsion between the molecules. In turn, the opposite end of the H_2 molecule obtains the same Lewis function as the interacting Lewis center. This fact can be clearly seen from Figure 3.12, which shows the frontier orbitals of the binary systems. The HOMO of the phosphine + H_2 fragment has a significant contribution from the distal H atom, and its orbital energy differs only by +0.015 au from the HOMO of the free phosphine in its relaxed geometry (see Table 3.1). Accordingly, the LUMO of the H_2 + borane system extends onto the H atom opposite to B, and the orbital energy difference with respect to the free borane is only +0.006 au. The H_2 molecule, which itself is a poor Lewis acid and base, "relays" the interacting Lewis property.

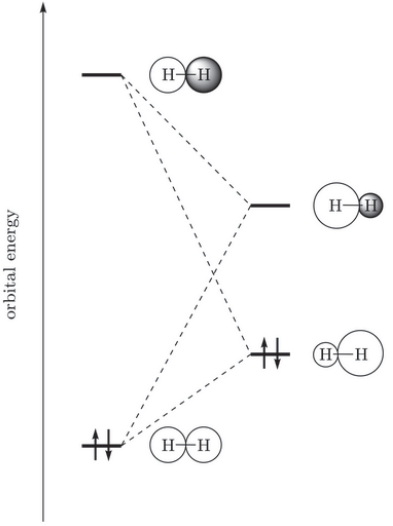

Figure 3.11: Schematic diagram showing the deformation of the orbitals of an H_2 molecule as a result of mixing the HOMO and LUMO

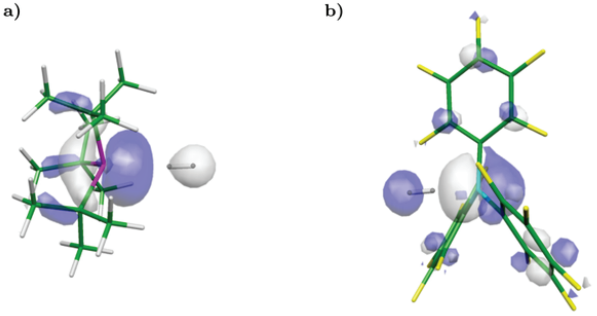

Figure 3.12: HOMO of the phosphine + H_2 fragment (a) and LUMO of the H_2 + borane fragment (b) at the TS geometry

Structure	ϵ_{HOMO}	ϵ_{LUMO}
tBu$_3$P	−0.250	
B		−0.087
tBu$_3$P + H_2 (TS geometry)	−0.235	
H_2 + **B** (TS geometry)		−0.081
H_2	−0.503	0.113
tBu$_3$P···**B**	−0.258	−0.081

Table 3.1: Calculated frontier orbital energies (in atomic units) of some species

3.4.3 Frontier Orbitals of the Frustrated Complex

Classical, sterically not hindered Lewis acids and bases react with each other by forming a D−A dative bond. The exothermicity of the process is related to the favorable mixing between the original HOMO of the Lewis base and the LUMO of the Lewis acid, which is depicted schematically in Figure 3.13a. In contrast, the principal motif of frustration is the unquenched nature of the Lewis acid and base. In the frustrated D···A complex, the components are in close vicinity without chemical reaction, as the orbital overlap is hindered by the large distance between the donor and acceptor centers, and the frustrated complex is expected to inherit its HOMO and LUMO from the free base and acid molecules, respectively (see Figure 3.13b).

The calculated HOMO and LUMO of the tBu$_3$P···**B** frustrated complex are shown in Figure 3.14. Their shapes perfectly correspond to the orbitals of the isolated components (see Figure 3.9), and the orbital energies are also hardly altered: the orbital energy changes of the HOMO and LUMO upon complexation are only −0.008 au and +0.006 au, respectively (Table 3.1).

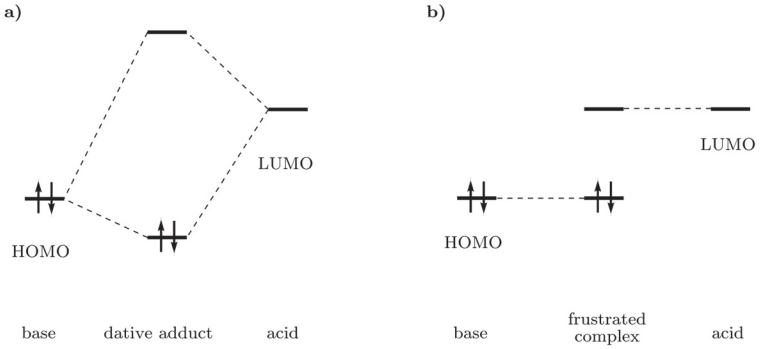

Figure 3.13: Orbital interactions upon the formation of classical Lewis adducts (a) and frustrated complexes (b)

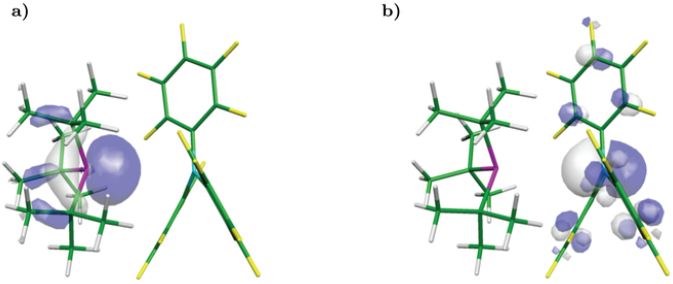

Figure 3.14: Frontier orbitals of the tBu$_3$P···**B** frustrated complex: HOMO (a) and LUMO (b)

These features clearly show that the steric congestion of the FLP members prevents the frontier orbitals of the acid and base to efficiently overlap for dative bond formation. On the other hand, secondary forces acting between the substituents stabilize a geometry in which both orbitals are perfectly aligned for a simultaneous interaction with the H_2 molecule. The complex formation not only brings the Lewis partners close together, but also implies a remarkable preorganization of the HOMO and the LUMO of the components to form a "reactive pocket", which is the active site of the frustrated complex and the key to the unique reactivity.

3.4.4 Ternary Interactions and the Splitting Process

In the reactive, ternary system, the H_2 molecule simultaneously interacts with both the Lewis acidic and basic centers of the frustrated complex. Both sites induce polarization on H_2 in the same direction, which thus leads to reduced repulsion on both sides of the molecule, and to a shift of electron density in the P→B direction. This partial electron transfer can be identified clearly on the electron density difference map, and it is also corroborated by the population analysis (Figure 3.15). The pyramidal distortion of the borane and the large absolute value of the computed dipole moment vector ($\mu = 5.1\,\mathrm{D}$) provide further support for this observation.

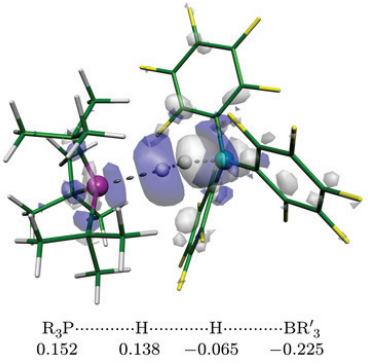

Figure 3.15: Electron density difference map of $\mathbf{TS}_{\mathrm{PB}}$. Gray and blue surfaces (obtained with a cutoff of ±0.001 au) indicate the electron density gain and loss as compared to the isolated $t\mathrm{Bu_3P}\cdots\mathbf{B}$ and H_2 components, frozen in the TS geometry. Numbers indicate NPA charges on the corresponding hydrogen atoms or fragments.

Considering the structure of the reactants as well as the properties of the binary interactions it can be concluded that the electron transfer process in the TS is made possible by the H_2 molecule acting as a bridge between the phosphine and borane fragments and thus ensuring favorable orbital overlaps. Due to the structural flexibility of the frustrated complex, the activation energy is dominated by the work required to create this bridge. Indeed, the interaction energy of the frozen phosphine and borane fragments in the TS geometry (without H_2) amounts to $-10.7\,\mathrm{kcal\,mol^{-1}}$, which is only slightly less than the binding energy of the frustrated complex with respect to the relaxed reactants ($-13.1\,\mathrm{kcal\,mol^{-1}}$ at the present level of theory). The activation energy ($7.4\,\mathrm{kcal\,mol^{-1}}$ with respect to $t\mathrm{Bu_3P}\cdots\mathbf{B} + H_2$) is mainly required to distort the geometry of the phosphine, borane and H_2 and to overcome the repulsion between H_2 and $t\mathrm{Bu_3P}\cdots\mathbf{B}$.

Inside the frustrated complex, the H_2 molecule participates in two concerted Lewis acid–base reactions, allowing the electron transfer to occur via simultaneous

$t\mathrm{Bu_3P} \rightarrow \sigma^*(\mathrm{H_2})$ and $\sigma(\mathrm{H_2}) \rightarrow \mathbf{B}$ donations in a push–pull manner (Figure 3.16). These donations lead to progressive weakening of the H−H bond along the reaction pathway, and, ultimately, to bond cleavage and to the formation of two new covalent bonds (P−H and H−B). This process can be clearly seen from the evolution of the two natural localized molecular orbitals having the largest contribution from the H atoms. At the early transition state, these correspond to the σ(H−H) orbital, and to the lone pair on the phosphorous atom, denoted as n(P) (Figure 3.17a). A closer look at their shape reveals that the σ(H−H) orbital involves contributions from the p orbital on the B atom, while the n(P) lone pair also has a slight σ^*(H−H) antibonding character. These chemically relevant delocalization tails of the localized MOs are obvious signs of the electron donations mentioned above. During the reaction, these orbitals are gradually transformed into two new σ-type bonding orbitals, as illustrated by Figures 3.17b and 3.17c.

The progress of formation of the new dative bonds as well as the cleavage of the H−H bond can be traced by calculating Mayer bond orders along the pseudo-IRC of the reaction. The results for the P−H, H−B and H−H bonds (shown in Figure 3.18) clearly demonstrate the remarkably parallel formation of the P−H and H−B bonds, i.e., the synchronous nature of the process.

3.5 The Notion of Frustration*

It might be useful at this point to highlight the key features of frustrated pairs, i.e., the nature and the role of frustration that allow their remarkable reactions to take place.

From our computational studies on the $t\mathrm{Bu_3P}$ + **B** pair, we proposed a general mechanistic model that involves the intermolecular association of the nonlinked Lewis acidic and basic components to a "frustrated complex", with an arrangement similar to a classical Lewis donor–acceptor adduct, but having a much looser structure. This flexibility provides a range of optimal acid–base distances for bifunctional cooperativity. The synergistic interaction of $\mathrm{H_2}$ with both centers of this *preorganized ambiphilic system* can lead to its cleavage in a bimolecular, low-barrier process.

In our terminology frustration not only refers to steric effects, but also implies a strain, which can be utilized for bond activation. As compared to a hypothetical classical Lewis pair having the same intrinsic acid–base properties, the *reactant state* of the frustrated system is significantly *destabilized* due to the absence of the dative bond. This destabilization lowers the activation barrier and increases the exothermicity of the overall process.

The noncovalent forces, which act between the bulky substituents, play a crucial role here. By allowing frustrated complex formation, they render the cooperativity of the Lewis centers possible. They also provide additional stabilization for the transition state and for the product ion pair as well.

*This discussion was published as part of our paper [1].

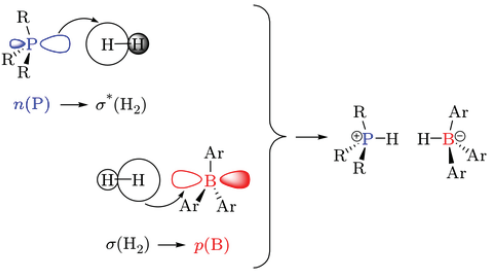

Figure 3.16: Schematic picture of electron donations leading to H−H bond cleavage

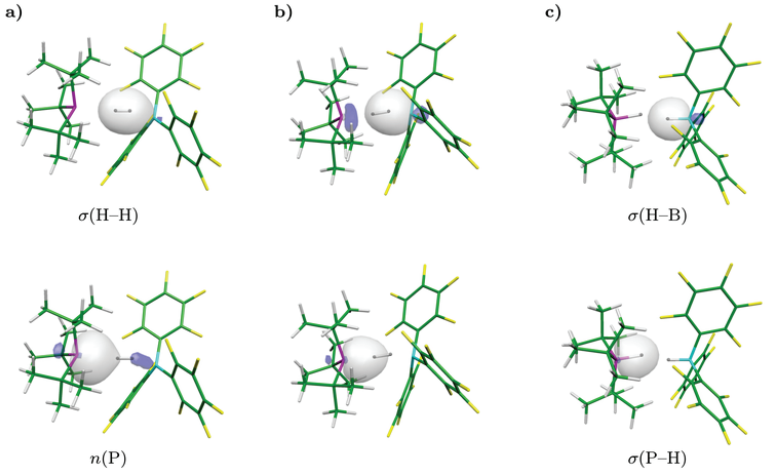

Figure 3.17: Natural localized molecular orbitals corresponding to the two participating electron pairs in the TS (a), in an intermediate point of the reaction path with H−H bond order of 0.326 (b), and in the product (c)

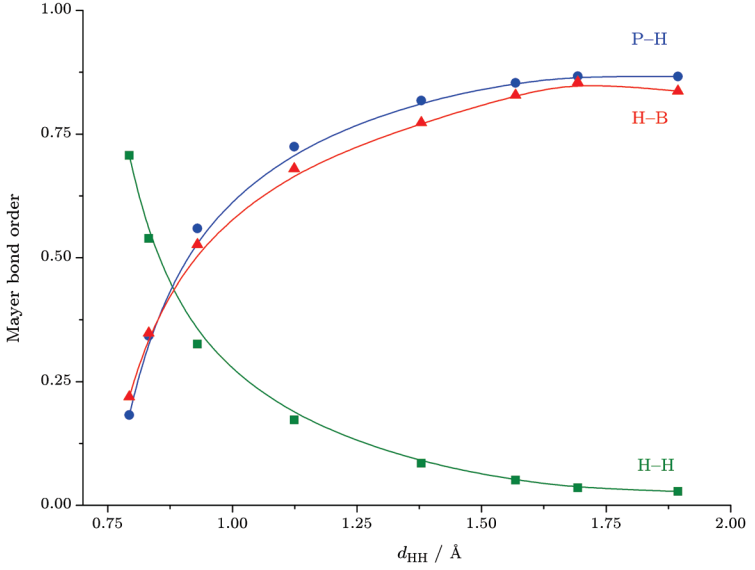

Figure 3.18: Evolution of the Mayer bond orders for the H−H (green squares), H−B (red triangles) and P−H (blue dots) bonds along the pseudo-IRC path, depicted as a function of the H−H distance

3.6 Other Modes of Hydrogen Activation*

The above results showed that the hydrogen splitting by the tBu$_3$P + **B** frustrated pair, and presumably by other FLPs as well, is based on a cooperative action of the free Lewis centers, involving electron donation to the $\sigma^*(H_2)$ and electron acceptance from the $\sigma(H_2)$ orbitals. Preorganization of the nonlinked centers owing to secondary interactions is the key that allows this concerted process to take place easily. Given the large number of known hydrogen activation reactions, we think it is interesting to compare the present mechanism with literature results, and to point out the similarities and differences.

3.6.1 Transition Metal Systems

Hydrogen cleavage at single transition metal centers has been extensively studied and the mechanism is now well understood [225–227]. Transition metals possess d

*The described comparison was published as the last section of our paper [2].

orbitals whose symmetry is particularly well suited for a process that involves electron donation to an empty d orbital from the occupied level of H_2 and a back donation from an occupied metal d orbital to the empty σ^* orbital (Figure 3.19a). Both donations occur in a symmetric fashion with respect to the H_2 giving rise to identical charge distribution for each H atom at any stage of the reaction. Therefore the H−H bond cleavage takes place homolytically, although no radical intermediates are present at any stage of the reacion. The reaction pathway involves a continuum of bonding situations, ranging from weakly bound metal–H_2 σ-complexes to metal dihydrides; the exact location of the stationary points is determined by the metal and the coordinating ligands.

Transition metal centers can also be involved in heterolytic splitting [225–227]. In this family of reactions, the metal atom serves as a Lewis acid accepting a hydride ion, while the proton is transferred to another Lewis donor atom, which may be either directly bonded to the metal, located on one of its ligands, or present in a separate molecule (Figure 3.19b).

Noteworthily, a third, slightly different type of transition-metal based hydrogen activation is also known, which is based on the cooperative action of two metalloradical

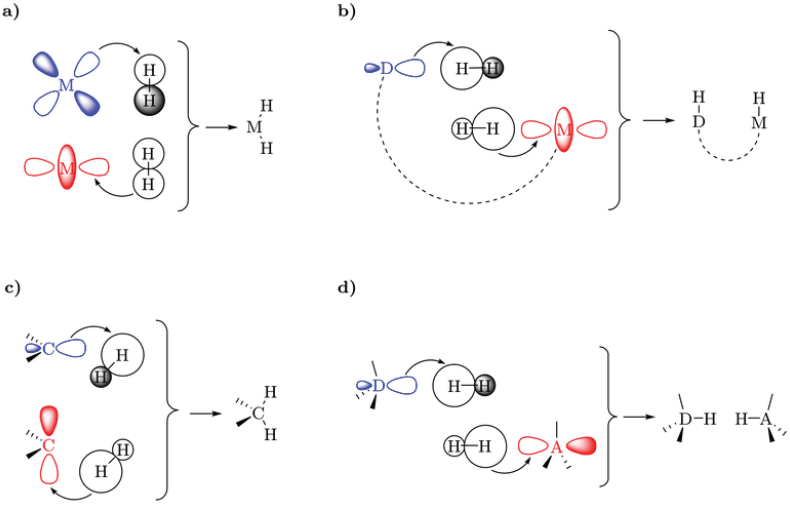

Figure 3.19: Schematic representation of various nonradical H_2 splitting mechanisms. Homolytic splitting on single transition metal centers (a), transition-metal-based heterolytic splitting (b), reaction of singlet carbenes (c) and FLPs (d). Blue and red colors indicate filled and vacant orbitals of the active center(s), respectively. Note the analogies horizontally (metal/nonmetal) and vertically (single-center/multi-center).

Figure 3.20: H_2 activation by cooperative metalloradicals

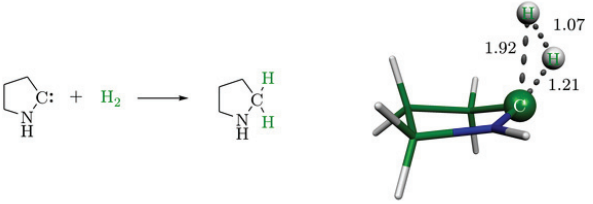

Figure 3.21: Hydrogen cleavage by a model carbene and the calculated transition state [128]

centers on H_2 (Figure 3.20) [234]. While the electronic reorganization is quite distinct from the Lewis acid–base type processes discussed here, the near-linear four-centered TS and the importance of preorganization are clearly analogous.

3.6.2 Singlet Carbenes

Singlet carbenes have an sp^2-type lone pair and an empty p orbital on the carbon atom, and therefore they are suitable for the same donation–back-donation process as transition metals (Figure 3.19c). As shown by recent experiments [128], (alkyl)(amino)carbenes can indeed cleave H_2 along with the formation of two C−H bonds.

In contrast to transition metals, the shape of the carbene orbitals does not allow symmetric back donation to the $\sigma^*(H_2)$ orbital. The calculated transition state structure [128] (Figure 3.21) reflects this asymmetry, the approach of hydrogen is consistent with expectations based on simple MO overlap arguments. Due to the asymmetric back-donation, the hydrogen becomes polarized in the transition state, and the cleavage can be described as heterolytic, albeit identical bonds are formed.

3.6.3 Comparison with Frustrated Pairs

The common feature of the above hydrogen activation processes and the H_2 cleavage by FLPs (Figure 3.19d) is the dual role of the reactants: H_2 donates electrons which are accepted by the reaction partner, and at the same time, it accepts electrons donated by its partner. Both electron transfers weaken the H−H bond, and if the partner has sufficiently strong Lewis acidic and basic character, the molecule is eventually splitted. The symmetry of the interacting orbitals determines whether the splitting is heterolytic, implying the spatial separation of the Lewis acidic and basic sites on H_2.

On the other hand, the various mechanisms differ in the way how the three interacting fragments (H_2, the donor and the acceptor) are brought together. The donor and acceptor sites may be located on the same atom, then no structural preorganization is required. Transition-metal-based processes may begin with the formation of a metal–H_2 σ-complex, which makes even a subsequent intermolecular hydrogen splitting (practically a proton transfer) feasible. Preorganizaton via a covalent bonding framework may connect the transition metal Lewis acid center and the Brønsted base, but intramolecular cooperativity of main group Lewis centers is possible as well. The nonlinked FLPs provide a fascinating example, where the organization is a result of purely secondary interactions.

3.7 Conclusions

We carried out a quantum chemical exploration of the mechanism of H_2 activation by the tBu$_3$P + B(C$_6$F$_5$)$_3$ frustrated Lewis pair. We identified the corresponding reaction pathway and analyzed the electronic reorganization along it. Consideration of the results allowed the formulation of a general mechanistic picture, and provided additional insight into the notion of frustration. The results described in this chapter can be summarized in the following main conclusions:

1. No theoretical evidence supports the previously suggested stepwise mechanisms for the heterolytic cleavage of H_2 by the tBu$_3$P + B(C$_6$F$_5$)$_3$ Lewis pair.

2. A novel mechanistic proposal, involving the preorganization of the bulky donor–acceptor molecules into a loosely bound and highly reactive, ambiphilic complex (the "frustrated complex"), accounts for all experimental observations for this reaction.

3. In the proposed mechanism, the key to break the strong H−H bond is the simultaneous interaction of H_2 with a filled and a vacant orbital. This feature is quite analogous to other hydrogen splitting processes, while the way of achieving the required preorganization differs markedly.

4. The role of frustration is to ensure the existence of an active, ambiphilic form (the frustrated complex) of the donor–acceptor system as well as to reduce the energetic costs of the reaction by reactant-state destabilization.

Chapter 4

Rationalizing the Reactivity of Frustrated Pairs

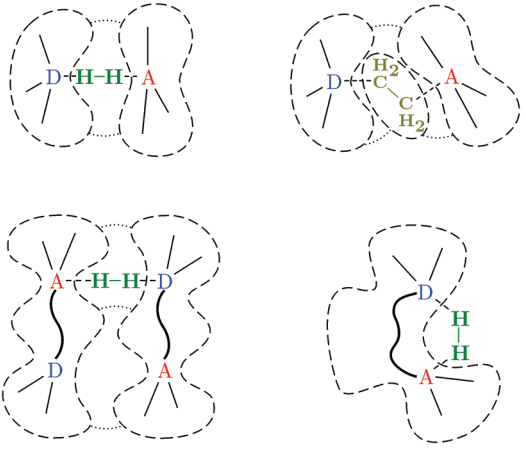

4.1 Introduction

Based on our studies on the tBu$_3$P + B(C$_6$F$_5$)$_3$ pair, we suggested a mechanism of bond splitting reactions via FLPs, which was described in the previous chapter. Apparently, the investigated system has no particular features, apart from the presence of the bulky substituents, we therefore expected that the suggested model would also account for the reactions of other pairs with various small molecules.

In this chapter, we first present related earlier examples, and then the reactivity of various FLP systems towards hydrogen, olefins, and carbon dioxide is analyzed based on our results and studies from other research groups. As the summary of the mechanistic considerations, an extension and generalization of our model is introduced.

4.2 Earlier Examples of Main-Group Lewis Cooperativity

Before the discovery of the unique reactivity of FLPs, a couple of studies on heterolytic hydrogen splitting reactions by cooperative main-group Lewis centers were already present in the literature, which are worth discussing at this point. One example is the homogeneous hydrogenation of ketones catalyzed by alkali metal alkoxides, which was discovered by Walling and Bollyky in 1961 (Figure 4.1a) [130]. Some forty years thereafter, Berkessel and coworkers carried out a detailed experimental mechanistic study [131], which was later complemented by the theoretical work of Chan and Radom [132]. The proposed mechanism of this process involves heterolytic H_2 splitting with an alkoxide ion as the base and the carbonyl carbon atom as the acid (Figure 4.1b). The reaction requires harsh conditions (150–200 °C, 80–160 atm pressure, strong base), which was explained by the fact that a highly ordered transition structure, featuring a six-membered ring, must be assembled. In order to enhance the efficiency of the process, the importance of improving the preorganization was underlined [131].

Nature provides numerous examples of the excellent preorganization of the reactive sites in enzymes. While the active centers usually only comprise a handful of functional groups, thousands of atoms work together to ensure their appropriate position and flexibility. Enzymatic hydrogen activation has been known for almost hundred years, but it was also discovered rather early that hydrogenases contain transition metal centers responsible for the hydrogen splitting [159]. In 1990, a new hydrogenase enzyme termed H_2-forming methylene-tetrahydromethanopterin dehydrogenase (Hmd) was found, which catalyzes the reversible reaction shown in Figure 4.2 [160]. This enzyme also contains an iron center, but due to its EPR- and redox-inactivity, it was thought to have structural rather than functional roles [153, 154]. Although the iron was later shown to be a part of the active site [157, 158], the concept of metal-free hydrogenase enzymes emerged, and it motivated theoretical studies directed toward the understanding of such enzyme activity.

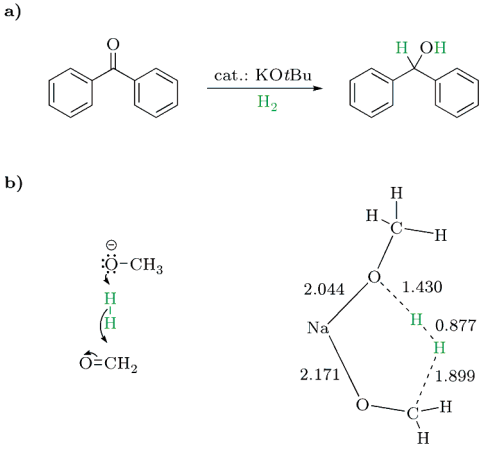

Figure 4.1: Base-catalyzed hydrogenation of ketones [130] (a); scheme and calculated transition state [131, 132] of a corresponding model reaction (b)

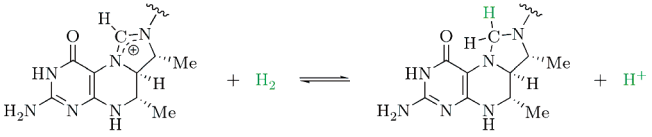

Figure 4.2: Reversible hydrogenation reaction catalyzed by H_2-forming methylene-tetrahydromethanopterin dehydrogenase [160]

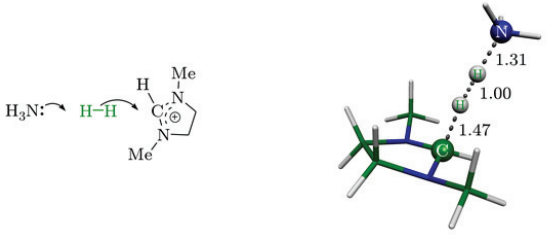

Figure 4.3: Scheme and calculated transition state [156] of a model reaction of the hypothetical metal-free enzymatic hydrogenation

The computational works of Berkessel [155] and Radom [156] showed that a heterolytic splitting of H_2 between an amidinium cation Lewis acid and different Brønsted bases (ammonia, formate anion, methylamine etc.) is both kinetically and thermodynamically feasible. The identified transition states (see an example in Figure 4.3) are clearly analogous to the hydrogen activation by FLPs, with the necessary preorganization provided by the protein backbone. Although the enzymes prefer other ways of hydrogen cleavage, these studies highlight potential compound classes that may be useful in hydrogen activation chemistry by FLPs.

4.3 Hydrogen Activation with Nonlinked Frustrated Pairs

Following our study on the $t\mathrm{Bu_3P}$ + **B** pair, several examples appeared in the literature that demonstrate the applicability of the established mechanistic picture to hydrogen splitting via nonlinked pairs. As part of our studies on catalytic imine hydrogenation by FLPs, we also presented results that corroborate the generality of the mechanism. This section is devoted to the presentation of these contributions.

4.3.1 Carbene–Borane and Carbonyl–Borane Pairs

The research group led by Matthias Tamm published a joint experimental–theoretical study on the heterolytic hydrogen splitting by a carbene–borane pair [97]. In accordance with an independent experimental work of Stephan et al. [96], they found that this pair is also capable of hydrogen activation, yielding an amidinium hydridoborate salt (see Figure 4.4). Interestingly, upon standing at room temperature this pair quickly loses its reactivity towards hydrogen through the formation of an "abnormal" dative adduct [97]. On the other hand, no interaction between the carbene and the borane can be detected at −78 °C [96].

In their computational work, the Tamm group identified a noncovalent, preorganized **carb**···**B** complex between the Lewis components with an association energy of $\Delta E = -10.9\,\mathrm{kcal\,mol^{-1}}$. They were also able to locate the transition state for hydrogen splitting, which is completely analogous to that found by us for the $t\mathrm{Bu_3P}$ + **B** pair. The carbene–borane reaction has a lower barrier ($\Delta E^{\neq} = +1.1\,\mathrm{kcal\,mol^{-1}}$ relative to **carb**···**B** + H_2) and significantly higher exothermicity than the phosphine–borane system, which may be attributed to the higher basicity of the carbene than the phosphine (see also later, in Chapter 5). The calculations also confirmed the existence of two carbene–borane dative adducts, the sterically less hindered "abnormal" adduct being much more stable.

In their calculations, Privalov et al. addressed the possibility of hydrogen cleavage via carbonyl–borane pairs [116]. This reaction has not yet been observed experimentally, but it could serve as the basis for Lewis-acid-catalyzed direct hydrogenation of C=O bonds. The authors identified the corresponding transition state of H_2 activation, in

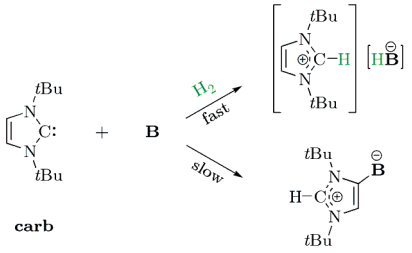

Figure 4.4: Hydrogen activation and "abnormal" dative bond formation by the **carb** + **B** pair [96, 97]

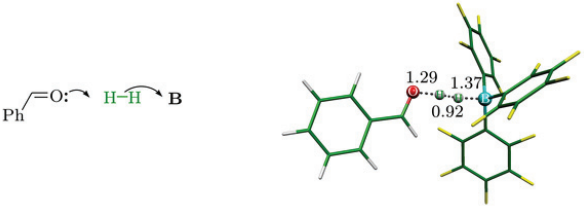

Figure 4.5: Scheme and transition state for hydrogen splitting by a carbonyl–borane pair [116]

which the carbonyl oxygen atom and the boron center serve as the Lewis base and acid, respectively (Figure 4.5). The structure of the TS is consistent with the systems discussed up to this point. On the reactant side, the existence of a datively bound carbonyl–borane adduct was shown. The cleavage reaction step is predicted to be moderately endergonic, but the overall reaction leading to an alcohol product was found to be both thermodynamically and kinetically feasible.

4.3.2 Imine–Borane and Amine–Borane Pairs*

Whilst addressing the mechanism of borane-catalyzed imine reduction, we explored the PES of the reaction of an imine–borane and an amine–borane pair with hydrogen. Experimentally [90], the hydrogen activation by the **btim** + **B** pair proceeds similarly to the $t\mathrm{Bu_3P}$ + **B** system in that there is no datively bound adduct [148], and room temperature and ambient pressure are sufficient to induce the reaction (Figure 4.6). The expected iminium hydridoborate salt product can not be isolated, as it rapidly

*Results in this section appeared as part of our paper on catalytic imine hydrogenation [3].

forms an amine–borane dative adduct via hydride transfer.* Interestingly, despite the dative bond, the amine–borane adduct is also capable of hydrogen activation, albeit only at elevated temperature.

The results of our related computational studies are summarized in the form of an energy profile in Figure 4.7, while the corresponding structures are displayed in Figures 4.8, 4.9 and 4.10. The calculations were done at the SCS-MP2/cc-pVTZ//M05-2X/6-31G* level.

Apparently, the appropriate frustrated complexes exist for both the imine–borane and the amine–borane pairs. π–π stacking as well as C−H···π and C−H···F interactions are responsible for the association, and give rise to appreciable binding energies of $-12.0\,\mathrm{kcal\,mol^{-1}}$ and $-12.6\,\mathrm{kcal\,mol^{-1}}$ for **btim**···**B** and **btam**···**B**, respectively. Although formed in entropically unfavored processes, these D···A intermediates react rapidly with H_2 via transition states $\mathbf{TS}_{\mathrm{im}}$ and $\mathbf{TS}_{\mathrm{am}}$, which are analogous to $\mathbf{TS}_{\mathrm{PB}}$ found in the phosphine–borane system and represent only a modest barrier in this case, too. The heterolytic cleavage of the H−H bond is an exothermic process and yields the appropriate $[\mathrm{DH}]^+[\mathrm{HA}]^-$ ion pairs.

The datively bound amine–borane adduct was also identified in our calculations. However, the optimized structure of **btam**−**B** suggests a notable degree of strain, which is also borne out by its relatively small binding energy of $26.7\,\mathrm{kcal\,mol^{-1}}$. For a comparison, the binding energy of the notably less strained $(CH_3)_2$NH−**B** adduct is predicted to be $39.3\,\mathrm{kcal\,mol^{-1}}$.

As a result of the existence of **btam**−**B**, corresponding to a deep energy minimum, higher activation energy is needed to reach the transition state in the amine–borane case, which is in full agreement with the experimental finding that the formation of the ammonium hydridoborate ion pair product occurs only at 80 °C [90]. It is also reassuring to see that the optimized geometry of $[\mathbf{btam}\mathrm{H}]^+[\mathrm{H}\mathbf{B}]^-$ is in good accordance with the structure determined from X-ray diffraction measurements.

4.4 Reactivity of Linked Donor–Acceptor Pairs towards Hydrogen

4.4.1 Linked Systems without Intramolecular Cooperation†

In the first linked phosphinoboranes investigated in the FLP context ($t\mathrm{Bu_2P}-\mathrm{C_6F_4}-\mathbf{B'}$ and $\mathrm{Mes_2P}-\mathrm{C_6F_4}-\mathbf{B'}$), which were described by Stephan et al. [76, 80, 90, 107], the phosphorus and boron centers are linked by a large and rigid $-p\text{-}\mathrm{C_6F_4}-$ moiety, which makes a direct intramolecular cooperation in these D∼A systems impossible. Together with the experimentally observed first-order hydrogen loss kinetics, this led

*The role of iminium hydridoborate as an intermediate was confirmed by a different experiment with a sterically more crowded imine, in which the subsequent step is apparently blocked. See also section 6.2.1, page 92.

†Based on preliminary results, we suggested the applicability of our model to such systems in our paper [1].

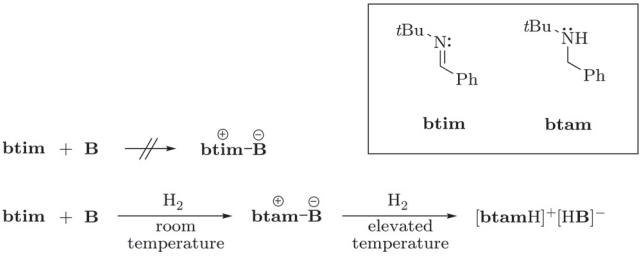

Figure 4.6: Reactions of an imine–borane and an amine–borane pair with hydrogen [90]

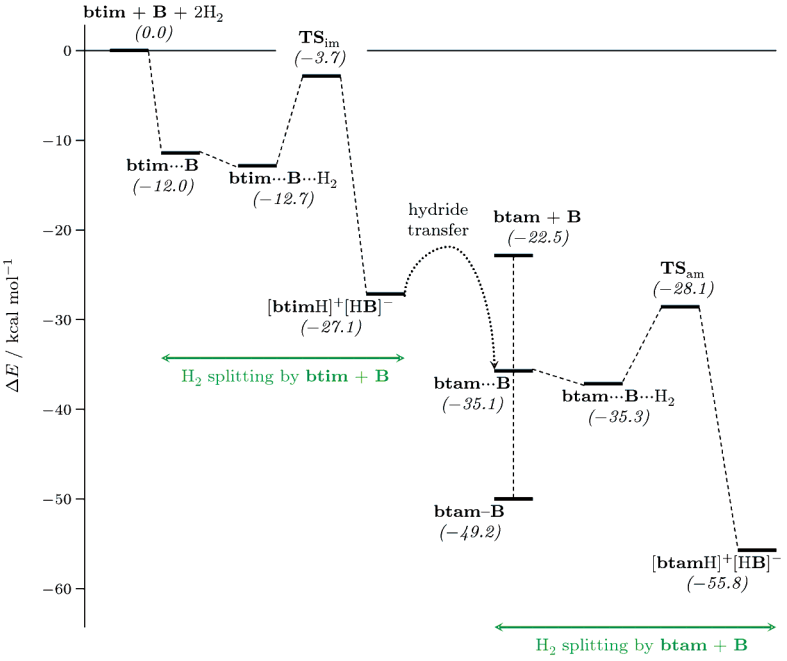

Figure 4.7: Electronic energy profile for the hydrogen splitting reactions by the **btim** + **B** and **btam** + **B** pairs, calculated at the SCS-MP2/cc-pVTZ//M05-2X/6-31G* level of theory

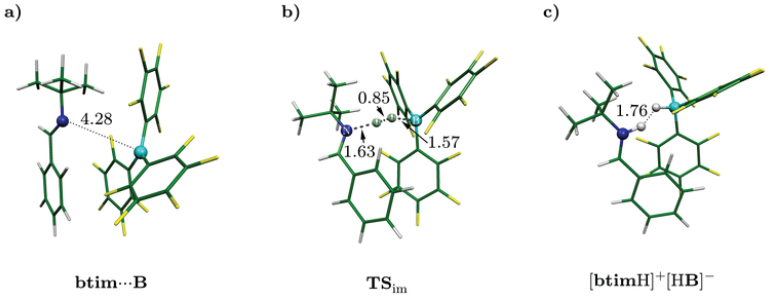

Figure 4.8: Optimized geometries of stationary points along the hydrogen splitting process by the **btim** + **B** pair: frustrated complex (a), transition state (b), product ion pair (c)

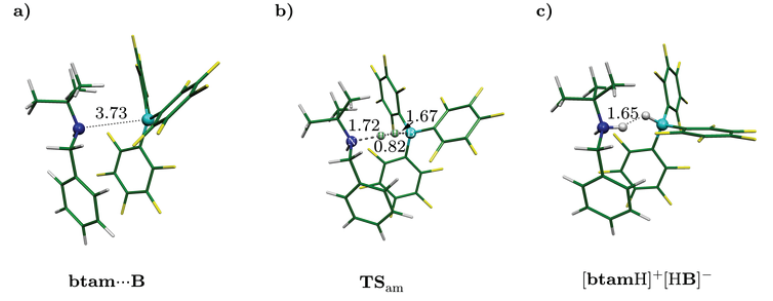

Figure 4.9: Optimized geometries of stationary points along the hydrogen splitting process by the **btam** + **B** pair: frustrated complex (a), transition state (b), product ion pair (c)

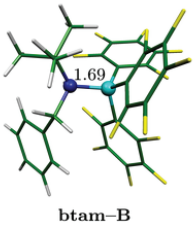

Figure 4.10: Optimized geometry of the amine–borane dative adduct

Stephan and coworkers to formulate an intramolecular mechanism, involving hydrogen splitting over the B−C or P−C bonds, followed by proton or hydride migration (recall Figure 1.17 on page 12) [80]. In our preliminary investigations, we found these migration intermediates to lie very high in energy, but we were able to identify D∼A···D∼A frustrated complexes formed from two phosphinoborane molecules (Figure 4.11). We therefore suggested that hydrogen splitting may proceed via similar mechanism as in nonlinked pairs, involving intermolecular cooperation of the phosphorus and boron centers.

Guo and Li carried out detailed calculations on this system [117], and concluded that the migration channels are unfavorable, but they found the intermolecular pathway feasible. Their suggested reaction route involves frustrated complex formation at one end of the phosphinoboranes, splitting of a molecule of hydrogen, complex formation at the other end, and splitting another H_2. As the authors pointed out, this mechanism interprets the observed bimolecular exchange process, which was anticipated by Stephan et al. [80] to rationalize the scrambling of deuterium labels when a mixture of [$^{+}$HMes$_2$P−C$_6$F$_4$−**B′**H^{-}] and [$^{+}$DMes$_2$P−C$_6$F$_4$−**B′**D^{-}] is heated. On the other hand, the observed first-order kinetics of hydrogen loss is seemingly inconsistent with this bimolecular process. Further experimental and theoretical investigation is therefore necessary to provide a thorough understanding of this system.

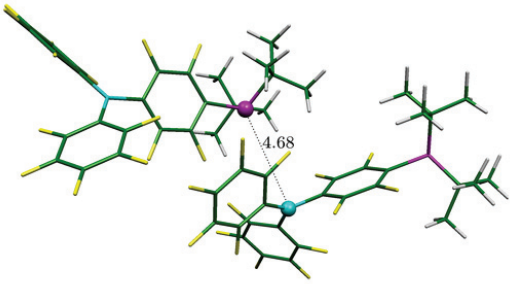

Figure 4.11: B3LYP/6-31G*-optimized geometry of the frustrated *t*Bu$_2$P−C$_6$F$_4$−**B′**···*t*Bu$_2$P−C$_6$F$_4$−**B′** complex. Alternative, parallel head-to-tail dimer structures were also found.

4.4.2 Intramolecular Cooperativity of Linked Systems

With an appropriate arrangement of the active Lewis centers, intramolecular cooperative hydrogen splitting was expected to be realizable. An early attempt to utilize such reactivity was done by Roesler, Piers and Parvez [41]. The authors synthesized an *ortho*-phenylene bridged aminoborane compound (see Figure 4.12), in part with the aim of obtaining a "molecular dihydrogen storage device". Unfortunately, the

triphenylamine moiety proved to be a very poor base, and the hydrogenated form of the compound could not be prepared.

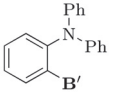

$Ph_2N–C_6H_4–\mathbf{B}'$

Figure 4.12: An aminoborane compound intended for Lewis bifuncionality [41]

While the $-p$-C_6F_4- linker of the first intramolecular frustrated pairs excludes intramolecular cooperation of the P and B centers in H_2 splitting, the ethylene moiety in $Mes_2P-C_2H_4-\mathbf{B}'$, prepared by Erker et al. [103], possesses significant flexibility. Computational results indicate that a *gauche* conformer without dative bond exists, which could provide the necessary preorganized active sites for H_2 splitting (Figure 4.13) [103]. *gauche*-$Mes_2P-C_2H_4-\mathbf{B}'$ was predicted to be only $7\,\mathrm{kcal\,mol^{-1}}$ less stable than the closed, cyclic form, and it should thus be readily accessible even at room temperature, although a larger value of $13\,\mathrm{kcal\,mol^{-1}}$ was later reported at a more sophisticated level of theory [114].

Other D∼A pairs capable of intramolecular hydrogen splitting include the "directly linked" phosphinoboranes, such as $t\mathrm{Bu}_2\mathrm{P}-\mathbf{B}'$ [106]. The calculations of Stephan et al. revealed that the π-type overlap between the phosphorus lone pair $n(\mathrm{P})$ and the borane p orbital is present but limited, and the centers retain sufficient Lewis acidic and basic character to react with H_2 directly [106]. In the transition state, which was located later by Privalov [118], the approach of hydrogen is asymmetric, with end-on-like interaction with the phosphine and side-on-like with the borane moiety (Figure 4.14). This picture is consistent with the expected $n(\mathrm{P}) \rightarrow \sigma^*(\mathrm{H_2})$ and $\sigma(\mathrm{H_2}) \rightarrow p(\mathrm{B})$ donations. Privalov et al. also carried out a detailed analysis on the substituent effects on the barrier [119], and concluded that decreasing the π-interaction between $n(\mathrm{P})$ and $p(\mathrm{B})$ via geometrical constraints or placing electron withdrawing substituents on the borane facilitates the reaction.

Intramolecular cooperativity of the active centers was also demonstrated for the methyl-*ortho*-phenyl-linked aminoborane compound $\mathbf{tmp}-CH_2-C_6H_4-\mathbf{B}'$, synthesized by Repo, Rieger and coworkers (Figure 4.15) [102]. No dative bond in the dehydrogenated D∼A form can be detected by NMR spectroscopy, and the compound readily cleaves hydrogen at 20 °C. The reaction is reversed at 110 °C. Computational investigation confirmed the possibility of intramolecular hydrogen activation via the identification of the corresponding transition state (Figure 4.15), which represents the only significant barrier along the reaction route towards $[^{+}\mathrm{HD}{\sim}\mathrm{AH}^{-}]$. The TS bears numerous common features with the $t\mathrm{Bu}_3\mathrm{P} + \mathbf{B} + \mathrm{H_2}$ system, in particular, it is rather early and low-lying ($\Delta E^{\neq} = 3.3\,\mathrm{kcal\,mol^{-1}}$ with respect to $\mathbf{tmp}-CH_2-C_6H_4-\mathbf{B}' + H_2$).

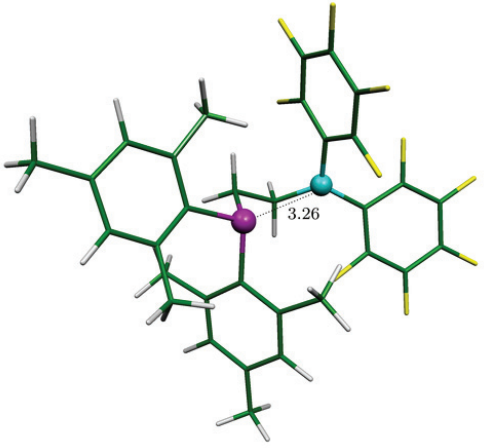

Figure 4.13: Calculated *gauche* conformer of $Mes_2P{-}C_2H_4{-}\mathbf{B}'$ [103]

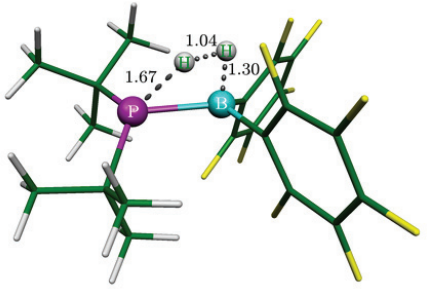

Figure 4.14: Transition state of hydrogen splitting by $t\mathrm{Bu}_2\mathrm{P}{-}\mathbf{B}'$ [118]

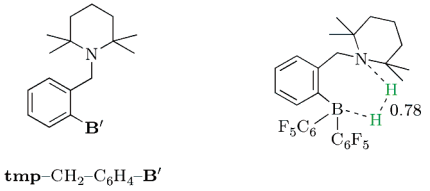

tmp–CH_2–C_6H_4–**B′**

Figure 4.15: Structure and transition state of hydrogen splitting of an aminoborane derivative [102]

4.5 Olefin Activation*

In the preceding sections, we discussed the mechanism of hydrogen splitting via frustrated Lewis pairs. We now present our studies directed toward the extension of this model to another family of mechanistically intriguing reactions, namely, to the addition of frustrated phosphine–borane pairs to olefins. We show that the cooperative action of Lewis acidic and basic centers in a preorganized environment easily explains the activation reaction of an olefinic π-bond as well. The results presented here are based on SCS-MP2/cc-pVTZ//B3LYP/6-31G* calculations.

4.5.1 Experimental Results

As noted in the introduction, Stephan and coworkers reported that ethylene or propylene react readily with mixtures of tBu$_3$P and **B** yielding alkanediyl-linked zwitterionic phosphonium borates (Figure 4.16) [109]. Both NMR and X-ray crystallographic data indicated that the Lewis components add to the opposite ends of the olefinic bond, and for substituted alkenes, the reaction is regioselective in that the secondary carbon center is attacked by tBu$_3$P. The authors suggested that these three-component reactions are initiated by activation of the olefin by the Lewis acidic borane, which is followed by phosphine addition. Nevertheless, no spectroscopic evidence of related binary adducts was found in experiments even at lower temperatures.

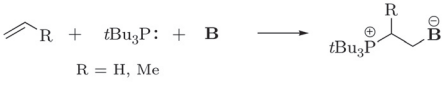

Figure 4.16: Activation of olefins by the tBu$_3$P + **B** pair [109]

*The theoretical analysis presented in this chapter was published in our paper [4].

4.5.2 Stationary Points and Reaction Pathways

On the basis of the model we put forward for H_2 activation, one expects that the addition of tBu$_3$P + **B** pair to alkenes takes place in a single step via synergistic phosphine–olefin and borane–olefin interactions. Our quantum chemical calculations carried out for the tBu$_3$P + **B** + C_2H_4 system confirm this assumption as seen from the structure of the identified transition state $\mathbf{TS}_{et}$. Figure 4.17 shows that the C_2H_4 molecule in $\mathbf{TS}_{et}$ interacts simultaneously with the two active centers of the frustrated Lewis pair in an antarafacial manner. The concerted addition has an early TS, but the distorted structure of C_2H_4 implies a considerable degree of activation already at this stage of the reaction. The relative energy of the TS (+1.8 kcal mol^{-1} with respect to the separated reactants) is comparable to that of the hydrogenation reaction and it is consistent with the observed reaction rate (see full energy profile in Figure 4.18, and compare with the hydrogen activation shown in Figure 3.7, page 37).

On the reactant side of the TS, a weakly bound ternary complex (tBu$_3$P···**B**···C_2H_4) is identified as an energy minimum, which corresponds to an open form of the tBu$_3$P···**B** frustrated complex interacting with a C_2H_4 molecule (Figure 4.19b). This transient species lies 12.0 kcal mol^{-1} below the reactants, and the stabilization arises partly from van der Waals and C–H···F contacts between the aryl groups of the phosphine–borane pair and also from weak borane–ethylene attraction. All these interactions contribute to the preorganization of reacting molecules to an arrangement favorable for cooperative interactions.

According to our calculations, formation of this ternary complex can occur in two pathways. One of them, analogously to the hydrogen splitting process, involves

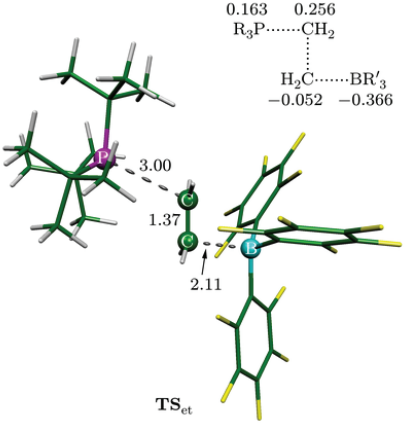

Figure 4.17: Transition state $\mathbf{TS}_{et}$ of ethylene activation. Numbers in the upper part indicate calculated NPA charges of the respective fragments.

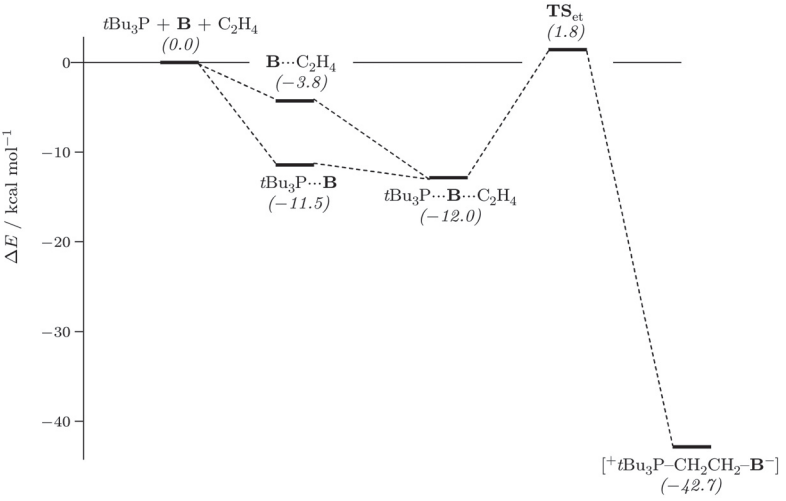

Figure 4.18: Electronic energy profile of ethylene activation, calculated at the SCS-MP2/cc-pVTZ//B3LYP/6-31G* level of theory

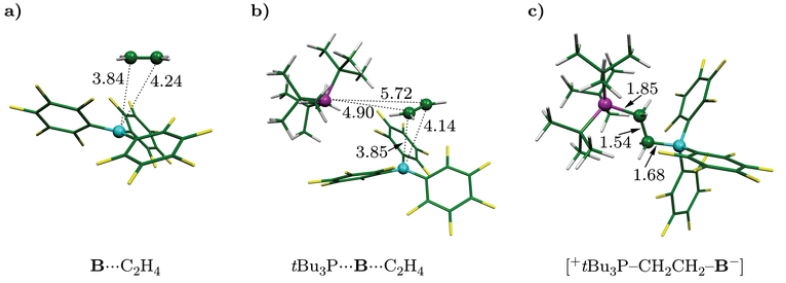

Figure 4.19: Stationary points of ethylene activation: ethylene–borane complex (a), ternary complex (b), product (c)

formation of a frustrated complex, which then interacts with the incoming ethylene. However, the reaction may also commence with the formation of a weak $\mathbf{B}\cdots C_2H_4$ complex (Figure 4.19a), which is then attacked by the phosphine. The association energy for the $\mathbf{B}\cdots C_2H_4$ adduct is predicted to be $-3.8\,\mathrm{kcal\,mol^{-1}}$, which is slightly larger than that reported for the $F_3B\cdots C_2H_4$ complex identified previously in liquid argon or nitrogen [36], but much smaller than the stabilization energy of the $t\mathrm{Bu_3P}\cdots\mathbf{B}$ complex ($-11.5\,\mathrm{kcal\,mol^{-1}}$).

Importantly, the ethylene molecule in $\mathbf{B}\cdots C_2H_4$ does not interact covalently with the B center as revealed from the long B···C distances. The charge transfer is thus absent, the stabilization is rather due to van der Waals and C−H···F contacts. Therefore, contrary to the suggestion of Stephan et al. [109], this weak association does not represent a real olefin activation step.

We also investigated the possibility of a stepwise mechanism beginning with either P−C or B−C covalent bond formation. Our calculations indicate that the interaction of **B** and C_2H_4 in the covalent bond region as well as interaction between $t\mathrm{Bu_3P}$ and C_2H_4 at all distances are repulsive for chemically relevant geometrical arrangements.

On the product side of the TS, we identified the $[^{+}t\mathrm{Bu_3P}{-}\mathrm{CH_2CH_2}{-}\mathbf{B}^{-}]$ product on the PES (Figure 4.19c), whose calculated structure agrees well with the available X-ray data [109]. The charge separation in this zwitterionic species is confirmed by the large dipole moment ($\mu = 18.7\,\mathrm{D}$). The relative stability of the addition product is predicted to be $-42.7\,\mathrm{kcal\,mol^{-1}}$ with respect to separated reactants, which points to a highly exothermic and irreversible reaction.

4.5.3 Electronic Structure Analysis

The natural population analysis of the transition state (see Figure 4.17) indicates significant charge density redistribution relative to the reactants. The ethylene molecule undergoes polarization and electron transfer is observed corresponding to $t\mathrm{Bu_3P} \rightarrow \pi^*(C_2H_4)$ and $\pi(C_2H_4) \rightarrow \mathbf{B}$ donations. These electronic effects are very similar to those found for the heterolytic cleavage of H_2, and underline the mechanistic analogy between the two reactions.

The progress of bond formation along the reaction pathway was monitored by inspecting the deviation of the olefinic CCH_2 units from planarity. The deviation from planarity is measured as the angle ϕ between the imaginary elongation of the C−C bond and the sum of the C−H vectors of a given C atom (see Figure 4.20). For ethylene, $\phi = 0°$, while for a regular tetrahedral center, $\phi = \arccos\left(\sqrt{3}/3\right) \approx 54.74°$.

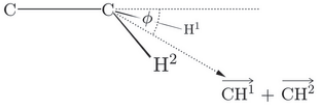

Figure 4.20: Definition of angle ϕ measuring the deviation of the CCH_2 unit from planarity

As seen in Figure 4.21, the transition from sp^2 to sp^3 hybrid states occurs asynchronously, as the deviation from planarity at the boron site (ϕ_B) is always larger than that at the phosphorus side (ϕ_P). In other words, the development of the B−C bond is somewhat ahead the formation of the P−C bond.

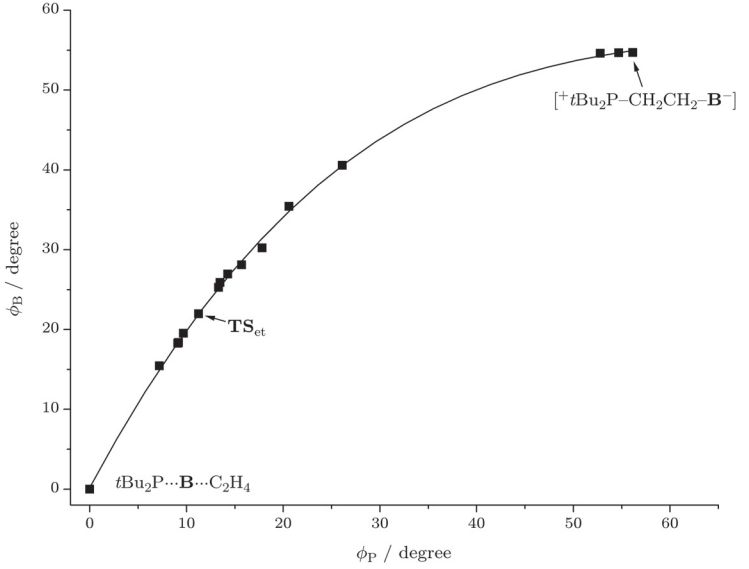

Figure 4.21: Progress of P−C and B−C bond formation, expressed as the deviation from planarity of the respective CCH_2 units (ϕ_P and ϕ_B) along the reaction pathway of ethylene activation

4.5.4 Regioselectivity

The early nature of the located TS and the irreversibility of the reaction allows us to associate the regiochemistry with reaction rates expected from the electron distribution of the reactants. Due to the excess of electron density on the terminal carbon of the olefinic bond in alkylated ethylenes, the CH_2 group is expected to preferentially act as a Lewis base in the concerted addition and react more favorably with borane, while the phosphine favors to attack the substituted CHR group [235].

In order to assess the relevance of this reasoning, we located a series of transition states for the reaction of $t\mathrm{Bu_3P}$ + **B** with propylene. The initial structures in these transition state optimizations were constructed from the TS identified for addition to

C_2H_4 by corresponding methyl substitutions. Due to the helical chirality caused by the aryl rings of the borate fragment, four different TSs can be identified, their relative energies are shown in Figure 4.22. It is apparent that the lowest TS corresponding to the experimentally observed product (methyl on the phosphine side) lies 1.3 kcal mol^{-1} lower in energy than that identified for the reverse addition pathway. These results are in qualitative agreement with the observed regioselectivity [109].

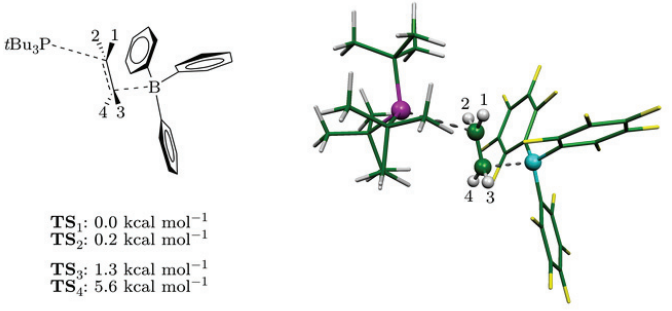

Figure 4.22: Structures and relative energies of the four possible transition states for the addition of the tBu$_3$P + **B** pair to propylene. Numbers 1–4 indicate possible positions of the methyl group.

4.5.5 Related Literature Results on π-Bonded Systems

Independently from our work, Guo and Li published a paper discussing the mechanism of FLP addition to olefins [120], with conclusions mainly in agreement with ours. They also carried out calculations for the tBu$_3$P + BPh$_3$ pair, showing that its reaction with ethylene is both thermodynamically and kinetically unfavorable. It is interesting to recall that addition of this pair to the triple bond of 1,2-didehydrobenzene was found to occur experimentally (see Figure 1.27 on page 18).

On the other hand, the authors reject the possibility that the formation of the tBu$_3$P···**B** frustrated complex could initiate the addition reaction, because "it is difficult for olefins to insert into the narrow space between the B(C$_6$F$_5$)$_3$ moiety and the tBu$_3$P moiety". Supported by our results on the flexibility of the frustrated complex, we maintain our hypothesis about the two possible pathways.

Very recently, joint experimental and theoretical studies on the addition of Mes$_2$P−C$_2$H$_4$−**B**′ to norbornene were published [110]. The authors addressed the question whether the addition is stepwise, starting with B−C bond formation, or concerted. Their analysis is based on the possibility of Wagner–Meerwein rearrangements of the norbornyl cation moiety in the case of a stepwise addition, which could lead to a mixture of products (Figure 4.23). As this is not observed experimentally, they

conclude that either the reaction is concerted, or the second step is faster than the rearrangement. The computational identification of the corresponding transition state in that system corroborates that the process is a concerted, asynchronous addition, similarly to what we found for $t\mathrm{Bu_3P}$ + **B** + etyhlene or propylene.

As mentioned at the end of section 1.6, frustrated Lewis pairs were reported by Stephan, Erker, Grimme and coworkers to react easily with one of the π-bonds of carbon dioxide in a reversible reaction [114]. The authors also presented a theoretical investigation on the reaction of CO_2 with $\mathrm{Mes_2P{-}C_2H_4{-}}\mathbf{B'}$. According to the results, the open isomer *gauche*-$\mathrm{Mes_2P{-}C_2H_4{-}}\mathbf{B'}$, which only lies 13.0 kcal/mol above the cyclic structure, forms a weak complex with CO_2, and the reaction then proceeds in a concerted, synchronous step towards the product (Figure 4.24). The simultaneous interaction of the Lewis centers with the substrate and the resulting low barrier are obviously analogous to the above studied hydrogen and ethylene activation reactions.

4.6 Conceptual Issues*

Since the publication of the basic concepts on the role of frustration in our study on $t\mathrm{Bu_3P}$ + **B**, numerous FLP systems have been considered briefly or analyzed in detail. While the key points of the early model (preorganization and reactant-state destabilization) remained valid, we think it useful to provide a refined and expanded description of frustration.

First, the computational studies indicate that there exist an "active" form of the pair, in which the Lewis centers create a preorganized ambiphilic environment. In nonlinked pairs (and in linked pairs with certain linkers), this active form is the intermolecular frustrated complex, which is bound by secondary forces between the bulky substituents. Linked pairs may possess an isomer or conformer that is suitable for intramolecular cooperation; the existence and stability of such a conformer may also be related to the presence of steric effects.

Second, population of the above mentioned "active" form is energetically feasible. By hindering the formation of the datively bound (or in any other way quenched) form of the pair, the steric effects provide reactant-state destabilization that lowers the energetic cost of reaching the active state, and also makes the reaction more exothermic.

Reactant-state destabilization by steric effects was formulated as a general concept by Brown in as early as 1960, and the term "steric assistance" was coined to it [18]. More recently, the concept is utilized, e.g., in the description of enzymatic reactions, where strained reactant states are called "entatic states" [236].

In several pairs, e.g., in the previously investigated $t\mathrm{Bu_3P}$ + **B**, the reactant-state destabilization is so effective that it causes the active form, the frustrated complex, to be the global energy minimum of the system (the minimum corresponding to the

*This discussion is a slightly extended version of that published as part of our paper [3].

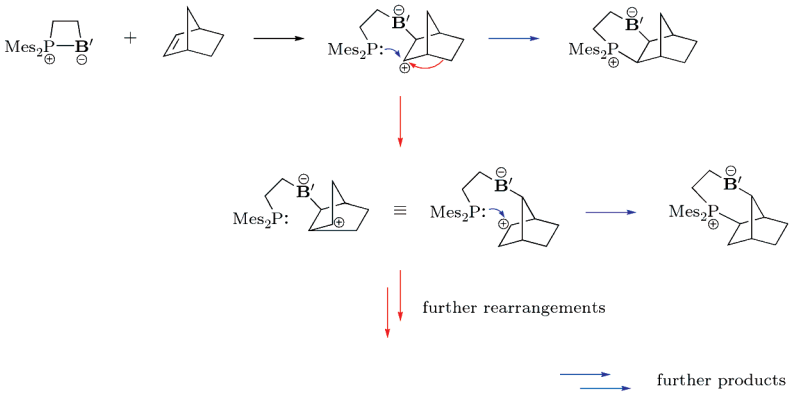

Figure 4.23: Possible formation of multiple products from the stepwise addition of a linked FLP to norbornene [110]

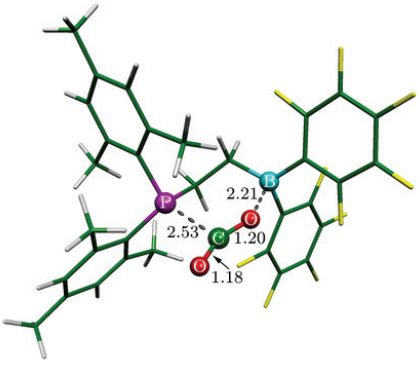

Figure 4.24: Transition state for CO_2 activation [114]

datively bound form may even be absent). In this sense, these pairs can be termed as "inherently frustrated" systems (red curve in Figure 4.25).

There also exist pairs, e.g., **btam** + **B**, that exhibit a datively bound global minimum lying well below the frustrated complex form. Although high strain may be present in the dative adduct, the active sites are still quenched and thermal activation is required to reach the reactive state. These pairs can be regarded to show "thermally induced frustration" (blue curve in Figure 4.25).

It is important to emphasize that the above classification is based on a zero-kelvin PES. At finite temperature, entropy change (usually loss) associated with (strong or weak) bonding markedly influences the tendency of adduct formation. For the nonlinked pairs, a certain binding energy is necessary for any adduct to be the dominant species over the entropically preferred, dissociated state.

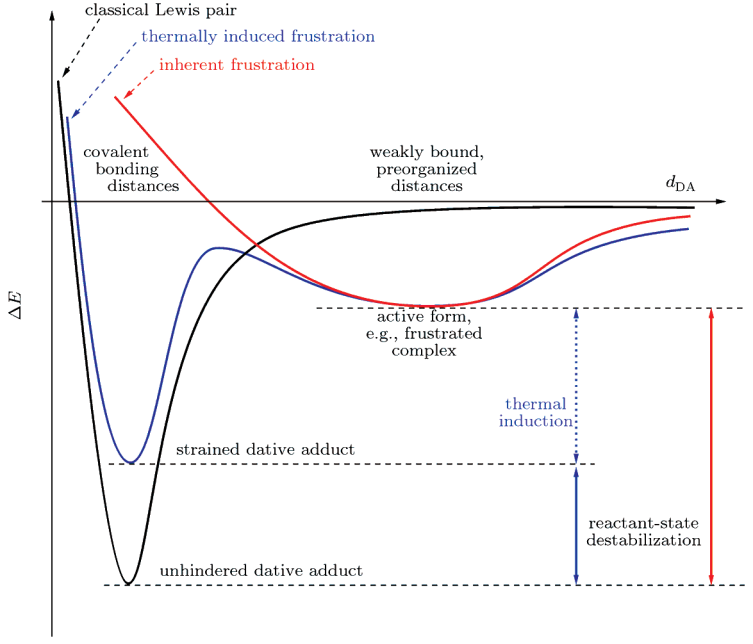

Figure 4.25: Characteristic potential energy curves of different donor–acceptor pairs as a function of donor–acceptor distance. Classical Lewis pairs (black curve) only possess a datively bound deep minimum. FLPs (blue and red curves) exhibit a preorganized active form, which may or may not be the global minimum of the system, depending on the destabilization of the dative bond.

Thermally induced frustration, presumably a consequence of "intermediate" steric bulk, is not uncommon among the recently investigated systems. However, temperatures required to induce FLP-type reactivity may vary significantly; a couple of experimental examples are collected in Figure 4.26. It is also apparent from this figure that the concept of thermal induction may also cover situations where the FLP-type reactivity is quenched reversibly but in a different way than simple dative adduct formation.

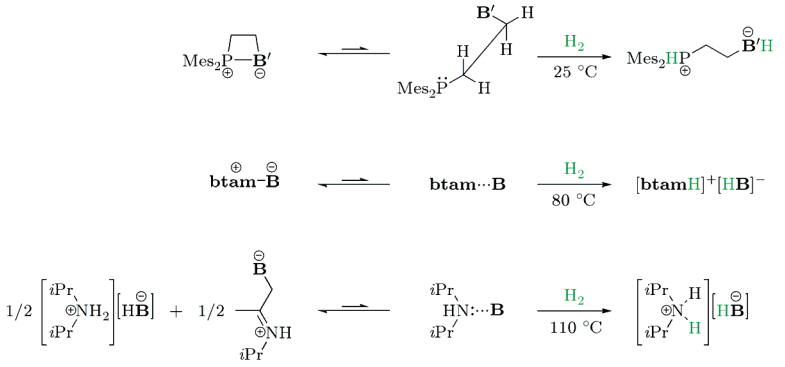

Figure 4.26: Some Lewis pairs reported to show thermally induced frustration [90, 93, 103]

4.7 Conclusions

Quantum chemical analyses on the reactivity of various frustrated pairs have been presented in this chapter. Besides our investigations on imine–borane, amine–borane hydrogen activation, and addition reactions to olefins, literature results were also summarized to provide a more complete picture of FLP-type reactivity. Our work allows the following conclusions to be drawn:

1. The model proposed for the tBu$_3$P + **B** + H$_2$ system accounts for the hydrogen splitting reactivity of **btim** + **B** and **btam**–**B** pairs.

2. Reactivity and selectivity of frustrated Lewis pairs in addition reactions with olefins can be interpreted computationally in terms of the same model. In this case, the olefin molecule may also participate in the preorganization.

3. The picture of FLP-type reactivity can be refined to involve intermediate case Lewis pairs that do not exhibit inherent but only thermally induced frustration. The temperature-dependent equilibria between the dative structure, the frustrated complex, and the dissociated components might serve as an additional possibility of fine-tuning or switching their chemical behavior.

Chapter 5

Thermodynamics of Hydrogen Splitting and the Role of Acid–Base Properties

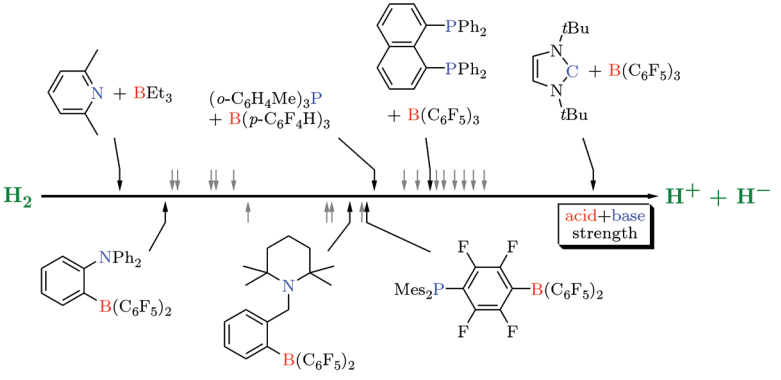

5.1 Introduction

In the previous chapters, a mechanism was presented that allows the interpretation of hydrogen splitting reactivity of ambiphilic Lewis systems as well as their reactions with other small molecules. Preorganization and reactant-state destabilization were identified as key factors in this behavior. However, a significant amount of experimental data highlights the fact that solely steric factors are not sufficient to induce the H_2 cleavage reactivity.

In one of their early studies [83], Stephan et al. investigated a series of different phosphines and boranes, and found that pairs consisting of less acidic or basic compounds are unreactive towards H_2. The authors concluded that a certain cumulative strength of the Lewis acid and base is necessary for a successful reaction.

On the other hand, Repo, Rieger et al. emphasized that it is the favorable electrostatic interaction between the charged fragments of the zwitterionic products that can "pay for the loss of the strong Heitler–London covalent bond of H_2" [102], but they also entitled the dihydrogen bonds [237] in the product as "key actors" in the hydrogen liberating process [94].

Besides the too low acid–base strength or other factors affecting the thermodynamics of the reaction, kinetic effects alone may also prevent the hydrogen cleavage by FLPs. This has been demonstrated by Erker et al. via the synthesis of phosphinoborane compounds $Mes_2P{-}CH{=}CR{-}\mathbf{B}'$, R = CH_3 or Ph, which are unreactive towards H_2 but readily accept the cleaved hydrogen from other systems (Figure 5.1) [105].

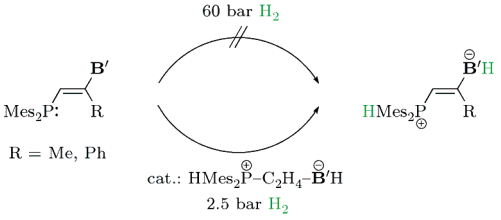

Figure 5.1: Example of a linked FLP that is kinetically unreactive towards hydrogen [105]

In the literature, thermodynamics of several hydrogen activating or releasing systems has been studied with the aim of exploring the reactivity-determining factors [238–243]. DuBois and DuBois presented an analysis of transition-metal-based systems, discussing the influence of hydride affinity and ligand basicity as well as various structural, electronic and steric effects [238]. Manners et al. investigated substituent effects in aminoborane systems via a partitioning of the reaction enthalpy comprising several hypothetical steps [239].

While keeping in mind the importance of kinetic effects, we decided to carry out a detailed computational investigation on the thermodynamics of the hydrogen splitting process by a series of frustrated Lewis acid–base pairs. We intended to assess the

importance of various factors, namely, the acid–base properties, the effects of possible dative bond formation between the donor and acceptor sites, and the stabilizing electrostatic interactions between the charged fragments of the product. Our results, presented in this chapter,* interpret the reasons for the reactivity or unreactivity of the investigated pairs, and highlight fundamental differences between the properties of linked and nonlinked systems as well.

5.2 Examined Systems and Molecular Geometries

In order to get a comprehensive picture of the thermodynamics of the H_2 splitting reactions, we included a large set of Lewis pairs in our study, for which experiments either clearly indicated hydrogenated product formation (Figure 5.2), or the absence of any reaction with H_2. The simple, nonlinked D + A combinations of the donor and acceptor compounds and the linked donor–acceptor (D∼A) systems we have considered in our study are listed in Table 5.1, together with the experimental results. Besides the FLPs introduced in Chapter 1, we also carried out calculations for $Ph_2N{-}C_6H_4{-}\mathbf{B}'$ (Figure 4.12 on page 60), which was synthesized by Piers et al. prior to the first successes in this field [41]. As mentioned earlier, this latter compound was intended to be potential hydrogen storage device, but the authors did not succeed in the preparation of the hydrogenated form, which they attributed to the low basicity of the triaryl-substituted nitrogen atom.

As indicated in Table 5.1, we adopted the experimentally found stable forms (datively bound or unbound) of the cooperative Lewis acid–base systems on the reactant side. Geometries of the free Lewis acids and bases possess no remarkable features. Our calculations agree well with reported X-ray crystal structures for the $Me_3P{-}\mathbf{B}$ [42] and $Ph_3P{-}\mathbf{B}$ [43] adducts. In particular, the nearly eclipsed conformation around the P−B bond is reproduced well in the calculations [19].

For the nonlinked pairs, the product was treated as a solvated cation–anion pair $[DH]^+[HA]^-$. Geometry optimizations of the product molecules were performed from initial structures having the D−H and H−A bonds oriented toward each other, which may give rise to D−H···H−A-type dihydrogen bonds. This procedure indeed gave structures with H···H distances around 1.5−2.0 Å, with the protonic hydrogen pointing towards the hydride, or (if steric factors allow it) towards the H−B σ-bond. A single exception is the $[\mathbf{carb}H]^+[H\mathbf{B}]^-$ product, where the C−H moiety of $[\mathbf{carb}H]^+$ is not expected to be a good hydrogen bond donor, and the orientation of the molecules confirm that other types of intermolecular interactions stabilize a geometry without a dihydrogen bond.

Although the suggested mechanism of heterolytic H_2 splitting makes it probable that an intermediate with dihydrogen-bonded arrangement is formed first, further stabilization via isomerization may not be excluded. Such process was indeed observed by NMR spectroscopy in the case of **tmp** + **B** [93]. Furthermore, the calculated

*The material discussed in this chapter was published in our paper [5].

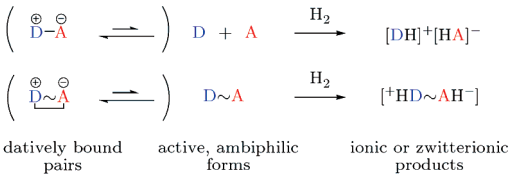

Figure 5.2: General equations of hydrogen splitting by FLPs

Entry	Reactant(s)	Reaction occurs experimentally?	Reference
nonlinked FLPs (D + A)			
1	tBu$_3$P + **B**	yes	[83]
2	Mes$_3$P + **B**	yes	[83]
3	(C$_6$F$_5$)$_3$P + **B**	no	[83]
4	tBu$_3$P + BPh$_3$	yes	[83]
5	Mes$_3$P + BPh$_3$	no	[83]
6	tBu$_3$P + BMes$_3$	no	[83]
7	Ph$_3$P–**B**	no	[83]
8	Me$_3$P–**B**	no	[83]
9	**naph** + **B**	yes, reversibly	[86]
10	tBu$_3$P + B(p-C$_6$F$_4$H)$_3$	yes	[87]
11	(o-C$_6$H$_4$Me)$_3$P + B(p-C$_6$F$_4$H)$_3$	yes, reversibly	[87]
12	Cy$_3$P + B(p-C$_6$F$_4$H)$_3$	yes	[87]
13	(o-C$_6$H$_4$Me)$_3$P + **B**	yes	[87]
14	**carb** + **B**	yes	[96, 97]
15	**diim** + **B**	yes	[90]
16	**tmp** + **B**	yes	[93]
17	**tmp** + BPh$_3$	no	[93]
18	**btam**–**B**	yes	[90]
19	**lut** + BEt$_3$	no	[95]
20	**lut**–**B**	yes	[95]
linked FLPs (D∼A)			
21	Mes$_2$P–C$_6$F$_4$–**B′**	yes, reversibly	[80]
22	tBu$_2$P–C$_6$F$_4$–**B′**	yes	[76, 90, 107]
23	Mes$_2$P–C$_2$H$_4$–**B′**	yes	[103]
24	tBu$_2$P–C$_2$HMe–**B′**	yes	[105]
25	**tmp**–CH$_2$–C$_6$H$_4$–**B′**	yes, reversibly	[102]
26	Ph$_2$N–C$_6$H$_4$–**B′**	no	[41]
27	tBu$_2$P–**B′**	yes	[106]

Table 5.1: Reactions of Lewis pairs with H$_2$. Notations of compounds can be found in Figures 1.13–1.15 on page 10.

dihydrogen-bonded structure does not correspond to the arrangement found in crystalline phase in the cases of Cy_3P + B(p-$C_6F_4H)_3$ [87], **tmp** + **B** [93] and **carb** + **B** [96,97] pairs. However, as the structure in solution is largely unknown, and for the sake of comparison, the reported energetics refers to the structures optimized from the D−H···H−A arrangement for all $[DH]^+[HA]^-$ compounds.

The products of the linked systems were treated as solvated single zwitterionic species $[^+HD{\sim}AH^-]$. Their calculated structures are in agreement with the available crystallographic data.

The M05-2X/6-311++G**//M05-2X/6-31G* density functional level of theory was used to obtain the results presented in this chapter. Solvation effects were addressed via the IEF-PCM model.

5.3 Overall Thermodynamics

To address the thermodynamic feasibility of the H_2 cleavage reaction, we first calculated the overall solvent-phase Gibbs free energies (ΔG) of the H_2 activation for the investigated D + A and D∼A systems (see reactions in Figure 5.2).

In all calculations, toluene was used as a solvent since the majority of experiments were carried out in this reaction medium, and using the same solvent for the entire series of reactions allowed us to examine the trends systematically. The results obtained with the actually used solvents (see Table 5.2) confirm that reaction free energies are only altered by a few kcal mol^{-1} with this choice, and none of our conclusions are affected.

Lewis pair	Toluene	Actual solvent	
naph + **B**	−2.1	−2.5	(benzene*)
tBu$_3$P + B(p-$C_6F_4H)_3$	−13.5	−16.2	(bromobenzene**)
(o-C_6H_4Me)$_3$P + B(p-$C_6F_4H)_3$	−0.1	−3.0	(bromobenzene**)
Cy_3P + B(p-$C_6F_4H)_3$	−9.4	−11.3	(bromobenzene**)
(o-C_6H_4Me)$_3$P + **B**	−1.4	−4.3	(bromobenzene**)
Mes$_2$P−C_2H_4−**B′**	−2.3	−1.4	(pentane***)
Ph_2N−C_6H_4−**B′**	7.1	5.5	(dichloromethane)

*The H_2 splitting was done in toluene, and the reverse reaction was observed in benzene.

**No PCM parameters were available, chlorobenzene was used in the calculations.

***No PCM parameters were available, heptane was used in the calculations.

Table 5.2: Solution-phase Gibbs free energies of various H_2 splitting reactions, calculated in toluene and in the actually used solvent. Values are given in kcal mol^{-1}.

The computed solvent-phase ΔG data of the investigated Lewis pairs are presented on an energy scale shown in Figure 5.3. It is apparent from these results that the calculated free energies vary in a remarkably wide range (from -40 to $+30\,\mathrm{kcal\,mol^{-1}}$). All systems that were shown to be unreactive experimentally are characterized by positive ΔG values typically above $+10\,\mathrm{kcal\,mol^{-1}}$, which suggests that the absence of the H_2 cleavage can be attributed to the thermodynamically unfavorable nature of these reactions. On the other hand, for all reactive systems but one, we obtained free energy values that are slightly, or in some cases well below zero. The exception is the $t\mathrm{Bu_3P}$ + $\mathrm{BPh_3}$ pair, which was found to be reactive, yet the calculated $\Delta G = +18.2\,\mathrm{kcal\,mol^{-1}}$ clearly falls into a region of several non-reactive systems. This sharp contradiction between theory and experiment will be commented on later.

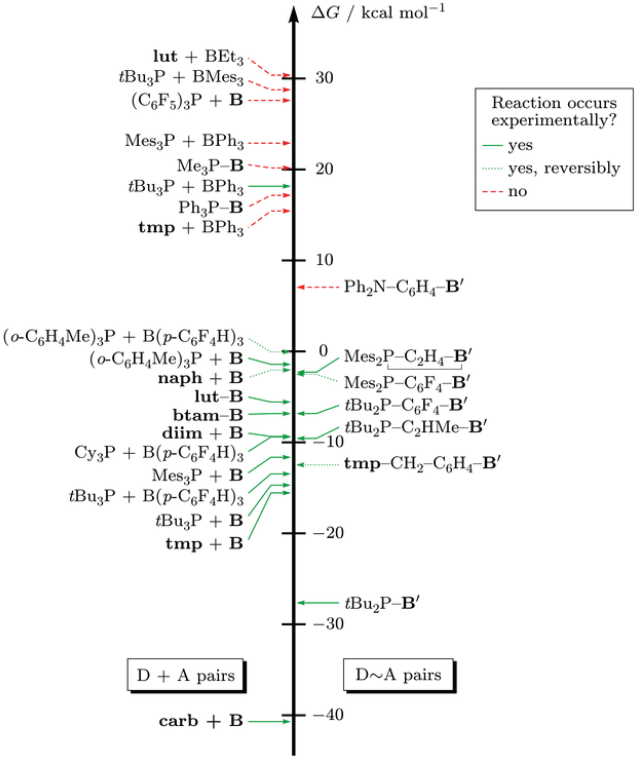

Figure 5.3: Calculated solvent-phase Gibbs free energies for the hydrogen splitting reaction of Lewis pairs

Some of the FLPs listed in Table 5.1 are known to activate H_2 reversibly (entries 9, 11, 21, 25), i.e., they lose H_2 and re-form the original compounds upon exposure to heat or/and reduced pressure. Although these nonequilibrium conditions are not taken into account in our present theoretical approach, one expects that reversible FLP/H_2 systems are slightly exergonic in the direction of H_2 uptake at standard conditions. The calculated free energies for the (o-$C_6H_4Me)_3P$ + $B(p\text{-}C_6F_4H)_3$ and **naph** + **B** pairs (-0.1 and $-2.1\,\mathrm{kcal\,mol^{-1}}$) are in good accordance with this expectation. The agreement is still acceptable for the tBu$_2$P$-$C$_6$F$_4-$**B′** + H_2 reaction ($\Delta G = -2.5\,\mathrm{kcal\,mol^{-1}}$), but the computed Gibbs free energy for H_2 splitting with the **tmp**$-$CH$_2-$C$_6$H$_4-$**B′** "molecular tweezer" [102] seems too low ($\Delta G = -12.5\,\mathrm{kcal\,mol^{-1}}$). This apparent contradiction could probably be attributed to the uncertainties of the applied methodology and additional efforts will be required for comprehensive understanding.

5.4 Partitioning of the Overall Free Energy

To understand the origin of the remarkable differences between the free energies of the various reactions, we partitioned the hydrogen splitting reaction into five hypothetical, but chemically meaningful steps. The primary motivation behind this partitioning was to include quantitative measures of the acidity and basicity of the reacting Lewis centers, which were suggested by the Stephan group to play an essential role in determining the reactivity [83]. As mentioned in Chapter 1, no single acidity or basicity scale is appropriate to cover all possible Lewis acid–base interactions, but for the present purpose, the Gibbs free energies of proton and hydride attachments to the donors and acceptors represent an adequate choice. These two quantities form the basis of the partitioning, which were supplemented by additional terms that were chosen to be as simple as possible yet to sum up to the overall free energy of the hydrogen splitting. The general partitioning scheme is presented in Figure 5.4a, whereas the thermodynamic cycles associated with the hydrogenation reactions of D + A and D∼A Lewis pairs are shown in Figures 5.4b.

According to the energy decomposition we propose, the first step of the thermodynamic cycle is the heterolytic cleavage of dihydrogen into H^+ and H^- ions in toluene. This is a rather endergonic process with a calculated free energy of $\Delta G_{\mathrm{HH}} = +128.8\,\mathrm{kcal\,mol^{-1}}$, which is constant for all FLPs. For most of the examined systems, where no dative bond between the Lewis centers exists in equilibrium, this is the only step uphill in free energy. However, if the active sites are quenched, an additional amount of free energy (ΔG_{prep}) is required to break the intra- or intermolecular dative bonds, so that the donor and acceptor centers become *prepared* to receive the H^+ and H^- ions.

For the nonlinked systems, we adopted the Gibbs free energies of the *attachment of a proton* (ΔG_{pa}) and a *hydride ion* (ΔG_{ha}) to the donor or acceptor molecules as the following two terms of the partitioning. As a consequence, the final, *stabilization*

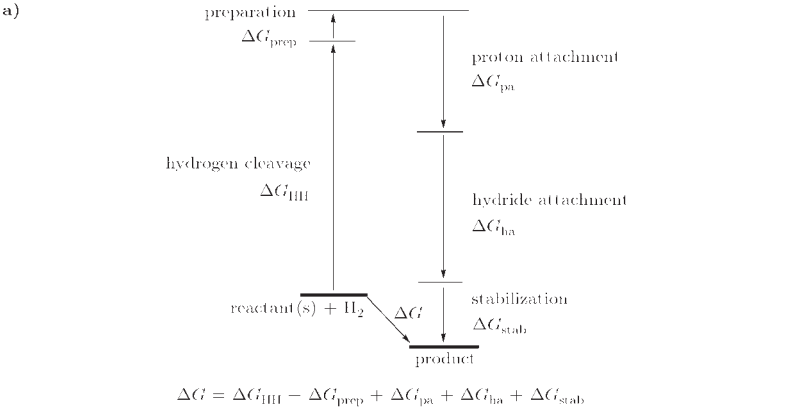

Figure 5.4: Partitioning scheme of the reaction free energy (a) and the associated thermodynamic cycles for nonlinked and linked pairs (b). Reaction steps shown in gray refer to FLPs forming dative bonds in equilibrium.

step corresponds to the formation of the product ion pair from the separated $[DH]^+$ and $[HA]^-$ ions (see Figure 5.4b). The free energy ΔG_{stab} associated with this step is simply the binding free energy of the ion pair.

For the linked pairs, which are in fact ambiphilic molecules, the acid and base strengths of the corresponding sites are defined as the free energies of proton and hydride attachments to the D∼A compounds (ΔG_{pa} and ΔG_{ha} in Figure 5.4b). Consequently, the last step of the thermodynamic cycle is the reaction of the ionic $[HD\sim A]^+$ and $[D\sim AH]^-$ species that yields the zwitterionic $[^+HD\sim AH^-]$ product and a neutral D∼A molecule. The free energy of this step (ΔG_{stab}) is a measure of stabilizing effects arising from the acid–base cooperativity of active centers, i.e., the enhancement of Lewis acidity upon protonation of the basic site or vice versa.

5.5 Term by Term Analysis

The partitioning of the overall reaction free energy allows a quantitative assessment of the most important factors that control the thermodynamic feasibility of hydrogenation processes. We shall therefore analyze each term of the decomposition separately.

5.5.1 Preparation

One of the key elements of the FLP concept is that the steric effects of the bulky substituents preclude or weaken the dative donor–acceptor bonding giving rise to inherent or thermally induced frustration. As pointed out previously, the reactant-state destabilization decreases the activation barrier and contributes to the exothermicity of the reaction. In the present partitioning, this aspect of FLP-type H_2 activation is reflected by the fact that most of the Lewis pairs possess zero free energy of preparation, i.e., the active sites are free in equilibrium. Three reactive systems (**btam**–**B**, **lut**–**B** and $Mes_2P\underline{-C_2H_4-}\mathbf{B}'$ were calculated to have small ΔG_{prep} values ranging between 5 and 8 kcal mol^{-1} (see Table 5.3). As expected, the sterically less crowded Me_3P and Ph_3P donors form stronger dative bonds with **B**, although the calculated data suggest that the Ph_3P–**B** adduct exhibits a considerable degree of strain [121].

It is worth noting that the same partitioning of the reaction electronic energies was applied by Mo and coworkers in an independent study to assess the role of frustration via a comparison of tBu$_3$P + **B** and the hypothetical H_3P + $B(CF_3)_3$ pairs [122]. Their conclusions fully support our findings about the importance of reactant-state destabilization.

Lewis pair	ΔG_{prep} / kcal mol^{-1}
Me_3P–**B**	23.4
Ph_3P–**B**	11.1
btam–**B**	7.1
$Mes_2P\underline{-C_2H_4-}\mathbf{B}'$	5.8
lut–**B**	5.5

Table 5.3: Calculated solvent-phase preparation Gibbs free energies of some Lewis pairs. For all other investigated pairs, $\Delta G_{\text{prep}} = 0$.

5.5.2 Acid–Base Properties

The basicity of the donor compounds or donor sites of the linked systems is quantified by the Gibbs free energy of proton attachment (ΔG_{pa}, see Figure 5.5) [215]. We note that commonly used definitions of proton affinity or pK_a involve thermodynamic data of the reverse process. With the opposite sign convention used here, a more negative ΔG_{pa} value corresponds to a stronger donor ability.

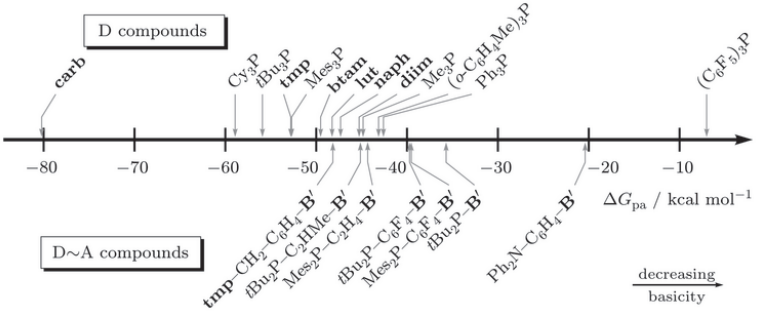

Figure 5.5: Calculated solvent-phase Gibbs free energies of the proton attachment to the Lewis donors

The calculated data reveal that most nonlinked bases with N or P donor atoms fall into a range of only about 15 kcal mol^{-1}. Despite the variety in the structures of the substituents, some trends can be clearly identified. As expected, phosphines with bulky alkyl groups are more basic than Ph_3P. The increasing basicity in the order of Ph_3P, $(o\text{-}C_6H_4Me)_3P$ and Mes_3P reflects the electronic effect of methyl substitution, whereas the introduction of electron-withdrawing substituents on the aromatic rings dramatically decrease the basicity of $(C_6F_5)_3P$. The extremely high proton affinity of base **carb** is borne out by its separation from the group of phosphines and amines on the ΔG_{pa} scale.

The relative ordering of the linked systems also lends itself easily to chemical interpretation. The three most basic compounds possess alkylamine, alkylphosphine or mesitylphosphine fragments and form a group between −49 and −44 kcal mol^{-1}. The electron-withdrawing effect of the fluorophenylene linker in $Mes_2P{-}C_6F_4{-}\mathbf{B'}$ and $t\text{Bu}_2P{-}C_6F_4{-}\mathbf{B'}$, or the directly attached $B(C_6F_5)_2$ moiety in $t\text{Bu}_2P{-}\mathbf{B'}$ notably reduces the basicity of the phosphorus. The triaryl amine fragment of $Ph_2N{-}C_6H_4{-}\mathbf{B'}$, featuring an almost completely planar nitrogen atom, has significantly diminished basicity.

The calculated acidity of the acceptor centers, measured by the Gibbs free energy of hydride attachment (ΔG_{ha}), is shown in Figure 5.6. Thermodynamic quantities pertinent to the reverse process are usually referred to as "hydride affinity" or "hydride donor ability", and they are often used to characterize Lewis acids including transition metal complexes [44–49, 238].

According to the data presented in Figure 5.6, the number of fluorine atoms on the substituents plays a quite important role in determining the acceptor strength of the boron atom. The scale starts from the strongest and the most frequently employed Lewis acid **B**. Replacement of *para*-fluorines with hydrogen atoms ($B(p\text{-}C_6F_4H)_3$) or with an R_2P fragment ($Mes_2P{-}C_6F_4{-}\mathbf{B'}$ and $t\text{Bu}_2P{-}C_6F_4{-}\mathbf{B'}$) leads to a slight

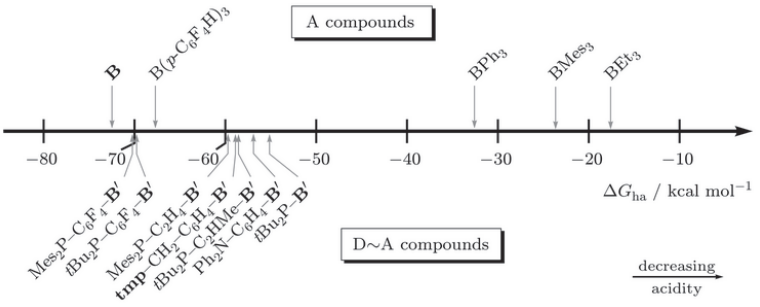

Figure 5.6: Calculated solvent-phase Gibbs free energies of the hydride attachment to the Lewis acceptors

decrease in acidity. A greater skip on the scale stems from substituting the alkyl or R_2P groups for a whole C_6F_5 ring (five D∼A compounds between −60 and −55 kcal mol^{-1}). The complete removal of the F atoms drops the acidity by ∼30−40 kcal mol^{-1} and yields remarkably lower acceptor strength for BPh_3 as compared to **B**, which is consistent with previous experimental and theoretical findings [50–53]. Among the nonfluorinated compounds (BPh_3, $BMes_3$ and BEt_3), electronic effects of the substituents easily explain the ordering.

5.5.3 Stabilization Step

The final contribution to the overall free energy of the hydrogen splitting reaction is ΔG_{stab} (recall the definition in Figure 5.4), which covers the inter- or intramolecular interaction of the charged fragments of the product. In order to assess the effect of the molecular structure on ΔG_{stab} and the significance of electrostatics, we plot the calculated data as a function of the reciprocal of the distance of the donor and acceptor atoms in the product ($d_{DA}{}^{-1}$; see Figure 5.7).

It is apparent from these results that the vast majority of the nonlinked systems can be characterized by a stabilization free energy lying in a fairly narrow range between −24 and −14 kcal mol^{-1}. The modest variation of this term originates from the structural similarity of the $[DH]^+[HA]^-$ ion pairs. In all cases, D and A bear +1 and −1 formal charges, which are shielded by bulky apolar groups, and their distance falls in the range of approximately 3.5−4.5 Å ($d_{DA}{}^{-1} = 0.22$−0.29 Å^{-1}). The stabilization in $[\mathbf{tmp}H]^+[HBPh_3]^-$ and $[\mathbf{lut}H]^+[HBEt_3]^-$ is stronger than the average, which can be related to the weaker steric repulsion owing to the small size of the constituent molecules.

The reduced ΔG_{stab} values obtained for the $[Ph_3PH]^+[H\mathbf{B}]^-$, $[\mathbf{naph}H]^+[H\mathbf{B}]^-$ and $[Cy_3PH]^+[HB(p\text{-}C_6F_4H)_3]^-$ products are due to better accessibility of the P−H bond by the solvent in the phosphonium cations, as compared to product ion pairs. While the

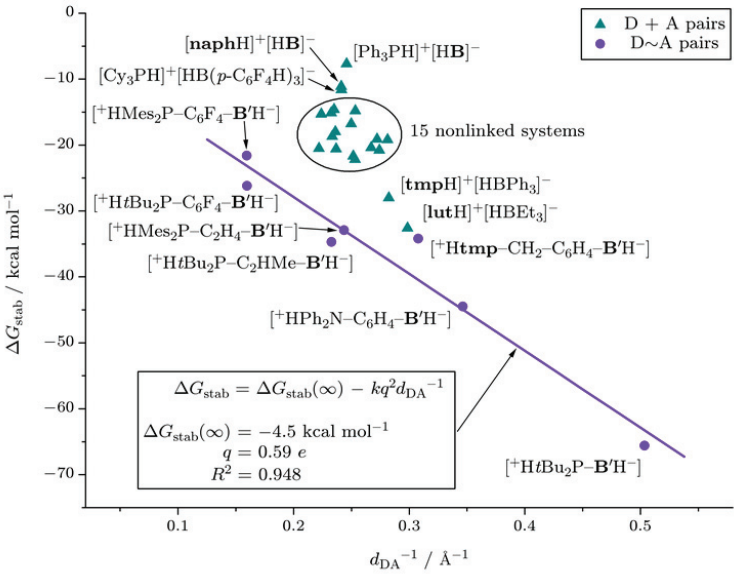

Figure 5.7: Calculated solvent-phase stabilization Gibbs free energies of the products of the hydrogen splitting reactions, plotted as a function of the reciprocal of the distance of the donor and acceptor atoms in the product ($d_{DA}{}^{-1}$). Linear fit of linked systems corresponds to the Coulomb interaction of q point charges at distance d_{DA}.

P−H bonds of these three cations are readily accessible by the solvent (Figure 5.8a), this unit is shielded in the product ion pairs, and the stabilization step therefore yields a decrease in the solvation stabilization. In other systems such as $[t\mathrm{Bu_3PH}]^+$, $[(o\text{-}\mathrm{C_6H_4Me})_3\mathrm{PH}]^+$ and $[\mathrm{Mes_3PH}]^+$, the methyl groups hinder the solvation already in the phosphonium cation (Figure 5.8b), and the variation in solvation is smaller upon ion pair formation.

According to Figure 5.7, no clear correlation between ΔG_{stab} of the nonlinked systems and $d_{DA}{}^{-1}$ can be observed. Although the gas-phase stabilization electronic energies do exhibit a notable linear relationship with $d_{DA}{}^{-1}$ (see Figure 5.9), the damping effect of the solvent renders this correlation completely undetectable in the solvent-phase ΔG_{stab} values, partly due to the relatively small $d_{DA}{}^{-1}$ range. These figures together indicate that the interaction strength is the result of an interplay of more factors (electrostatics, dispersion, repulsion, solvation effects etc.).

The existence of intermolecular D−H···H−A dihydrogen bonds in the $[DH]^+[HA]^-$ ion pairs, which have been noted previously in several reports [86, 90, 93, 95, 117, 123]

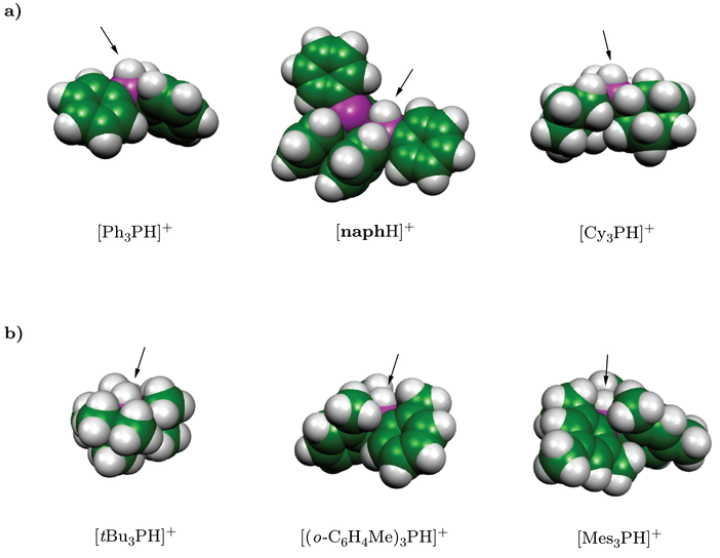

Figure 5.8: Phosphonium cations with solvent-accessible (a) and shielded (b) PH^+ units

and analyzed theoretically in this context [94, 122, 244, 245], may also contribute to the product stabilization. Indeed, we find rather short H···H contact distances (d_{HH}) in the equilibrium structures of the $[DH]^+[HA]^-$ species, typically in the 1.5−1.9 Å range, but interestingly, a correlation is absent between the stabilization energies and d_{HH} for the investigated systems, both in the solvent and in gas phase. These results suggest that the formation of dihydrogen bonds in H_2 splitting processes is not a major factor for favorable energetics. This is further supported by the results obtained for two isomers of the $[Cy_3PH]^+[HB(p\text{-}C_6F_4H)_3]^-$ product ion pair, which indicate that the structure characterized by a rather short dihydrogen bond ($d_{HH} = 1.54$ Å) is notably less stable (by 4.5 kcal mol^{-1}) than that corresponding to the X-ray data [87]. In the latter structure, the P−H and B−H vectors are aligned into the same direction, however, the noncovalent Cy···aryl contacts give rise to considerable stabilization (see Figure 5.10).

Figure 5.7 reveals that the linked systems tend to have more favorable stabilization free energies than the nonlinked pairs, which can partly be attributed to the difference in the stoichiometry of the stabilization step (see Figure 5.4). This step of the thermodynamic cycle involves entropy loss for nonlinked systems due to the ion association, whereas the number of molecules does not vary in the stabilization step of linked pairs. In the present partitioning, this step accounts for the different entropy changes of the overall reactions, which represents a fundamental difference between

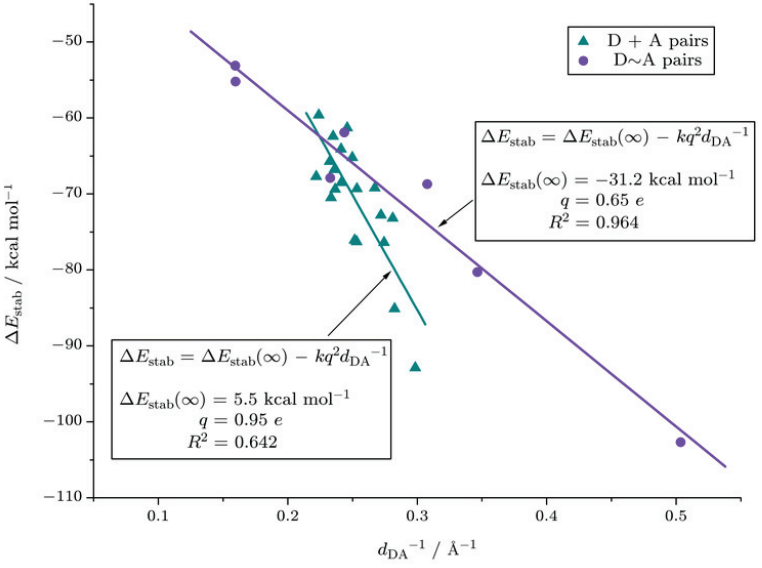

Figure 5.9: Calculated stabilization electronic energies of the products of the hydrogen splitting reactions, plotted as a function of the reciprocal of the distance of the donor and acceptor atoms in the product ($d_{DA}{}^{-1}$). Linear fits correspond to the Coulomb interaction of q point charges at distance d_{DA}.

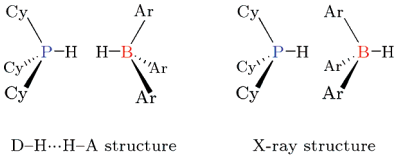

Figure 5.10: Two product isomers of $[Cy_3PH]^+[HB(p\text{-}C_6F_4H)_3]^-$

the two families of FLPs.* We furthermore find that the ΔG_{stab} values of linked FLPs vary in a broader energy interval than those of the D + A pairs, and their trends are consistent with a simple electrostatic interpretation (see Figure 5.7). The directly linked $t\mathrm{Bu}_2\mathrm{P}{-}\mathbf{B}'$ molecule is of course a unique case owing to the short P−B distance, however, the Coulomb stabilization in the anticipated hydrogenation product of the *ortho*-phenylene bridged aminoborane ($[^{+}\mathrm{HPh}_2\mathrm{N}{-}\mathrm{C}_6\mathrm{H}_4{-}\mathbf{B}'\mathrm{H}^{-}]$) with $d_{\mathrm{NB}} = 2.88\,\text{Å}$ is still significant. The stabilizing effect is reduced gradually with increasing intramolecular d_{DA} separations, and ΔG_{stab} is calculated to be about −25 to −20 kcal mol^{-1} for p-$\mathrm{C}_6\mathrm{F}_4$-linked products. One can conclude from these results that the intramolecular distance of the active sites has a significant and well-defined effect on the acid–base cooperativity and the variations in this term can easily exceed those found in the ion pair binding energies of nonlinked pairs.

5.6 Assessment of the Role of Acid–Base Properties

Inspecting the magnitude of the overall reaction free energies and their constituent terms we see that all three negative contributions (proton attachment, hydride attachment and stabilization terms) are essential to obtain exergonic hydrogenation processes. Among these factors, the acid–base properties are found to show the largest diversity for the series of investigated compounds. In order to correlate the cumulative acid–base strength of Lewis pairs with the thermodynamics of H_2 splitting reactions, we plotted the overall reaction free energies as a function of $\Delta G_{\mathrm{pa}} + \Delta G_{\mathrm{ha}}$ (see Figure 5.11).

The figure clearly demonstrates that for most of the nonlinked systems studied so far, the absence of the dative bond and the near invariance of the ion pair binding energy infers decisive role for the donor–acceptor strength in determining the thermodynamic feasibility of H_2 activation. Significant deviations from the linear relationship between ΔG and $\Delta G_{\mathrm{pa}} + \Delta G_{\mathrm{ha}}$ can be attributed either to the formation of dative bonds (e.g. $\mathrm{Me}_3\mathrm{P}{-}\mathbf{B}$ and $\mathrm{Ph}_3\mathrm{P}{-}\mathbf{B}$) or to unusually large ion pair binding energies (e.g. **lut** + BEt_3 and **tmp** + BPh_3), emphasizing the importance of these factors in particular cases. For the datively bound $\mathrm{Me}_3\mathrm{P}{-}\mathbf{B}$ and $\mathrm{Ph}_3\mathrm{P}{-}\mathbf{B}$ systems, the cumulative acid–base strengths are comparable to those obtained for several reactive pairs, but the ΔG_{prep} terms lead to notable endergonicities.

For most of the reactive D + A pairs, the calculated $\Delta G_{\mathrm{pa}} + \Delta G_{\mathrm{ha}}$ values fall between −130 and −110 kcal mol^{-1} and these systems are combinations of bulky P and N donors with strong Lewis acids (**B** or $\mathrm{B}(p\text{-}\mathrm{C}_6\mathrm{F}_4\mathrm{H})_3$). The reaction free energies for these D + A pairs are predicted to be between −15 and 0 kcal mol^{-1}. The most exergonic systems in this group involve strong bases (**tmp** and $t\mathrm{Bu}_3\mathrm{P}$) combined with **B**, which indicates that further electronic modifications in the perfluoroaryl groups of **B** can be carried out while still retaining the exergonic character of H_2 splitting reactions. The **carb** + **B** combination is characterized by particularly

*Eleven translational or rotational degrees of freedom are converted to internal motions in the D + A + H_2 → $[\mathrm{DH}]^{+}[\mathrm{HA}]^{-}$ reaction, while only five are affected in D∼A + H_2 → $[^{+}\mathrm{HD}{\sim}\mathrm{AH}^{-}]$.

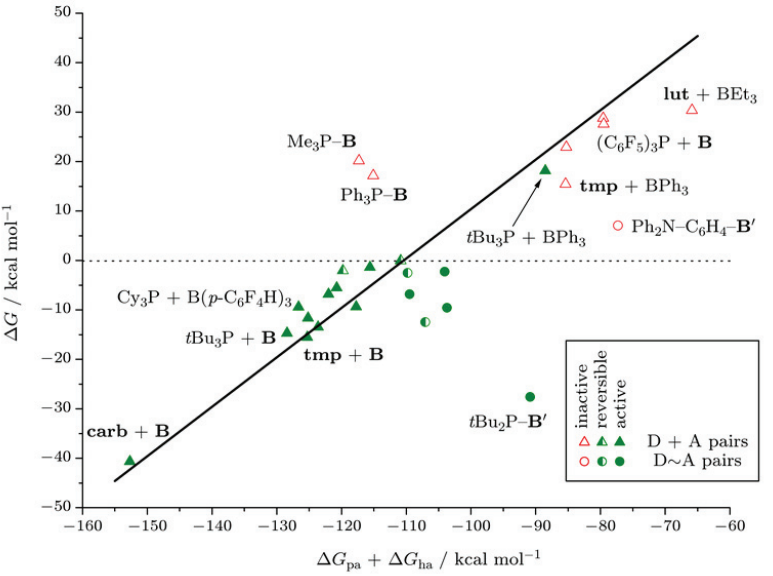

Figure 5.11: Overall Gibbs free energy of the reactions plotted as a function of the cumulative acid–base strength. The straight line was drawn using $\Delta G_{\text{prep}} = 0$ and the mean ΔG_{stab} of the nonlinked systems ($-18.4\,\text{kcal mol}^{-1}$).

enhanced cumulative acid–base strength, which however suggests that bulky carbenes or analogous compounds might be used successfully to activate H_2 in conjunction with Lewis acceptors considerably less acidic than **B**. At the other limit of the $\Delta G_{\text{pa}} + \Delta G_{\text{ha}}$ scale, the D + A pairs involve either boranes with significantly reduced acidities (BPh_3, $BMes_3$ and BEt_3), or the electron deficient $(C_6F_5)_3P$ phosphine, and accordingly, the H_2 splitting reactions are predicted to be thermodynamically unfavorable.

As noted before, the calculated $\Delta G = +18.2\,\text{kcal mol}^{-1}$ for the $t\text{Bu}_3\text{P}$ + BPh_3 pair, which belongs to this group of D + A pairs as well, contradicts with experimental findings [83]. The systematic trends revealed in our study for the reaction free energies and the agreement found for all other investigated reactions suggest that revision of the experimental data might be necessary in this particular case.

Although a much smaller number of linked systems were investigated in our study, a few general observations can be made from the data presented in Figure 5.11. As discussed above, lower entropic cost is associated with the hydrogen splitting in linked systems as compared to nonlinked pairs. As a consequence, smaller cumulative acid–base strength is generally sufficient to render a linked system thermodynamically

feasible. This is apparent from the $\Delta G_{\mathrm{pa}} + \Delta G_{\mathrm{ha}}$ values obtained for the reactive D∼A systems, which are all between −110 and −90 kcal mol^{-1}. Another important observation is that no clear correlation between the overall free energy and the cumulative acid–base strength can be established for the investigated linked pairs, which is due to larger variations in the ΔG_{stab} components as pointed out in the previous section. This feature provides an additional degree of freedom to control the thermodynamics of H_2 splitting reactions. It is interesting to note in this regard that the unreactive nature of the $Ph_2N{-}C_6H_4{-}\mathbf{B}'$ system indeed stems from the low basicity of the N atom as pointed out by Piers et al. [41], but despite the unfavorable acid–base properties, the calculated $\Delta G = +7.1$ kcal mol^{-1} is surprisingly low owing to unusually high stabilization free energy. These results indicate that *o*-phenylene bridged donor–acceptor pairs could be promising candidates in future developments.

5.7 Conclusions

We considered a series of experimentally described FLP systems, and carried out quantum chemical calculations to characterize the thermodynamics of the hydrogen activation reactions. A partitioning of the reaction free energy was also introduced to help the separation of various influencing factors. The main conclusions of the work presented in this chapter can be summarized as follows:

1. Among the systems we studied, the absence of reactivity towards H_2 originates from the unfavorable thermodynamics of the processes.

2. Acidity, basicity, and product stabilization (either as ion pair binding energy or as intramolecular cooperativity) are all important aspects of these reactions that should be considered to overcome the energetic cost of the heterolytic H−H bond splitting, and in particular cases, the cleavage of the donor–acceptor bonds. The overall reaction energy is the result of these five terms, four of which can, in general, be tuned by varying the molecular structure.

3. Nonlinked Lewis pairs that do not form dative bond in equilibrium show good correlation between cumulative acid–base strength and the overall reaction free energy due to the similar structure of the products. In contrast, the remarkable variation of the intramolecular cooperativity in linked systems may easily become a decisive factor in reactivity.

4. Linked systems lose less entropy when reacting with H_2 than do unbound, nonlinked systems. As a consequence, smaller acid–base strength and stabilization may be sufficient to produce reactive compounds.

Chapter 6

Metal-Free Hydrogenation Catalysis

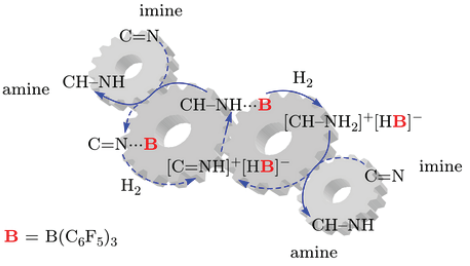

6.1 Introduction

We have so far presented studies on the cleavage of the hydrogen molecule by several FLPs, including analyses of the mechanism and the reactivity-determining factors. However, a catalytic hydrogenation procedure involves not only activation of H_2, but also its transfer to the substrate to be reduced. In order to provide a more complete picture of FLP-based hydrogenation, we now address the quantum chemical characterization of a full catalytic cycle.

We decided to carry out this detailed computational investigation on the direct imine hydrogenation mediated by **B**. In the subsequent sections, we examine the elementary steps and intermediates of the catalytic cycle, which was suggested by Stephan and coworkers for this process. An additional, autoinductive pathway, which has emerged from our calculations, is also described. Literature results concerning related reactions are presented and discussed as well.

6.2 B-Catalyzed Imine Hydrogenation

6.2.1 Experimental Results

The research groups of Stephan [90] and Klankermayer [91] independently described that hydrogenation of bulky imines, which is a valuable transformation from a synthetic point of view [246], can be readily accomplished under mild conditions using the Lewis acid **B** as catalyst. However, the rate of the reaction strongly depended on the structure of the substrate. The highly reactive imine **btim** gave good isolated yields of the **btam** product in only 2 hours at moderate conditions (see Figure 6.1). In contrast, the strongly crowded imine **diim** showed no reaction after 48 hours at higher temperature and H_2 pressure.

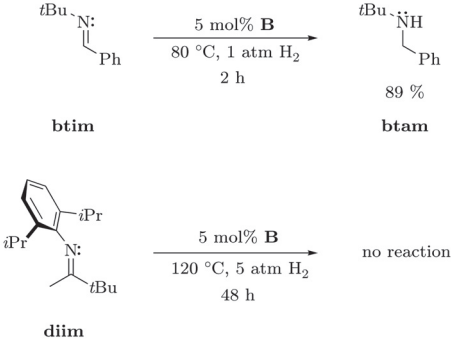

Figure 6.1: Selected experimental results on Lewis-acid-catalyzed hydrogenation of imines [90]

In an effort to garner mechanistic insight, Stephan et al. also carried out reduction experiments using stoichiometric amounts of **B** [90]. Imine **btim** readily gave the stoichiometric reduction product **btam**–**B** even at 25 °C. Upon heating to 80 °C, this dative adduct cleaved another H_2 molecule, yielding the ammonium hydridoborate product $[\mathbf{btam}H]^+[H\mathbf{B}]^-$. The more crowded imine **diim**, which showed no reaction in the catalytic system, gave the iminium hydridoborate $[\mathbf{diim}H]^+[H\mathbf{B}]^-$ under stoichiometric conditions, thereby corroborating the role of this ion pair as a mechanistically relevant intermediate (see Figure 6.2). These results led Stephan et al. to formulate the catalytic cycle already introduced in Chapter 1. This cycle involves hydrogen splitting by the imine–borane pair, hydride transfer to the activated iminium yielding an amine–borane dative adduct, and dissociation of this adduct to regenerate the catalyst (recall Figure 1.24a on page 16).

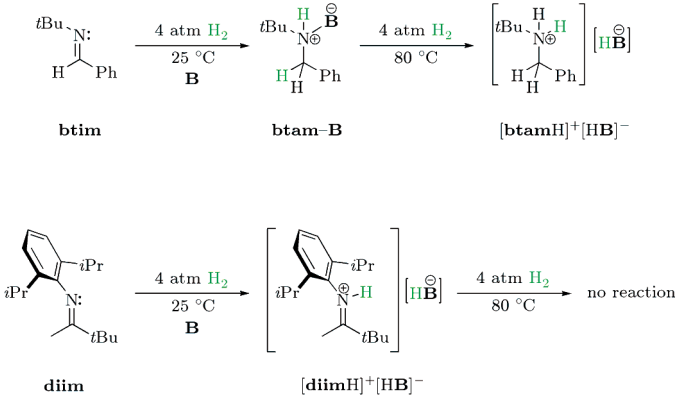

Figure 6.2: Stoichiometric reactions of imines with **B** and H_2 [90]

6.2.2 Elementary Steps of the Reaction*

A quantum chemical analysis of the hydrogen splitting by the **btim** + **B** and **btam**–**B** systems was already presented in section 4.3.2 (page 55). As described there, reactivity of these Lewis pairs towards hydrogen is readily interpreted in terms of **btim**···**B** and **btam**···**B** frustrated complex formation, followed by concerted reactions with H_2 to yield the $[\mathbf{btim}H]^+[H\mathbf{B}]^-$ and $[\mathbf{btam}H]^+[H\mathbf{B}]^-$ ion pairs. Therefore, we can now turn our attention to the reduction step, the hydride transfer to an imine molecule. The results presented here were obtained from SCS-MP2/cc-pVTZ//M05-2X/6-31G* calculations.

*Results in this section were published as part of our paper [3].

Experimental observations for a number of related systems indicate that hydride attack on the imine is only possible if the imine is activated, generally via protonation or Lewis adduct formation on the nitrogen atom [107,145,232]. Our calculations are in agreement with this finding, as we found that the reaction electronic energy of hydride transfer from $[\mathbf{HB}]^-$ to unactivated **btim** is as high as $\Delta E = 83.1\,\mathrm{kcal\,mol^{-1}}$. Considering the absence of a stable **btim**–**B** adduct, hydride transfer in $[\mathbf{btimH}]^+[\mathbf{HB}]^-$ is indeed the only pathway for the reduction that seems feasible. Our results for the reaction of $[\mathbf{btimH}]^+[\mathbf{HB}]^-$ are summarized in Figure 6.3 in the form of an energy diagram obtained for the explored reaction route. The structures of the identified stationary points are depicted in Figure 6.4 (also recall Figures 4.8, 4.9, 4.10 on page 58).

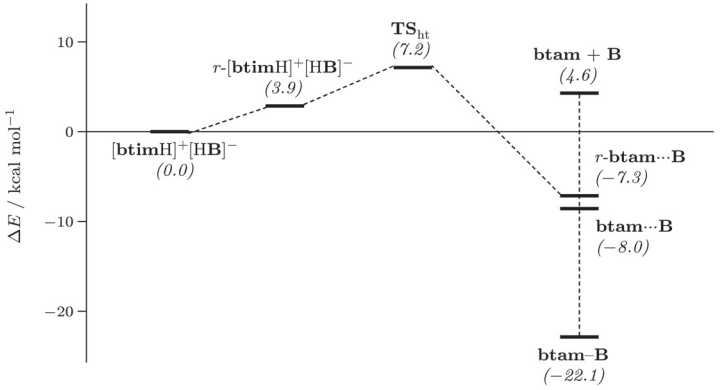

Figure 6.3: Electronic energy profile for the hydride transfer in the $[\mathbf{btimH}]^+[\mathbf{HB}]^-$ ion pair, calculated at the SCS-MP2/cc-pVTZ//M05-2X/6-31G* level of theory

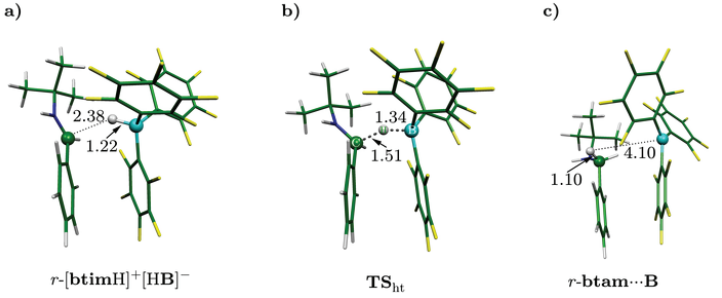

Figure 6.4: Optimized geometries of the stationary points along the hydride transfer process

The most stable, dihydrogen-bonded structure of the $[\mathbf{btim}H]^+[HB]^-$ ion pair does not allow direct hydride transfer, the reduction is thus initiated by an internal rearrangement. This step gives an isomer (r-$[\mathbf{btim}H]^+[HB]^-$) wherein the B−H bond points toward the unsaturated carbon atom of the iminium. The hydride transfer in r-$[\mathbf{btim}H]^+[HB]^-$ occurs via $\mathbf{TS}_{ht}$ with a rather low overall activation energy, which is in agreement with the expectations for a reaction that is rapid at room temperature. In contrast to the suggestion of Stephan et al. [90], the primary product of the exothermic reduction step is a *weakly bound* amine–borane complex. As its geometry markedly differs from the preorganized **btam**···**B** frustrated complex, we denote this isomer as r-**btam**···**B**. The binding energy of the r-**btam**···**B** species is $-11.9\,\mathrm{kcal\,mol^{-1}}$ with respect to **btam** + **B**, which means that it is only marginally less stable than **btam**···**B** ($-12.6\,\mathrm{kcal\,mol^{-1}}$). Depending on the reaction conditions, the formed r-**btam**···**B** can collapse to the datively bound **btam**−**B**, or dissociate to **btam** + **B**. An isomerization to the active **btam**···**B** form is also feasible.

For a comparison, we also calculated the barrier of hydride transfer in the $[\mathbf{diim}H]^+[HB]^-$ ion pair, formed from the more crowded imine **diim**. The obtained activation energy ($24.7\,\mathrm{kcal\,mol^{-1}}$) is significantly higher than for $[\mathbf{btim}H]^+[HB]^-$ ($7.2\,\mathrm{kcal\,mol^{-1}}$), which is in agreement with experiments showing that the hydrogenation reaction stops at the $[\mathbf{diim}H]^+[HB]^-$ species.

6.2.3 Possible Catalytic Cycles*

Our computational results described up to this point provided us with a firmly established picture of the key steps of the imine hydrogenation reaction. We shall now discuss how these elementary steps are combined in a catalytic process. To monitor the kinetic and thermodynamic feasibility of the reaction steps, we present solvent phase Gibbs free energy data in this section, calculated for imine **btim** using the experimentally applied conditions ($T = 80\,^\circ\mathrm{C}$, $p = 1\,\mathrm{atm}$).

The main steps and the free energy profile of the catalytic cycle suggested by Stephan and coworkers [90] (hereafter referred to as cycle 1) are depicted in Figure 6.5. It is apparent that the hydrogen splitting represents the rate limiting step in this cycle with an estimated activation free energy of $16.5\,\mathrm{kcal\,mol^{-1}}$. The **btim**···**B** species is predicted to lie $2.0\,\mathrm{kcal\,mol^{-1}}$ above the reactants indicating that this reactive intermediate is present only in rather low concentrations in the solution. The $[\mathbf{btim}H]^+[HB]^-$ ion pair forms in an exergonic step and gives the weakly bound r-**btam**···**B** species in a low-barrier hydride transfer process. In the last step, this complex releases the amine product and the borane catalyst via an exergonic dissociation.

It should be pointed out that as the reaction proceeds and **btam** develops in considerable amount, the free **B** catalyst is quenched in the stable amine–borane dative adduct. This implies that the free energy required to dissociate the **btam**−**B** dative bond ($7.0\,\mathrm{kcal\,mol^{-1}}$) must be included in the barrier of the rate determining step. Thus, the overall barrier of the H_2 splitting is estimated to be $23.5\,\mathrm{kcal\,mol^{-1}}$.

*This section was published as part of our paper [3].

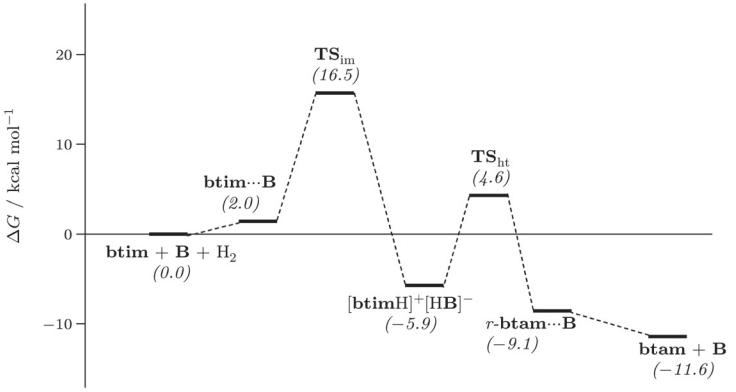

Figure 6.5: Solvent-phase Gibbs free energy profile at $T = 80\,^{\circ}\mathrm{C}$ for catalytic cycle 1

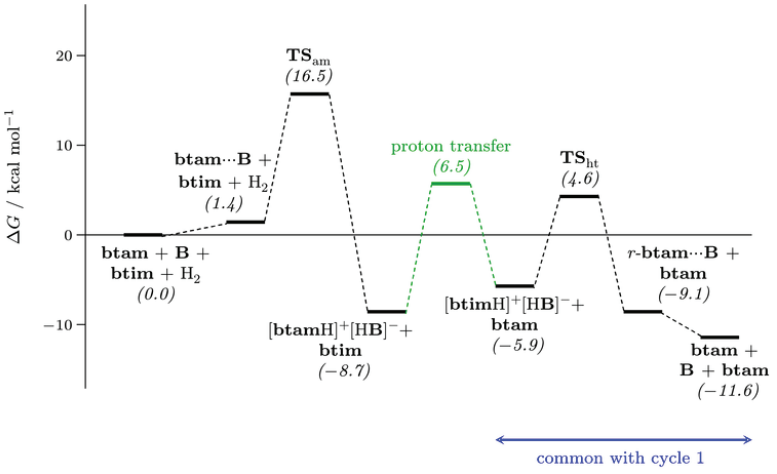

Figure 6.6: Solvent-phase Gibbs free energy profile at $T = 80\,^{\circ}\mathrm{C}$ for catalytic cycle 2. The overall barrier for the proton exchange step (shown in green) was estimated from a PES scan calculation.

On the other hand, sterically more crowded amines might not be able to quench the catalyst effectively.

The results for the hydrogen activation reactions have pointed out that the amine–borane pair **btam** + **B** is able to cleave H_2 at elevated temperatures. We envisioned that this process may also play a role in the catalytic hydrogenation of **btim**. In Figure 6.6, we display the calculated free energy profile for a catalytic pathway that can be associated with the amine–borane H_2 cleavage (cycle 2). Although not indicated in the figure, the dissociation of the **btam**−**B** adduct must be taken into account in this case as well.

The first stable intermediate of the cycle is the ammonium hydridoborate compound $[\mathbf{btam}H]^+[H\mathbf{B}]^-$, which is formed via $\mathbf{TS}_{am}$. The activation free energy of this step is almost identical to that predicted for the imine–borane pair pointing to competing reaction channels in H_2 activation.

To interpret the production of an activated imine, we thereafter considered proton exchange between the ammonium ion and the imine molecule. Our calculations confirmed that a protonation reaction, producing the free amine and the iminium hydridoborate ion pair $[\mathbf{btim}H]^+[H\mathbf{B}]^-$, is feasible. The amine–imine proton transfer is expected to take place in a ternary **btim**···$[\mathbf{btam}H]^+[H\mathbf{B}]^-$ complex (see Figure 6.7).

Although the transition state for the actual proton transfer can be easily located, a further intramolecular rearrangement is necessary to allow the dissociation of the product **btam**, leaving behind the ion pair $[\mathbf{btim}H]^+[H\mathbf{B}]^-$. Due to the size of the ternary species and the complex PES with numerous close-lying minima, we only determined an upper estimate for the barrier of this rearrangement from a PES scan, gradually decreasing a nonbonded distance between the aromatic rings of $[\mathbf{btim}H]^+$ and $[H\mathbf{B}]^-$. This rearrangement turned out to be the step determining the overall barrier of the proton exchange process.

The obtained activation free energy (15.2 kcal mol^{-1} with respect to the separated imine and ammonium hydridoborate) clearly supports that the reaction is kinetically allowed. Although the proton activation of imine in terms of the $[\mathbf{btam}H]^+[H\mathbf{B}]^-$ + **btim** → $[\mathbf{btim}H]^+[H\mathbf{B}]^-$ + **btam** reaction is slightly endergonic, the subsequent hydride transfer (via $\mathbf{TS}_{ht}$) and the dissociation of the *r*-**btam**···**B** species (already described for cycle 1) provide notable stabilization along the reaction pathway and render the overall reduction process thermodynamically feasible as well.*

These considerations suggest that cycle 1 proposed by Stephan et al. [90] can be extended by cycle 2 involving the cleavage of hydrogen via the amine–borane pair, which is followed by its transfer to the imine. The two catalytic routes form interconnecting cycles as illustrated in Figure 6.8. The catalytic process starts necessarily with cycle 1, which is based on imine-mediated heterolytic H_2 splitting, but as soon as the amine product appears in notable amount in the reaction mixture, cycle 2 represents a competing reaction pathway.

*The hydride transfer may also occur before the dissociation of the $[\mathbf{btim}H]^+[H\mathbf{B}]^-$···**btam** complex as well, yielding a weak ternary **btam**···**B**···**btam** complex.

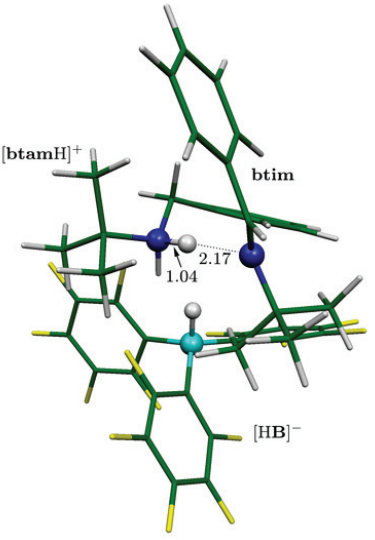

Figure 6.7: Calculated structure of the imine–ammonium-hydridoborate ternary complex, in which the proton transfer can occur

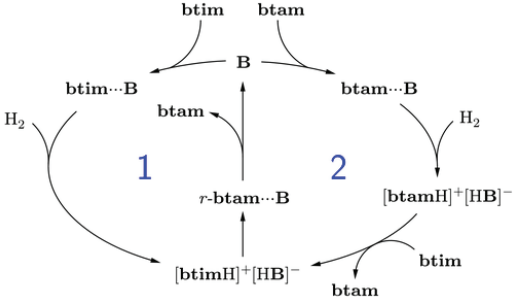

Figure 6.8: Interconnected catalytic cycles for imine hydrogenation

This second cycle bears some characteristics of an autocatalytic route, the possibility of which has been mentioned by Klankermayer et al. [91], but no details have been reported in their paper. However, the original catalyst **B** is still required for the operation of this second cycle, it is therefore better classified as an autoinductive route [247]. Cycle 2 can also be regarded as a transfer hydrogenation pathway, wherein the $[\mathbf{btam}H]^+[H\mathbf{B}]^-$ species serves as the hydrogen donor and reduces **btim** to **btam**. Similar transfer mechanism (without autoinductivity) has also been suggested by Stephan and coworkers [107] to operate in reactions where the substrate to be reduced does not readily participate in hydrogen cleavage requiring the presence of both bulky Lewis base and acid components [90, 107].

6.2.4 Related Literature Results

In an independent, later study, Privalov also analyzed the possible catalytic pathways of imine reduction mediated by **B** [123]. In addition to essentially reproducing our results, he also located the transition states for the proton and hydride transfer steps in the ternary $\mathbf{btim}\cdots[\mathbf{btam}H]^+[H\mathbf{B}]^-$ complex. His conclusions generally agree with ours, although some points are worth discussing.

An important element of our model for hydrogen splitting is the preorganization provided by secondary forces. In its absence, a termolecular collision would be required to achieve a transition state featuring acid–base cooperativity, which can hardly explain the observed high reaction rates. This consideration and the characterization of the respective frustrated complexes are completely missing from Privalov's work.

He furthermore states that the hydride transfer in $[\mathbf{btim}H]^+[H\mathbf{B}]^-$ yields directly the dative $\mathbf{btam}{-}\mathbf{B}$ adduct; this may be due the errors of the B3LYP functional applied in his calculations. As this functional fails to describe dispersion-dominated complexes, the minimum on the PES corresponding to the weakly bound r-$\mathbf{btam}\cdots\mathbf{B}$ form may be so shallow that the calculated reaction pathway misses it.

Finally, a comment concerning the applied terminology is appropriate. Privalov denotes the imine–borane based pathway (cycle 1 in Figure 6.8) as "the autocatalytic pathway". In our opinion, cycle 2 does have certain autocatalytic features (involvement of the product in the catalytic cycle), but application of this term to cycle 1 is quite misleading.

In another, related paper, Privalov et al. presented a theoretical analysis of the **B**-catalyzed hydrogenation of oxo compounds (Figure 6.9) [116]. Such reduction process has not yet been carried out experimentally; the aim of the analysis was to address the feasibility of this reaction. Due to the low basicity of the carbonyl oxygen atom and the presence of the carbonyl–borane dative bond, the hydrogen splitting step was found to be somewhat endergonic, but the subsequent hydride transfer provides thermodynamic stabilization for the product. The calculated barriers are reasonably low, and suggest that, for oxo compounds with appropriate steric encumbrance, a catalytic route similar to cycle 1 of imines can probably be realized. The possible role

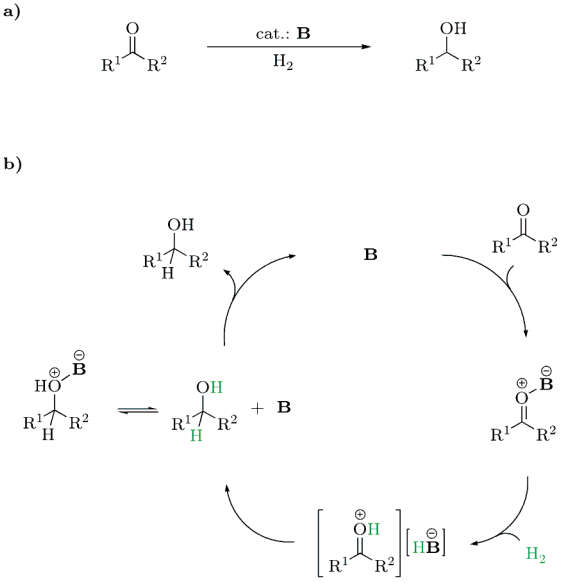

Figure 6.9: Supposed Lewis-acid-catalyzed hydrogenation of carbonyl compounds (a) and the suggested catalytic cycle (b) [116]

of the product alcohols, forming an analogue of cycle 2, was also mentioned but not analyzed in detail.

6.3 Hydrogenation via Linked Systems

In order to provide a more complete overview of catalytic hydrogenation processes by FLPs, we briefly summarize the results of two other theoretical studies [118,124], both written by Privalov, that appeared in the literature almost at the same time as our paper about imine hydrogenation by **B**. These studies are concerned with catalytic hydrogenation or hydrogen transfer processes mediated by linked phosphine–borane systems.

One of these contributions addresses the imine hydrogenation catalyzed by the *p*-C_6F_4 linked phosphonium borates (see Figure 6.10) [124]. As the mechanism of hydrogen splitting by these systems had already been investigated (see the discussion in section 4.4.1, page 56), Privalov's work was directed towards the reduction step.

The presented detailed calculations confirm that a stepwise proton and hydride transfer from [$^{+}$H*t*Bu$_2$P–C_6F_4–**B**′H^{-}] to the imine **btim**, suggested by Stephan

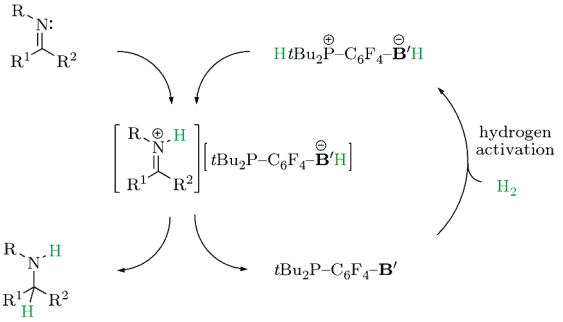

Figure 6.10: Main steps of the catalytic cycle of imine hydrogenation by linked phosphonium borates [107]

et al. on the basis of experimental results [107], are feasible. Besides emphasizing the key steps, the author highlights the possibility of alternative reaction channels. A plausible pathway, also discussed by Stephan et al. [107], involves intermolecular hydrogen activation, with the imine or the amine as Lewis base in conjunction with the boron center of $t\mathrm{Bu_2P{-}C_6F_4{-}}\mathbf{B'}$ acting as the Lewis acid. However, hydrogen splitting via the linked $t\mathrm{Bu_2P{-}C_6F_4{-}}\mathbf{B'}$ system is probably favored as it was found experimentally to be significantly faster [107]. In addition, Privalov points out that due to its high basicity, an amine molecule may mediate the proton transfer between the phosphonium center and the imine. The essential point of this discussion is that all Lewis acidic and basic centers in the solution must be considered, as they all may play a role in the mechanism.

The other Privalov study is devoted to the reaction between alcohols and the linked phosphanylboranes $\mathrm{R_2P{-}BR'_2}$, both in the forward and in the reverse directions (see Figure 6.11) [118]. Such processes have not yet been reported in the literature; the presented computational work addresses whether they may be realizable. The results show that the reactions have modest barriers, and are slightly exothermic in the direction of alcohol oxidation. The dehydrogenation of methanol was found to be almost thermoneutral. Contrary to the procedures discussed so far, a concerted hydrogen transfer mechanism is predicted (Figure 6.12), owing to the arrangement of the acidic–basic groups on $\mathrm{R_2P{-}BR'_2}$ and the acid–base properties of alcohols and oxo compounds. Transition-metal-catalyzed hydrogenation of C=O bonds were often found to proceed via similar mechanism [232].

In combination with the hydrogen activation via $\mathrm{R_2P{-}BR'_2}$, the author envisions various possible applications of the investigated reaction, such as catalytic racemization of alcohols and catalytic hydrogenation of oxo compounds. However, considering the calculated energetics, he also points out that tuning the R and R′ groups on the phosphanylborane is still necessary to obtain desirable reactivity.

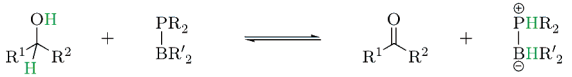

Figure 6.11: Hydrogen transfer between alcohols and linked phosphanylboranes [118]

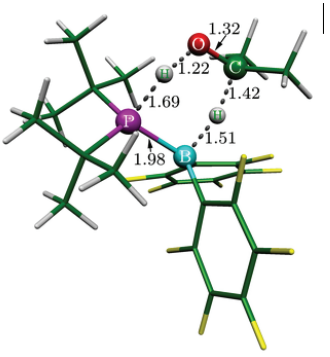

Figure 6.12: Transition state of hydrogen transfer between isopropanol and $t\mathrm{Bu_2P}-\mathbf{B'}$ [118]

6.4 Conclusions

Aiming at the comprehensive understanding of an FLP-based catalytic hydrogenation process, we carried out a computational characterization of several relevant reaction pathways and catalytic cycles of the $B(C_6F_5)_3$-mediated imine hydrogenation. To place the results in a broader scope, related works from the literature have also been presented. The main conclusions emerging from our theoretical studies can be formulated as follows:

1. The key imine reduction step, the hydride transfer, requires previous activation of the imine. It proceeds readily in the iminium hydridoborate ion pair, provided that steric bulk around the imine carbon is not prohibitively large. The primary product of this step is a weakly bound amine–borane complex.

2. The catalytic route involving imine–borane hydrogen splitting, proposed by Stephan et al., is corroborated by the calculations.

3. The reduced product amine can participate in the hydrogen activation process, and therefore opens up an alternative, autoinductive pathway. This pathway is suggested to be competitive to the imine–borane hydrogen activation route. Generally speaking, such alternatives may be important in all cases where more than a single frustrated pair is present in the reaction mixture.

Summary and Outlook

In the last few years, the chemistry of frustrated Lewis pairs underwent a spectacular development. The discovered reactions opened a new chapter in small molecule activation. Theoretical studies allowed the establishment of a reasonable mechanistic picture, which will, hopefully, contribute to the invention of improved systems. However, several questions concerning the mechanism are still open, and a number of problems hamper the widespread application of frustrated pairs. While recalling and summarizing the key results of our theoretical work, we also try to highlight some of these issues, which may eventually become future research directions.

Our studies on frustrated pairs revealed that *activation of small molecules (in particular, H_2) is attained by Lewis cooperativity. Compared to a classical Lewis pair, the energetics is made favorable by reactant-state destabilization. In intermolecular cases, complexes held together by secondary forces provide the necessary preorganized ambiphilic environment.* Nevertheless, direct experimental evidence of such preorganized assocation has not yet been presented. The contradiction between the observed first-order hydrogen loss from $[^{+}\mathrm{HMes_2P{-}C_6F_4{-}B(C_6F_5)_2H^{-}}]$ and the proposed bimolecular process is also still to be resolved.

The quest for frustrated complexes might be facilitated by computational studies that address the dynamical properties of complex formation, providing more accurate formation free energies and lifetime data. Such studies could be of particular interest in cases where dative bonds also exist.

The thermodynamics of hydrogen splitting was found to be governed by dative bond strength, acid–base properties, and the strength of intramolecular cooperation. Further investigation is still required to completely understand the reversibility, and to clear up the controversial issue of $t\mathrm{Bu_3P}$ + $\mathrm{BPh_3}$. Knowledge of the reasons for high kinetic barriers (e.g., in the case of $\mathrm{Mes_2P{-}CH{=}CR{-}B(C_6F_5)_2}$) would also be expedient for the fine-tuning of new systems.

The key step of catalytic imine hydrogenation was corroborated to be the hydride transfer to the protonated imine molecule. The hydrogen activation by various Lewis pairs in the solution, including compounds formed during the reaction, represent competitive pathways.

The wide interest in FLP chemistry is partly originated in the efforts to develop practical procedures for the catalytic activation of small molecules without transition

metals. Despite the promising results, several difficulties have yet to be tackled. The air- and moisture sensitivity of the hitherto investigated compounds, and the high catalyst loads make the procedures too complicated and expensive. Increased function group tolerance is required to allow reactions of diverse substrates, including sterically less encumbered ones. Methodology should be elaborated for chemo-, regio-, and stereoselective transformations, which are already accessible via transition metal catalysts.

The chemistry of frustrated Lewis pairs, and particularly, their applications, are still in infancy. It will be intriguing to see what directions the development will take, and how the lessons learned here will prove useful in other branches of chemistry.

References

R.1 Papers Forming the Basis of the Dissertation

[1] T. A. Rokob, A. Hamza, A. Stirling, T. Soós, I. Pápai, "Turning Frustration into Bond Activation: A Theoretical Mechanistic Study on Heterolytic Hydrogen Splitting by Frustrated Lewis Pairs", *Angew. Chem., Int. Ed.* **2008**, *47*, 2435. Highlighted in *Chemical and Engineering News* **2008**, *86*, issue 11, 42.

[2] A. Hamza, A. Stirling, T. A. Rokob, I. Pápai, "Mechanism of Hydrogen Activation by Frustrated Lewis Pairs: A Molecular Orbital Approach", *Int. J. Quantum Chem.* **2009**, *109*, 2416.

[3] T. A. Rokob, A. Hamza, A. Stirling, I. Pápai, "On the Mechanism of $B(C_6F_5)_3$-Catalyzed Direct Hydrogenation of Imines: Inherent and Thermally Induced Frustration", *J. Am. Chem. Soc.* **2009**, *131*, 2029.

[4] A. Stirling, A. Hamza, T. A. Rokob, I. Pápai, "Concerted Attack of Frustrated Lewis Acid–Base Pairs on Olefinic Double Bonds: A Theoretical Study", *Chem. Commun.* **2008**, 3148.

[5] T. A. Rokob, A. Hamza, I. Pápai, "Rationalizing the Reactivity of Frustrated Lewis Pairs: Thermodynamics of H_2 Activation and the Role of Acid–Base Properties", *J. Am. Chem. Soc.* **2009**, *131*, 10701.

R.2 Lewis Acids and Bases

[6] G. N. Lewis, *Valence and the Structure of Atoms and Molecules*, Chemical Catalogue Company, Inc., New York, **1923**.

[7] W. B. Jensen, *Chem. Rev.* **1978**, *78*, 1.

[8] I. Fleming, *Frontier Orbitals and Organic Chemical Reactions*, John Wiley & Sons, Ltd., London, **1976**.

[9] M. B. Smith, J. March, *March's Advanced Organic Chemistry, Fifth Edition*, John Wiley & Sons, Inc., New York, **2001**.

[10] For scales and methods of determination of Lewis acid or base strength, see papers [11, 12, 76] as well as references therein.

[11] S. E. Denmark, G. L. Beutner, *Angew. Chem., Int. Ed.* **2008**, *47*, 1560.

[12] W. E. Piers, *Adv. Organomet. Chem.* **2004**, *52*, 1.

[13] R. G. Pearson, *J. Am. Chem. Soc.* **1963**, *85*, 3533.

[14] R. S. Mulliken, *J. Am. Chem. Soc.* **1952**, *74*, 811.

[15] R. S. Drago, B. B. Wayland, *J. Am. Chem. Soc.* **1965**, *87*, 3571.

[16] R. S. Drago, *Coord. Chem. Rev.* **1980**, *33*, 251.

[17] H. C. Brown, H. I. Schlesinger, S. Z. Cardon, *J. Am. Chem. Soc.* **1942**, *64*, 325.

[18] H. C. Brown, *J. Chem. Soc.* **1956**, 1248.

[19] P. Spies, R. Fröhlich, G. Kehr, G. Erker, S. Grimme, *Chem. Eur. J.* **2008**, *14*, 333.

[20] G. Wittig, A. Rückert, *Liebigs Ann. Chem.* **1950**, *566*, 101.

[21] H. Meerwein, V. Hederich, H. Morschel, K. Wunderlich, *Liebigs Ann. Chem.* **1960**, *635*, 1.

[22] R. Damico, C. D. Broaddus, *J. Org. Chem.* **1966**, *31*, 1607.

[23] S. Doering, G. Erker, R. Fröhlich, O. Meyer, K. Bergander, *Organometallics* **1998**, *17*, 2183.

[24] D. W. Stephan, *Adv. Organomet. Chem.* **2006**, *54*, 267.

[25] E. Hollink, P. R. Wei, D. W. Stephan, *Organometallics* **2004**, *23*, 1562.

[26] W. Tochtermann, *Angew. Chem., Int. Ed.* **1966**, *5*, 351.

[27] W. E. Piers, T. Chivers, *Chem. Soc. Rev.* **1997**, *26*, 345.

[28] F. Focante, P. Mercandelli, A. Sironi, L. Resconi, *Coord. Chem. Rev.* **2006**, *250*, 170.

[29] G. Erker, *Dalton Trans.* **2005**, 1883.

[30] S. Bontemps, G. Bouhadir, P. W. Dyer, K. Miqueu, D. Bourissou, *Inorg. Chem.* **2007**, *46*, 5149.

[31] A. Moroz, R. L. Sweany, S. L. Whittenburg, *J. Phys. Chem.* **1990**, *94*, 1352.

[32] P. R. Schreiner, H. F. Schaefer III, P. v. R. Schleyer, *J. Chem. Phys.* **1994**, *101*, 7625.

[33] J. D. Watts, R. J. Bartlett, *J. Am. Chem. Soc.* **1995**, *117*, 825.

[34] B. S. Jursic, *J. Mol. Struct.* **1999**, *492*, 97.

[35] T. J. Tague, L. Andrews, *J. Am. Chem. Soc.* **1994**, *116*, 4970.

[36] W. A. Herrebout, B. J. van der Veken, *J. Am. Chem. Soc.* **1997**, *119*, 10446.

[37] P. Tarakeshwar, K. S. Kim, *J. Phys. Chem. A* **1999**, *103*, 9116. Erratum: *J. Phys. Chem. A* **1999**, *103*, 11486.

[38] G. Wittig, E. Benz, *Chem. Ber.* **1959**, *92*, 1999.

[39] A. Fukazawa, H. Yamada, S. Yamaguchi, *Angew. Chem., Int. Ed.* **2008**, *47*, 5582.

[40] M. E. Jacox, W. E. Thompson, *J. Chem. Phys.* **2006**, *124*, 204304.

[41] R. Roesler, W. E. Piers, M. Parvez, *J. Organomet. Chem.* **2003**, *680*, 218.

[42] P. A. Chase, M. Parvez, W. E. Piers, *Acta Crsyt.* **2006**, *E62*, o5181.

[43] H. Jacobsen, H. Berke, S. Döring, G. Kehr, G. Erker, R. Fröhlich, O. Meyer, *Organometallics* **1999**, *18*, 1724.

[44] D. J. Goebbert, P. G. Wenthold, *Int. J. Mass Spectrom.* **2006**, *257*, 1.

[45] R. Vianello, Z. B. Maksić, *Inorg. Chem.* **2005**, *44*, 1095.

[46] Z. B. Maksić, R. Vianello, *Pure Appl. Chem.* **2007**, *79*, 1003.

[47] P. R. Campodónico, A. Aizman, R. Contreras, *Chem. Phys. Lett.* **2009**, *471*, 168.

[48] X.-Q. Zhu, H. Liang, Y, Zhu, J.-P. Cheng, *J. Org. Chem.* **2008**, *73*, 8403.

[49] G. Kovács, I. Pápai, *Organometallics* **2006**, *25*, 820.

[50] A. Y. Timoshkin, G. Frenking, *Organometallics* **2008**, *27*, 371.

[51] D. J. Morrison, W. E. Piers, *Org. Lett.* **2003**, *5*, 2857.

[52] D. C. Bradley, I. S. Harding, A. D. Keefe, M. Motevalli, D. H. Zheng, *J. Chem. Soc., Dalton Trans.* **1996**, 3931.

[53] G. J. P. Britovsek, J. Ugolotti, A. J. P. White, *Organometallics* **2005**, *24*, 1685.

R.3 Applications of Ambiphilic Systems

[54] Y. Hamashima, D. Sawada, M. Kanai, M. Shibasaki, *J. Am. Chem. Soc.* **1999**, *121*, 2641.

[55] R. Noyori, M. Kitamura, *Angew. Chem., Int. Ed.* **1991**, *30*, 49.

[56] J. M. Brunel, M. Maffei, G. Buono, *Tetrahedron: Asymmetry* **1993**, *4*, 2255.

[57] V. K. Aggarwal, A. Mereu, G. J. Tarver, R. McCague, *J. Org. Chem.* **1998**, *63*, 7183.

[58] S. France, M. H. Shah, A. Weatherwax, A., H. Wack, J. P. Roth, T. Lectka, *J. Am. Chem. Soc.* **2005**, *127*, 1206.

[59] F.-G. Fontaine, J. Boudreau, M.-H. Thibault, *Eur. J. Inorg. Chem.* **2008**, 5439.

[60] I. Kuzu, I. Krummenacher, J. Meyer, F. Armbruster, F. Breher, *Dalton Trans.* **2008**, 5836.

[61] T. Y. S. But, P. H. Toy, *Chem. Asian J.* **2007**, *2*, 1340.

[62] S. Moebs-Sanchez, G. Bouhadir, N. Saffon, L. Maron, D. Bourissou, *Chem. Commun.* **2008**, 3435.

[63] S. Bräse, C. Gil, K. Knepper, V. Zimmermann, *Angew. Chem., Int. Ed.* **2005**, *44*, 5188.

[64] M. W. P. Bebbington, S. Bontemps, G. Bouhadir, D. Bourissou, *Angew. Chem., Int. Ed.* **2007**, *46*, 3333.

[65] See references in L. Zhu, S. H. Shabbir, M. Gray, V. M. Lynch, S. Sorey, E. V. Anslyn, *J. Am. Chem. Soc.* **2006**, *128*, 1222.

[66] C. Bresner, S. Aldridge, I. A. Fallis, C. Jones, L.-L. Ooi, *Angew. Chem., Int. Ed.* **2005**, *44*, 3606.

[67] D. H. Paull, C. J. Abraham, M. T. Scerba, E. Alden-Danforth, T. Lectka, *Acc. Chem. Res.* **2008**, *41*, 655.

[68] M. Kanai, N. Kato, E. Ichikawa, M. Shibasaki, *Synlett* **2005**, 1491.

[69] I. Georgiou, G. Ilyashenko, A. Whiting, *Acc. Chem. Res.* **2009**, *42*, 756.

[70] H. Grützmacher, *Angew. Chem., Int. Ed.* **2008**, *47*, 1814.

[71] T. Ikariya, K. Murata, R. Noyori, *Org. Biomol. Chem.* **2006**, *4*, 393.

[72] J.-A. Ma, D. Cahard, *Angew. Chem., Int. Ed.* **2004**, *43*, 4566.

[73] M. Shibasaki, M. Kanai, K. Funabashi, *Chem. Commun.* **2002**, 1989.

[74] H. Gröger, *Chem. Eur. J.* **2001**, *7*, 5247.

[75] G. J. Rowlands, *Tetrahedron* **2001**, *57*, 1865.

R.4 Frustrated Lewis Pairs

[76] G. C. Welch, L. Cabrera, P. A. Chase, E. Hollink, J. D. Masuda, P. Wei, D. W. Stephan, *Dalton Trans.* **2007**, 3407.

[77] J. S. J. McCahill, G. C. Welch, D. W. Stephan, *Dalton Trans.* **2009**, DOI: 10.1039/b911489k.

[78] G. C. Welch, J. D. Masuda, D. W. Stephan, *Inorg. Chem.* **2006**, *45*, 478.

[79] L. Cabrera, G. C. Welch, J. D. Masuda, P. Wei, D. W. Stephan, *Inorg. Chim. Acta* **2006**, *359*, 3066.

[80] G. C. Welch, R. R. San Juan, J. D. Masuda, D. W. Stephan, *Science* **2006**, *314*, 1124.

[81] D. W. Stephan, *Org. Biomol. Chem.* **2008**, *6*, 1535.

[82] D. W. Stephan, *Dalton Trans.* **2009**, 3129.

[83] G. C. Welch, D. W. Stephan, *J. Am. Chem. Soc.* **2007**, *129*, 1880.

[84] G. J. Kubas, *Science* **2006**, *314*, 1096.

[85] A. L. Kenward, W. E. Piers, *Angew. Chem., Int. Ed.* **2008**, *47*, 38.

[86] H. Wang, R. Fröhlich, G. Kehr, G. Erker, *Chem. Commun.* **2008**, 5966.

[87] M. Ullrich, A. J. Lough, D. W. Stephan, *J. Am. Chem. Soc.* **2009**, *131*, 52.

[88] D. P. Huber, G. Kehr, K. Bergander, R. Fröhlich, G. Erker, S. Tanino, Y. Ohki, K. Tatsumi, *Organometallics* **2008**, *27*, 5279.

[89] A. Ramos, A. J. Lough, D. W. Stephan, *Chem. Commun.* **2009**, 1118.

[90] P. A. Chase, T. Jurca, D. W. Stephan, *Chem. Commun.* **2008**, 1701.

[91] D. Chen, J. Klankermayer, *Chem. Commun.* **2008**, 2130.

[92] K. V. Axenov, G. Kehr, R. Fröhlich, G. Erker, *J. Am. Chem. Soc.* **2009**, *131*, 3454.

[93] V. Sumerin, F. Schulz, M. Nieger, M. Leskelä, T. Repo, B. Rieger, *Angew. Chem., Int. Ed.* **2008**, *47*, 6001.

[94] V. Sumerin, F. Schulz, M. Nieger, M. Atsumi, C. Wang, M. Leskelä, P. Pyykkö, T. Repo, B. Rieger, *J. Organomet. Chem.* **2009**, *694*, 2654.

[95] S. J. Geier, D. W. Stephan, *J. Am. Chem. Soc.* **2009**, *131*, 3476.

[96] P. A. Chase, D. W. Stephan, *Angew. Chem., Int. Ed.* **2008**, *47*, 7433.

[97] D. Holschumacher, T. Bannenberg, C. G. Hrib, P. G. Jones, M. Tamm, *Angew. Chem., Int. Ed.* **2008**, *47*, 7428.

[98] P. A. Chase, A. L. Gille, T. M. Gilbert, D. W. Stephan, *Dalton Trans.* **2009**, 7179.

[99] D. Holschumacher, C. Taouss, T. Bannenberg, C. G. Hrib, C. G. Daniliuc, P. G. Jones, M. Tamm, *Dalton Trans.* **2009**, 6927.

[100] C. Jiang, O. Blacque, H. Berke, *Chem. Commun.* **2009**, 5518.

[101] C. Jiang, O. Blacque, H. Berke, *Organometallics* **2009**, *28*, 5233.

[102] V. Sumerin, F. Schulz, M. Atsumi, C. Wang, M. Nieger, M. Leskelä, T. Repo, P. Pyykkö, B. Rieger, *J. Am. Chem. Soc.* **2008**, *130*, 14117.

[103] P. Spies, G. Erker, G. Kehr, K. Bergander, R. Fröhlich, S. Grimme, D. W. Stephan, *Chem. Commun.* **2007**, 5072.

[104] P. Spies, G. Kehr, K. Bergander, B. Wibbeling, R. Fröhlich, G. Erker, *Dalton Trans.* **2009**, 1534.

[105] P. Spies, S. Schwendemann, S. Lange, G. Kehr, R. Fröhlich, G. Erker, *Angew. Chem., Int. Ed.* **2008**, *47*, 7543.

[106] S. J. Geier, T. M. Gilbert, D. W. Stephan, *J. Am. Chem. Soc.* **2008**, *130*, 12632.

[107] P. A. Chase, G. C. Welch, T. Jurca, D. W. Stephan, *Angew. Chem., Int. Ed.* **2007**, *46*, 8050. Erratum: *Angew. Chem., Int. Ed.* **2007**, *46*, 9136.

[108] G. C. Welch, R. Prieto, M. A. Dureen, A. J. Lough, O. A. Labeodan, T. Höltrichter-Rössmann, D. W. Stephan, *Dalton Trans.* **2009**, 1559.

[109] J. S. J. McCahill, G. C. Welch, D. W. Stephan, *Angew. Chem., Int. Ed.* **2007**, *46*, 4968.

[110] C. M. Mömming, S. Frömel, G. Kehr, R. Fröhlich, S. Grimme, G. Erker, *J. Am. Chem. Soc.* **2009**, *131*, 12280.

[111] M. Ullrich, K. S.-H. Seto, A. J. Lough, D. W. Stephan, *Chem. Commun.* **2009**, 2335.

[112] M. A. Dureen, D. W. Stephan, *J. Am. Chem. Soc.* **2009**, *131*, 8396.

[113] M. A. Dureen, A. Lough, T. M. Gilbert, D. W. Stephan, *Chem. Commun.* **2008**, 4303.

[114] C. M. Mömming, E. Otten, G. Kehr, R. Fröhlich, S. Grimme, D. W. Stephan, G. Erker, *Angew. Chem., Int. Ed.* **2009**, *48*, 6643.

[115] E. Otten, R. C. Neu, D. W. Stephan, *J. Am. Chem. Soc.* **2009**, *131*, 9918.

[116] J. Nyhlén, T. Privalov, *Dalton Trans.* **2009**, 5780.

[117] Y. Guo, S. Li, *Inorg. Chem.* **2008**, *47*, 6212.

[118] T. Privalov, *Chem. Eur. J.* **2009**, *15*, 1825.

[119] J. Nyhlén, T. Privalov, *Eur. J. Inorg. Chem.* **2009**, 2759.

[120] Y. Guo, S. Li, *Eur. J. Inorg. Chem.* **2008**, 2501.

[121] Group 13–15 donor–acceptor complex dissociation energies have been studied recently. See: A. L. Gille, T. M. Gilbert, *J. Chem. Theory Comput.* **2008**, *4*, 1681.

[122] S. Gao, W. Wu, Y. Mo, *J. Phys. Chem. A* **2009**, *113*, 8108.

[123] T. Privalov, *Eur. J. Inorg. Chem.* **2009**, 2229.

[124] T. Privalov, *Dalton Trans.* **2009**, 1321.

R.5 Hydrogen Activation and Hydrogenation by Main-Group Compounds

[125] H. Gilman, A. L. Jacoby, H. Ludeman, *J. Am. Chem. Soc.* **1938**, *60*, 2336.

[126] A. F. Bickel, C. J. Gaasbeel, H. Hogeveen, J. M. Oelderik, J. C. Platte, *Chem. Commun.* **1967**, 634.

[127] G. H. Spikes, J. C. Fettinger, P. P. Power, *J. Am. Chem. Soc.* **2005**, *127*, 12232.

[128] G. D. Frey, V. Lavallo, B. Donnadieu, W. W. Schoeller, G. Bertrand, *Science* **2007**, *316*, 439.

[129] Y. Peng, B. D. Ellis, X. Wang, P. P. Power, *J. Am. Chem. Soc.* **2008**, *130*, 12268.

[130] C. Walling, L. Bollyky, *J. Am. Chem. Soc.* **1964**, *86*, 3750.

[131] A. Berkessel, T. J. S. Schubert, T. N. Müller, *J. Am. Chem. Soc.* **2002**, *124*, 8693.

[132] B. Chan, L. Radom, *J. Am. Chem. Soc.* **2005**, *127*, 2443.

[133] F. L. Ramp, E. J. DeWitt, L. E. Trapasso, *J. Org. Chem.* **1962**, *27*, 4368.

[134] M. W. Haenel, J. Narangerel, U.-B. Richter, A. Rufińska, *Angew. Chem., Int. Ed.* **2006**, *45*, 1061.

[135] M. Siskin, *J. Am. Chem. Soc.* **1974**, *96*, 3641.

[136] J. Wristers, *J. Am. Chem. Soc.* **1975**, *97*, 4312.

[137] L. H. Slaugh, *Tetrahedron* **1966**, *22*, 1741.

[138] L. H. Slaugh, *J. Org. Chem.* **1967**, *32*, 108.

[139] M. Yalpani, R. Köster, *Chem. Ber.* **1990**, *123*, 719.

[140] J. Spielmann, F. Buch, S. Harder, *Angew. Chem., Int. Ed.* **2008**, *47*, 9434.

[141] S. J. Connon, *Org. Biomol. Chem.* **2007**, *5*, 3407.

[142] S. You, *Chem. Asian J.* **2007**, *2*, 820.

[143] S. G. Ouellet, A. M. Walji, D. W. C. MacMillan, *Acc. Chem. Res.* **2007**, *40*, 1327.

[144] H. Adolfsson, *Angew. Chem., Int. Ed.* **2005**, *44*, 3340.

[145] M. Rueping, E. Sugiono, C. Azap, T. Theissmann, M. Bolte, *Org. Lett.* **2005**, *7*, 3781.

[146] E. J. Corey, C. J. Helal, *Angew. Chem., Int. Ed.* **1998**, *37*, 1986.

[147] A. V. Malkov, A. J. P. S. Liddon, P. Ramírez-López, L. Bendová, D. Haigh, P. Kočovský, *Angew. Chem., Int. Ed.* **2006**, *45*, 1432.

[148] J. M. Blackwell, E. R. Sonmor, T. Scoccitti, W. E. Piers, *Org. Lett.* **2000**, *2*, 3921.

[149] D. J. Parks, J. M. Blackwell, W. E. Piers, *J. Org. Chem.* **2000**, *65*, 3090.

[150] S. Rendler, M. Oestreich, *Angew. Chem., Int. Ed.* **2008**, *47*, 5997.

[151] D. J. Parks, W. E. Piers, *J. Am. Chem. Soc.* **1996**, *118*, 9440.

[152] H. Nishikori, R. Yoshihara, A. Hosomi, *Synlett* **2003**, 561.

R.6 Hydrogen Activation in Biological Systems

[153] R. K. Thauer, A. R. Klein, G. C. Hartmann, *Chem. Rev.* **1996**, *96*, 3031.

[154] G. Buurman, S. Shima, R. K. Thauer, *FEBS Lett.* **2000**, *485*, 200.

[155] J. H. Teles, S. Brode, A. Berkessel, *J. Am. Chem. Soc.* **1998**, *120*, 1345.

[156] A. P. Scott, B. T. Golding, L. Radom, *New J. Chem.* **1998**, 1171.

[157] S. Shima, O. Pilak, S. Vogt, M. Schick, M. S. Stagni, W. Meyer-Klaucke, E. Warkentin, R. K. Thauer, U. Ermler, *Science* **2008**, *321*, 572.

[158] S. Shima, R. K. Thauer, *Chem. Rec.* **2007**, *7*, 37.

[159] S. P. J. Albracht, *Biochim. Biophys. Acta* **1994**, *1188*, 167.

[160] C. Zirngibl, R. Hedderich, R. K. Thauer, *FEBS Lett.* **1990**, *261*, 112.

R.7 Theoretical Methods

[161] F. Jensen, *Introduction to Computational Chemistry, Second Edition*, John Wiley & Sons, Ltd., Chichester, **2007**.

[162] K. Fukui, *Acc. Chem. Res.* **1981**, *14*, 363.

[163] J. Tomasi, B. Mennucci, E. Cancès, *J. Mol. Struct. (Theochem)* **1999**, *464*, 211.

[164] A. Ben-Naim, *J. Phys. Chem.* **1978**, *82*, 792.

[165] R. P. Bell, *The Proton in Chemistry, Second Edition*, Cornell University Press, Ithaca, New York, **1973**.

[166] J. R. Pliego, Jr., J. M. Riveros, *J. Phys. Chem. A* **2001**, *105*, 7241.

[167] Y. Fu, L. Liu, R.-Q. Li, R. Liu, Q.-X. Guo, *J. Am. Chem. Soc.* **2004**, *126*, 814.

[168] A. V. Marenich, R. M. Olson, C. P. Kelly, C. J. Cramer, D. G. Truhlar, *J. Chem. Theory Comput.* **2007**, *3*, 2011.

[169] J. Pfaendtner, X. Yu, L. J. Broadbelt, *Theor. Chem. Acc.* **2007**, *118*, 881.

[170] C. Y. Lin, E. I. Izgorodina, M. L. Coote, *J. Phys. Chem. A* **2008**, *112*, 1956.

[171] A. D. Becke, *J. Chem. Phys.* **1993**, *98*, 5648.

[172] C. Lee, W. Yang, R. G. Parr, *Phys. Rev. B* **1988**, *37*, 785.

[173] S. H. Vosko, L. Wilk, M. Nusair, *Can. J. Phys.* **1980**, *58*, 1200.

[174] P. J. Stephens, F. J. Devlin, C. F. Chabalowski, M. J. Frisch, *J. Phys. Chem.* **1994**, *98*, 11623.

[175] P. R. Schreiner, *Angew. Chem., Int. Ed.* **2007**, *46*, 4217.

[176] K. E. Riley, B. T. Op't Holt, K. M. Merz, Jr., *J. Chem. Theory Comput.* **2007**, *3*, 407.

[177] P. Jurečka, J. Černý, P. Hobza, D. R. Salahub, *J. Comput. Chem.* **2007**, *28*, 555.

[178] S. Grimme, M. Steinmetz, M. Korth, *J. Org. Chem.* **2007**, *72*, 2118.

[179] A. G. Baboul, L. A. Curtiss, P. C. Redfern, K. Raghavachari, *J. Phys. Chem.* **1999**, *110*, 7650.

[180] Y. Zhao, D. G. Truhlar, *Acc. Chem. Res.* **2008**, *41*, 157.

[181] Y. Zhao, D. G. Truhlar, *J. Chem. Theory Comput.* **2008**, *4*, 1849.

[182] Y. Zhao, N. E. Schultz, D. G. Truhlar, *J. Chem. Theory Comput.* **2006**, *2*, 364.

[183] T. Schwabe, S. Grimme, *Acc. Chem. Res.* **2008**, *41*, 569.

[184] S. Kristyán, P. Pulay, *Chem. Phys. Lett.* **1994**, *229*, 175.

[185] T. A. Rokob, A. Hamza, I. Pápai, *Org. Lett.* **2007**, *9*, 4279.

[186] R. Ditchfield, W. J. Hehre, J. A. Pople, *J. Chem. Phys.* **1971**, *54*, 724.

[187] W. J. Hehre, R. Ditchfield, J. A. Pople, *J. Chem. Phys.* **1972**, *56*, 2257.

[188] P. C. Hariharan, J. A. Pople, *Theor. Chim. Acta* **1973**, *28*, 213.

[189] J. D. Dill, J. A. Pople, *J. Chem. Phys.* **1975**, *62*, 2921.

[190] M. M. Francl, W. J. Pietro, W. J. Hehre, J. S. Binkley, M. S. Gordon, D. J. DeFrees, J. A. Pople, *J. Chem. Phys.* **1982**, *77*, 3654.

[191] R. Krishnan, J. S. Binkley, R. Seeger, J. A. Pople, *J. Chem. Phys.* **1980**, *72*, 650.

[192] A. D. McLean, G. S. Chandler, *J. Chem. Phys.* **1980**, *72*, 5639.

[193] T. Clark, J. Chandrasekhar, G. W. Spitznagel, P. v. R. Schleyer, *J. Comput. Chem.* **1983**, *4*, 294.

[194] E. R. Johnson, R. A. Wolkow, G. A. DiLabio, *Chem. Phys. Lett.* **2004**, *394*, 334.

[195] J. Gräfenstein, D. Izotov, D. Cremer, *J. Chem. Phys.* **2007**, *127*, 214103.

[196] E. R. Johnson, A. D. Becke, C. D. Sherrill, G. A. DiLabio, *J. Chem. Phys.* **2009**, *131*, 034111.

[197] C. A. Jiménez-Hoyos, B. G. Janesko, G. E. Scuseria, *Phys. Chem. Chem. Phys.* **2008**, *10*, 6621.

[198] *Phys. Chem. Chem. Phys.* **2008**, *10*, issue 23, partly devoted to local correlation methods, and references therein.

[199] M. Feyereisen, G. Fitzgerald, A. Komornicki, *Chem. Phys. Lett.* **1993**, *208*, 359.

[200] F. Weigend, M. Häser, *Theor. Chem. Acc.* **1997**, *97*, 331.

[201] F. Weigend, A. Kohn, C. J. Hattig, *J. Chem. Phys.* **2002**, *116*, 3175.

[202] S. Grimme, *J. Chem. Phys.* **2003**, *118*, 9095.

[203] Á. Szabados, *J. Chem. Phys.* **2006**, *125*, 214105.

[204] S. Grimme, *J. Comput. Chem.* **2003**, *24*, 1529.

[205] J. G. Hill, J. A. Platts, *J. Chem. Theory Comput.* **2007**, *3*, 80.

[206] Y. Jung, R. C. Lochan, A. D. Dutoi, M. Head-Gordon, *J. Chem. Phys.* **2004**, *121*, 9793.

[207] T. H. Dunning, *J. Chem. Phys.* **1989**, *90*, 1007.

[208] G. Lendvay, I. Mayer, *Chem. Phys. Lett.* **1998**, *297*, 365.

[209] J. Antony, S. Grimme, *J. Phys. Chem. A* **2007**, *111*, 4862.

[210] *J. Comput. Chem.* **2007**, *28*, special issue 1 entitled "90 Years of Chemical Bonding".

[211] K. A. Wiberg, *Tetrahedron* **1968**, *24*, 1083.

[212] I. Mayer, *Chem. Phys. Lett.* **1983**, *97*, 270.

[213] A. E. Reed, L. A. Curtiss, F. Weinhold, *Chem. Rev.* **1988**, *88*, 899.

[214] A. E. Reed, F. Weinhold, *J. Chem. Phys.* **1985**, *83*, 1736.

[215] Concerning ab initio determination of basicity of various compounds in organic solvents, see: J.-N. Li, Y. Fu, L. Liu, Q.-X. Guo, *Tetrahedron* **2006**, *62*, 11801 and references therein.

R.8 Software Packages

[216] M. J. Frisch, G. W. Trucks, H. B. Schlegel, G. E. Scuseria, M. A. Robb, J. R. Cheeseman, J. A. Montgomery, Jr., T. Vreven, K. N. Kudin, J. C. Burant, J. M. Millam, S. S. Iyengar, J. Tomasi, V. Barone, B. Mennucci, M. Cossi, G. Scalmani, N. Rega, G. A. Petersson, H. Nakatsuji, M. Hada, M. Ehara, K. Toyota, R. Fukuda, J. Hasegawa, M. Ishida, T. Nakajima, Y. Honda, O. Kitao, H. Nakai, M. Klene, X. Li, J. E. Knox, H. P. Hratchian, J. B. Cross, V. Bakken, C. Adamo, J. Jaramillo, R. Gomperts, R. E. Stratmann, O. Yazyev, A. J. Austin, R. Cammi, C. Pomelli, J. W. Ochterski, P. Y. Ayala, K. Morokuma, G. A. Voth, P. Salvador, J. J. Dannenberg, V. G. Zakrzewski, S. Dapprich, A. D. Daniels, M. C. Strain, O. Farkas, D. K. Malick, A. D. Rabuck, K. Raghavachari, J. B. Foresman, J. V. Ortiz, Q. Cui, A. G. Baboul, S. Clifford, J. Cioslowski, B. B. Stefanov, G. Liu, A. Liashenko, P. Piskorz, I. Komaromi, R. L. Martin, D. J. Fox, T. Keith, M. A. Al-Laham, C. Y. Peng, A. Nanayakkara, M. Challacombe, P. M. W. Gill, B. Johnson, W. Chen, M. W. Wong, C. Gonzalez, J. A. Pople, *Gaussian 03, Revisions B.05 and E.01*, Gaussian, Inc., Wallingford CT, **2004**.

[217] R. Ahlrichs, M. Bär, H. Baron, R. Bauernschmitt, S. Böcker, N. Crawford, P. Deglmann, M. Ehrig, K. Eichkorn, S. Elliott, F. Furche, F. Haase, M. Häser, C. Hättig, A. Hellweg, H. Horn, C. Huber, U. Huniar, M. Kattannek, A. Köhn, C. Kölmel, M. Kollwitz, K. May, P. Nava, C. Ochsenfeld, H. Öhm, H. Patzelt, D. Rappoport, O. Rubner, A. Schäfer, U. Schneider, M. Sierka, O. Treutler, B. Unterreiner, M. v. Arnim, F. Weigend, P. Weis, H. Weiss, *TURBOMOLE 5.9.1 and 5.10*, University of Karlsruhe, **2008**.

[218] I. Mayer, *Program "BORDER" Version 1.0*, Chemical Research Center, Hungarian Academy of Sciences, Budapest, **2005**.

[219] G. Schaftenaar, J. H. Noordik, *"Molden: a pre- and post-processing program for molecular and electronic structures", J. Comput.-Aided Mol. Design* **2000**, *14*, 123.

[220] P. Flükiger, H. P. Lüthi, S. Portmann, J. Weber, *MOLEKEL 4.3*, Swiss National Supercomputing Centre CSCS, Manno, Switzerland, **2000**.

R.9 Miscellaneous

[221] *Chem. Soc. Rev.* **2009**, *38*, issue 1 ("2009 Renewable Energy issue").

[222] U. Eberle, M. Felderhoff, F. Schüth, *Angew. Chem., Int. Ed.* **2009**, *48*, 6608.

[223] *Acc. Chem. Res.* **2007**, *40*, special issue 12 on hydrogenation and transfer hydrogenation.

[224] *Adv. Synth. Catal.* **2003**, *345*, special issue 1-2 on catalytic hydrogenation.

[225] G. J. Kubas, *Chem. Rev.* **2007**, *107*, 4152.

[226] G. J. Kubas, *Adv. Inorg. Chem.* **2004**, *56*, 127.

[227] P. G. Jessop, R. H. Morris, *Coord. Chem. Rev.* **1992**, *121*, 155.

[228] D. M. Heinekey, A. Lledos, J. M. Lluch, *Chem. Soc. Rev.* **2004**, *33*, 175.

[229] G. S. McGrady, G. Guilera, *Chem. Soc. Rev.* **2003**, *32*, 383.

[230] R. H. Crabtree, *Acc. Chem. Res.* **1990**, *23*, 95.

[231] G. J. Kubas, *Acc. Chem. Res.* **1988**, *21*, 120.

[232] J. S. M. Samec, J.-E. Bäckvall, P. G. Andersson, P. Brandt, *Chem. Soc. Rev.* **2006**, *35*, 237.

[233] G. J. Kubas, *Proc. Natl. Acad. Sci. USA* **2007**, *104*, 6901.

[234] W. Cui, B. B. Wayland, *J. Am. Chem. Soc.* **2004**, *126*, 8266 and references therein.

[235] L. J. Sæthre, T. D. Thomas, S. Svensson, *J. Chem. Soc., Perkin. Trans. 2* **1997**, 749.

[236] P. Comba, *Coord. Chem. Rev.* **2000**, *200–202*, 217.

[237] R. Custelcean, J. E, Jackson, *Chem. Rev.* **2001**, *101*, 1963.

[238] M. R. DuBois, D. L. DuBois, *Chem. Soc. Rev.* **2009**, *38*, 62.

[239] A. Staubitz, M. Besora, J. N. Harvey, I. Manners, *Inorg. Chem.* **2008**, *47*, 5910.

[240] C. R. Miranda, G. Ceder, *J. Chem. Phys.* **2007**, *126*, 184703.

[241] X. Yang, M. B. Hall, *J. Am. Chem. Soc.* **2008**, *130*, 1798.

[242] D. J. Grant, A. J. Arduengo III, D. A. Dixon, *J. Phys. Chem. A* **2009**, *113*, 750.

[243] H.-J. Himmel, H. Schnöckel, *Chem. Eur. J.* **2002**, *8*, 2397.

[244] D. Hugas, S. Simon, M. Duran, C. F. Guerra, F. M. Bickelhaupt, *Chem. Eur. J.* **2009**, *15*, 5814.

[245] A. Krapp, G. Frenking, E. Uggerud, *Chem. Eur. J.* **2008**, *14*, 4028.

[246] S. Kobayashi, H. Ishitani, *Chem. Rev.* **1999**, *99*, 1069.

[247] D. G. Blackmond, *Angew. Chem., Int. Ed.* **2009**, *48*, 386.

Abstract

Steric factors often hinder chemical reactions. It was observed more than fifty years ago that Lewis acid–base pairs with bulky substituents are unable to form a dative bond. Such pairs, in turn, can possess surprising reactivity: certain examples have very recently been shown to cleave molecular H_2 or other small molecules, and to catalyze direct hydrogenation of double bonds. Similar reactions under mild conditions have only been known on the surface or in complexes of transition metals.

In my PhD work, I have been involved in computational studies aimed at the mechanistic understanding of these intriguing reactions. Quantum chemical calculations at various density functional theory and ab initio levels allowed us to explore the reaction pathways on the relevant potential energy surfaces, and to formulate concepts concerning this reactivity.

Based on our thorough studies on the prototypical $t\mathrm{Bu_3P} + \mathrm{B(C_6F_5)_3} + \mathrm{H_2} \rightarrow [t\mathrm{Bu_3PH}]^+[\mathrm{HB(C_6F_5)_3}]^-$ reaction, we proposed a general mechanism. We pointed out that secondary interactions between the donor and acceptor molecules allow formation of a weak complex, in which the acidic and basic centers are preorganized for a cooperative interaction with the incoming H_2 (or other small) molecule. We described the fragments and molecular orbitals that participate in this interaction, which leads to the polarization and cleavage of the hydrogen molecule. We found that the absence or weakness of the dative bond represents reactant-state destabilization, which lowers the activation barrier and makes the reaction exothermic. Using this model, we could also interpret H_2 splitting by other acid–base pairs as well as the addition reaction to olefins and its regioselectivity.

We studied the thermodynamics of the hydrogen splitting by various Lewis pairs. Our calculations revealed that the outcome of the cleavage reaction is governed by the dative bond strength, the cumulative acid–base properties of the pair and the effectiveness of acid–base cooperativity. We furthermore gave a detailed description of the mechanism of a transition-metal-free catalytic hydrogenation system based on sterically encumbered Lewis pairs. We extended the catalytic cycle presented in the literature with a competitive, autoinductive pathway, which demonstrated that consideration of all Lewis centers in the reaction mixture is essential for a more complete understanding.

Összefoglalás

Kémiai reakciók végbemenetelét sokszor akadályozzák sztérikus tényezők. Már több, mint ötven évvel ezelőtt megfigyelték, hogy nagy térkitöltésű szubszituenseket hordozó Lewis sav–bázis párok esetén nem jön létre datív kötés. Ezek a párok azonban meglepő reaktivitást mutatnak: számos képviselőjükről derült ki a közelmúltban, hogy képes a H_2-t vagy más kis molekulákat elhasítani, illetve kettős kötések közvetlen hidrogénezését katalizálni. Ilyen reakciókat enyhe körülmények között korábban csak átmenetifémek felületén vagy komplexeiben figyeltek meg.

PhD munkám során elméleti kémiai számítások segítségével törekedtünk ezeknek a rendszereknek a megértésére. Különböző sűrűségfunkcionál-alapú és ab inito módszereket alkalmaztunk annak érdekében, hogy a megfelelő potenciálisenergia-felületeken a reakcióutakat felderítsük, majd a kapott eredmények segítségével egy átfogó mechanizmusképet alakítsunk ki.

A prototípusnak tekinthető $t\mathrm{Bu_3P} + \mathrm{B(C_6F_5)_3} + \mathrm{H_2} \rightarrow [t\mathrm{Bu_3PH}]^+[\mathrm{HB(C_6F_5)_3}]^-$ reakció részletes vizsgálata alapján javasoltunk egy általános modellt. Megmutattuk, hogy a donor- és akceptormolekula másodlagos kötőerők révén történő asszociációja létrehozhat egy gyenge komplexet, melyben a savas és bázisos centrumok organizálva vannak a H_2-vel (vagy más kis molekulával) való kooperatív kölcsönhatáshoz. Részletesen jellemeztük a fragmenseket és azokat molekulapályákat, melyek részt vesznek a hidrogénmolekula erős polarizálódásához, majd felszakításához vezető kölcsönhatásban. Megállapítottuk, hogy a datív kötés gyengesége vagy hiánya reaktánsoldali destabilizációt jelent, amelynek köszönhetően kicsi az aktiválási gát és exoterm lesz a reakció. Ezen modell keretében értelmezni tudtuk más hasonló pároknak hidrogénnel szembeni reaktivitását, továbbá az olefinekre történő addíciót és annak regioszelektivitását is.

Vizsgáltuk a hidrogénhasítási reakció termodinamikáját különböző Lewis párok esetén. Számításainkból kiderült, hogy a folyamat kimenetelét a datív kötés erőssége, a pár sav–bázis tulajdonságai, és a sav–bázis kooperativitás hatékonysága befolyásolja. Részletesen jellemeztük továbbá egy átmenetifémet nem alkalmazó, nagy térkitöltésű Lewis párokon alapuló katalitikus hidrogénezési rendszer reakciómechanizmusát. Az irodalomban javasolt katalitikus kört kiegészítettük egy kompetitív, autoinduktív úttal, amely egyben arra is rávilágított, hogy egy teljesebb mechanisztikus kép kialakításához a reakcióelegyben található összes Lewis savas vagy bázisos komponens figyelembevételére szükség van.